THESIS FOR THE DEGREE OF DOCTOR OF PHILOSOPHY

Study on a Fatigue Assessment Method for Ship Structures Considering the Stochastic Characteristics of the Whipping Vibration

（ホイッピング振動の統計的性質を考慮した船体構造部材の疲労強度評価法に関する研究）

Luis Carlos De Gracia Claude

July 2019

Division of Global Architecture

Department of Naval Architecture and Ocean Engineering

Osaka University

Japan 2019

Abstract

Recently, the size of container ships has increased to improve its economic efficiency and reduce their environmental impact. Then, the hydro-elastic vibratory phenomena, recognized as whipping and springing, are more likely to be more important due to the effect of large bow flare which induces higher slamming loads, higher ship speed service, the constant increase in the ship size, and the increase of the fatigue damage in fatigue sensitive detail. Recently, relevant information on the importance of the hull vibration effect on the fatigue strength has been reported from full-scale measurement, numerical analysis, and fatigue testing. Various have reported that the increase in the fatigue damage evaluated by RainFlow Cycle Counting (RFCC) due to whipping, but the validity of RFCC for those stress waveforms have not been fully verified yet.

This thesis presents the stochastic characteristics of hull vibration superimposed stress waveform (HVSSW) examined from a series of Non-Linear Hydro-Elasticity Analyses (NLHEA) for short seas, heading angles, and ship speeds. It is found that the stress waveform's characteristics can be simplified so that the slamming impact occurs once in every 3 to 5 waves and the impact stress range is comparable to the primary wave stress range. In order to make a reasonable assessment of the structural influence of hull vibration on the fatigue strength, it is essential to consider both the structural influence of whipping vibration and the probability of the slamming load. The validity of RFCC is examined by carrying out fatigue tests with stress histories which emulate the characteristics of the simulated whipping vibration. For these tests, it is developed an electric-driven fatigue testing apparatus which can apply whipping superimposed stress waveform in high speed and low cost.

Keywords: Fatigue, Whipping, Hydro-elasticity analysis, Electric exciter, Storm model, Fatigue testing.

Acknowledgments

First of all, I would like to express my utmost gratitude to my supervisor Professor Naoki Osawa, for giving me the opportunity to join the laboratory of Ocean Material Engineering of the Department of Naval Architecture and Ocean Engineering of Osaka University and helping me continue this interesting research topic. Your inspiring, experience and knowledge offered are an important part of my research.

Besides my supervisor, I want to express my sincere appreciation to Professor Hidekazu Murakawa, for giving me the opportunity to come to Japan and admitted me as a research student at the Joining and Welding Research Institute of Osaka University, for his patience, invaluable help and support not only in my studies, but in my daily life. I am also pleased to say thank you to Professor Sherif Rashed, Professor Kazuhiro Iijima and Professor Wengang Mao for their insightful suggestions.

My gratitude also goes to Professor Kazuhiro Iijima, Professor Munehiko Minoura and Professor Hitoi Tamaru for participating as members of the dissertation committee and providing corrections and valuable suggestions to improve the quality of this work.

Thankfulness to Nippon Kaiji Kyokai staff members, especially Dr. Norio Yamamoto and Mr. Tomohiro Sugimoto for their valuable discussions during this research.

Acknowledgment is also made to the Panamanian Government for providing fund for supporting my doctoral studies in Japan. Also my gratitude to my supervisor at Universidad Tecnologica de Panama, Dr. Adan Vega Saenz who always trusted in me and for his valuable pieces of advice while being in Japan.

Most of all, I am grateful to my family for their love, patience, support and for always believing in me. I consider myself nothing without them. To my friends for their tireless encouragement during my stay in Japan.

Luis De Gracia

Osaka, August 2019

Table of Contents

List of Abbreviations and Symbols

a	Threshold value parameter
BNF	Bending natural frequency
C, m	Material parameters
CFD	Computational fluid dynamics
CA	Constant amplitude
C_{wh}	Coefficient of whipping interval
$C_{wh,\mathrm{lim}}$	C_{wh} at limit ship forward speed
D_{rf}	RainFlow damage
DUF	RainFlow damage Up to the Failure
ECMWF	Europe Centre for Medium-Range Weather Forecasts
EE	Electric Exciter
EM	Eccentric Mass
FE	Finite Element
FEM	Finite Element Method
FFT	Fast Fourier Transformation
f_{PW}	PW frequency
f_{whip}	Frequency of whipping vibration

HFE	High-frequency Effect
H_S	Significant wave height
HV	Hull Vibration
HVSSW	Hull Vibration Superimposed Stress Waveform
IF	Intermittently superimposed with Fixed $\Delta\sigma_{eq}$
IFFT	Inverse Fast Fourier Transformation
JWA	Japan Weather Association
LFW	Low-frequency Wave
MTR	Minimum Time Route
N_0	N_b estimated by CA SN curve
N_b	Number of load cycles at which the crack propagation path turns into the main plate
n_{CA}	CA cycles
NLHEA	Non-Linear Hydro-Elasticity Analyses
N_{PW}	Number of PW
n_{PW}	PW cycles in each sea state
n_{slm}	Number of slamming impact
n_{SUP}	SUP cycles
n_{total}	Total number of cycles in one load set
PBV	Plate Bending Vibration
PW	Primary Wave

RAO	Response amplitude operator
RFCC	RainFlow Cycle Counting
$\sigma_{HV\text{-}PK}$	Peak stress of HV waveform
$\sigma_{HV\text{-}VL}$	Valley stress of HV waveform
SP	Setpoint
SUP	Superimposed
T_{HRES}	Threshold value
T_S	Mean zero-up cross period
VA	Variable amplitude
VBM	Vertical Bending Moment
VLCC	Very large crude carriers
$V_{\lim}(H_S)$	Maximum V_S achievable for a given H_S
V_S	Ship forward speed
$\Delta\sigma_{CREST}$	Crests of $\Delta\sigma_{PK}$ sequence
$\Delta\sigma_{PK}$	Difference between $\sigma_{HV\text{-}PK}$ and $\sigma_{HV\text{-}VL}$
$\Delta\sigma_{PK,\lim}$	Average values of $\Delta\sigma_{PK}$ for $V_{\lim}(H_S)$
$\Delta\sigma_{\mathrm{PK\_RNG,lim}}$	Slamming peak stress range at the limit ship forward speed
$\Delta\sigma_{PW}$	Stress range of PW stress waveform
$\Delta\sigma_{PW,\lim}$	Average values of $\Delta\sigma_{PK}$ for $V_{\lim}(H_S)$

$\Delta\sigma_{PW,lim}$	Primary stress range at the limit ship forward speed
$\Delta\sigma_{nb}$	Nominal bending stress range
$\Delta\sigma_{CA}$	$\Delta\sigma_{eq,rf}$ in CA cycles
$\Delta\sigma_{eq,rf}$	Equivalent stress range
$\Delta\sigma_{SUP}$	$\Delta\sigma_{eq,rf}$ in SUP cycles
s_{Rng}	Standard deviation of $\Delta\sigma_{PK}$

Chapter 1 Introduction

One of the main driver for ordering bigger container ships is to reduce the energy needed to transport each individual container. In this way, it improves the profitability and reduces the environmental impact of global supply chains (DNVGL 2018). Although that the slowing global world economy holds back the container growth in 2018, it is expected that the global volume overturns this trend over the next two years[1], since the international shipping industry represents over the 70% of global trade by value[2]. Thus, a comprehensive framework of safety regulations needs continuous improvement because actual ship design methods are associated with a number of different uncertainties. Therefore, when it comes to the ship structure the aim is to ensure that all parts of the hull structure subjected to dynamic loading have an adequate fatigue life to avoid human life casualties, loss of cargoes and environmental consequences due to catastrophic or nearly catastrophic failures.

1.1 Background and Motivation

Vessels sailing in ocean-going routes are continuously exposed to the influence of conditions caused by weather, e.g. wind, waves and ocean currents. Knowledge about wave-induced loads and motions of ships and offshores structures is important both in design and operational studies. The evaluation of the wave-induced loads on ships is a challenging task. In particular, vertical accelerations and relative vertical motions between the ship and the waves are important responses. Accelerations are an important factor to seasickness, to determine loads on cargo and equipment, and a significant effect on many marine applications, for example, subsea lifting

[1]IHS Markit: Trends in the World Economy and Trade report
[2]United Nations Conference on Trade and Development

operations, aircraft landing on vessels, hydrographic seabed mapping, oil exploration, and drilling vessels, among others. Large vertical accelerations are caused most frequently by heavy and pitch motions. An important cause of large pitch motion, especially in head seas, is whipping response to slamming impact and water on deck. For ships is imperative to avoid slamming as well as water on deck due to the possibility of local damage to the structure. Ocean waves are random in terms of both time and space. Therefore, the encountered waves are usually described by the stochastic random processes. The variability of the wave-induced loads leads to structural fatigue in ships. An example of the wave-induced load variability is the alternating sagging and hogging condition that causes repeated loading and unloading to the ship structure, accumulating fatigue damage since the ship is launched.

Fatigue has been an important design criterion in the shipbuilding industry for a long time, especially with the extensive use of higher tensile strength steel (HTS-steels) from the middle of the 1980s. The complexity of ship structures creates problems during the proof of sufficient fatigue strength, typically in the joint connecting ship and offshore structural members. When a material is subjected to cyclic loading, fatigue damage and fatigue cracks are progressive processes. The probability of fatigue-induced failure can conceptually be estimated using a series system description: a geometry (i.e. structural member assembly) is as weak as its weakest material link, introducing the statistics of extremes to the fatigue damage criteria formulations. Moreover, the structural analysis also involves the ultimate strength assessment. The evaluation of the ultimate capacity of ships is a very important issue on the structural design of the ship. It is associated with a global failure of the hull and the final results are normally the loss of the ship, its cargo and human lives.

For ships, classification societies mostly stipulate a simplified approach for the fatigue load determination by providing a set of simplified load cases defined in guidelines which provide expressions related to the principal arrangement of the ship navigating in various loading conditions for a given design wave environment. Recently, the drastic changes in ship type, size and complexity, and the use of new higher strength materials trigger the concerns about the adequateness of these guidelines for ships.

It is well known that ships at sea are not only subjected to wave-induced stresses. The ship is also subjected to hydro-elastic hull vibrations referred as 'whipping' and 'springing'. Whipping is known as a transient vibratory phenomenon due to wave impacts, called slamming, and 'springing' as a resonance of hull vibration, consequence of the oscillating wave loads. Nowadays, these hydro-elastic vibratory phenomena are more likely to be more important for larger container ships due to large bow flare which induces higher slamming loads, higher ship service speed, the increase in the ship size that reduces the natural frequencies, an increase of the fatigue damage in fatigue sensitive detail, etc. These as been observed on full-scale measurements as reported by Moe et al. (2005), Storhaug et al. (2007), Ogawa et al. (2012), among others. However, the classification society guidelines were developed to account for wave frequency loads and are unlikely to consider the effect of whipping/springing for safety assessment, due to the limited experience (see DNV-GL 2015; Almar Naess 1985).

As a result, one of the main repercussions are the fatigue cracks that have been known to occur in welded ships for several decades. These fatigue cracks sometimes start at a very early stage in the ship's service and the fatigue problem becomes more imminent (Moe et al. 2005; Storhaug et al. 2007). Figure 1.1 shows examples of fatigue cracks found in a double hull Very Large Crude Carriers (VLCC) reported

in the SR245 (2000). Therefore, a generalized methodology to manage fatigue life is definitely still open for further improvement. For ship owners and operators, the topic is of great interest due to the economics aspect associated with it (for example the repairing costs, maintenance or even expenses from environmental pollution or the increase of the insurance policies).

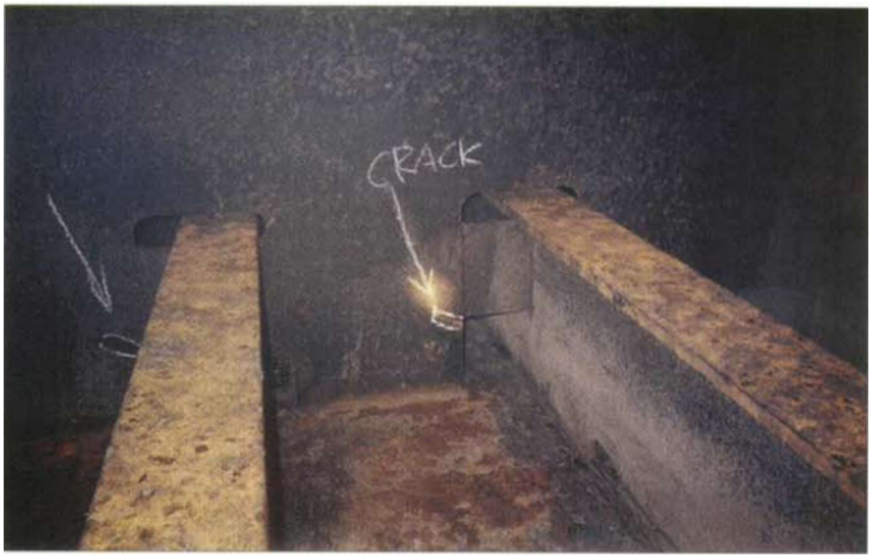

(a) fatigue cracks in way of the longitudinal cutouts.

(b) fatigue cracks in the base of the strut.

Fig. 1.1 Examples of fatigue cracks in a double hull VLCC. Adapted from (SR245 2000).

Furthermore, the severe environments encountered by ships may lead to an increase in extreme responses of ship structures during long-term sailing. It can cause structural failures due to local ultimate strength and buckling. Therefore, it is essential to get accurate long-term sea environmental data for the ship trade areas. In addition to the wave scatters provided by different classification societies, more realistic wave information for ship design and operation can be accessed from various sensors launched to collect wave data, e.g., onboard observations, buoy data, satellite measurements, and hindcast data (also known as reanalysis data), etc.

Meanwhile, in all industrial sectors, there is a strong drive towards increases asset life in order to reduce whole-life costs. Despite the great advance in the computational power, measurement and prediction of damage development during life and methods of accelerated testing to be able to predict performance and remnant strength after perhaps several decades of operation are necessaries. Then, the effect of repair strategies can be comprehensively understood.

In the recent past, a great number of fatigue failures occurred in ship structures. However, there are limited information and no formal database of structural or mechanical failures or near-miss events of ships in operation with enough and accurate background information. Due to the lack of a knowledge database, and uncertainties in design factors including human factors (captain decisions), the risk-based design has hardly been applied historically to ship structures. Hence, marine structures including offshore structures are designed for safe-life, but the still the environmental loads are often not well-understood.

1.1.1 Hydroelasticity of ships

The hydroelasticity of the ship is in the form of wave-induced vibrations, referred to as whipping and springing. Among other ship structural problems, they tend to aggravate extreme and fatigue loads of very large commercial ships. The

impact of the wave-induced vibrations on the ship structural strength depends on sizes, types and operational conditions of ships.

Recent studies have emphasized that wave-induced vibrations significantly increase design loads. Therefore, wave-induced vibrations should be considered in the ship design. For running container carriers, the effect of wave-induced vibrations was investigated with full-scale measurements (Storhaug et al. 2003; Storhaug et al. 2007; Drummen et al. 2008; Fukasawa et al. 2014; Storhaug et al. 2015; Ki HG et al. 2015). For a new design of ultra-large containerships, numerical methods have been applied for prediction of design loads (Im et al. 2015; Oberhagemann et al. 2015; Hwang et al. 2015; Kim et al. 2018). Wave-induced vibrations should be predicted via nonlinear hydro-elastic analysis methods because whipping and springing are mainly induced by nonlinear wave loads. The wave-induced vibrations can be predicted by either a numerical simulation or a model test. While the model test is considered a reliable method to represent real phenomena, the main obstacles are the high costs and problems handling errors. To the contrary, the resources needed to perform numerical simulations are much lower than that for the model test.

Furthermore, recently, for seakeeping analysis, various hydro-elastic methods to consider nonlinearities have been proposed (Jensen et al. 1996; Malenica et al. 2008; Kim et al. 2009). In addition, to establish reliable procedures for hydro-elastic response and fatigue analyses, the effect/characteristics of the wave-induced vibrations were examined by Non-Linear Hydro-Elasticity Analyses (NLHEA) for various wave conditions (Hirdaris et al. 2003; Iijima et al. 2008; Hirdaris et al. 2009; Tuitman 2010; Kim et al. 2014; Kim et al. 2015; Kim et al. 2016). A numerical method generally consists of three parts (Kim et al. 2015):

1) A fluid solver for the seakeeping problem: there are various methods utilized by fluid solvers, including the 2-D strip theory method, 3-D panel method, and 3-D CFD method. The 3-D panel method is presently considered to be the most practical for time-domain simulation; the 3-D CFD method is still too heavy for extended simulation;

2) A structural solver for the rigid-body and flexible motions: for the structural solver, either a 1-D beam model or a 3-D FE model can be used depending on the purpose. When considering structural discontinuity, a 1-D beam model exhibits almost the same structural behaviors as a 3-D FE model, including in the torsional response (Kim et al. 2014).

3) A slamming solver for calculating slamming loads (Kim et al. 2015): the slamming load acting on the bow flare, bottom, or stern should also be considered when the linear potential theory is used for the seakeeping problem; it is automatically included in the 3-D CFD method (Oberhagemann et al. 2012). Although a 3-D slamming model is desirable because a ship slamming is basically a 3-D problem (Korobkin et al. 2006), the theoretical study on the slamming of 3D for arbitrary body shape is no available at this moment. Further, although CFD can be a candidate for this purpose, its practicality and accuracy are very limited.

1.1.2 Ship slamming occurrence

Slamming event occurs when a ship experiences sufficiently large heave and pitch motions such that the bow emerges from the water and re-enters with a heavy impact or slam. The slamming loading is characterized by a rapid increase during water re-entry followed by high-frequency transient vibration in the structure, called whipping, which decays rapidly (Dessi et al. 2013). This type of slamming often occurs with smaller ships and increases with the ship's speed. For larger vessels, bottom slamming is more likely to occur in a ballast condition and in extreme sea

states. Several reports had shown that ships, especially sailing in the head waves with high forward speed, have suffered from local structural damage due to slamming loads (MAIB 2008; Boesten 2006). Therefore, the frequency of slamming occurrence is an important factor for a shipmaster to reduce the speed or to change the heading.

In order to improve understanding of the influence of slamming in the fatigue life, the slamming occurrence has been studied statistically since the ship motions and the free surface elevation in a sea state are both random in nature. Pioneer works on statistical characteristics of slamming were published by Tick (1958) and Ochi (1964). The general criteria of these works are based on a) relative vertical motion between the structure and the sea surface; b) the relative vertical velocity; c) the angle between the cross-structure and free surface. Further studies have been accepted considering the first two criteria for probabilistic slamming models (Faltinsen 1993; Wang et al. 2016a, 2016b).

Furthermore, various the slamming occurrence models concerning the fatigue life have been proposed based on the identification of slam event from full-scale measurements as shown in Ogawa et al. (2012), Toyoda et al. (2012), Magoga et al. (2014), and including full-scale experiment as in Thomas et al. (2011), French et al. (2015). Thomas et al. (2011) proposed a slamming identification technique by defining two slamming event criteria: a threshold center bow load and the change rate of the load. Additionally, French et al. (2015) identify slamming event using the presence of peak value in full-scale experiment data. On the other hand, Ogawa et al. (2012) investigated the effect of the whipping on the fatigue damage and the probability of whipping occurrence using full-scale measurements, while Toyoda et al. (2012) studied the effect of the difference of sea state on the occurrence probability of stress on the hull due to whipping using long term prediction and

hindcast data. An investigation into different approaches to identify slamming events using full-scale measurements in a high-speed craft was presented in Magoga et al. (2014). The characteristics of the slamming event were used to assess the importance of structural integrity assessment.

As French et al. (2015) reported, a slamming criterion was not necessary due to the large spike load found in the full-scale experimental data in the event of water impact, and only a peak detection method was required to identify peak pressure and thus slamming events. Therefore, slamming identification can be used to establish a practical approach to account for slamming loads in ship structural assessment.

Despite the great number of researches on the slamming load, currently, there is limited knowledge and data on the influence of occurrence frequency and loads with respect to sea conditions and speed in a systematic investigation. Therefore, analytical investigation on the slamming occurrences and severity may provide insight to designers and operators with valuable information and provide a basis for considering possible mitigation strategies.

1.1.3 Fatigue assessment of ship structures

Ship structural members are often found to have failed under the action of repeated or fluctuating stresses called fatigue failure. The actual maximum repeated stresses are well below the ultimate strength of the material and quite frequently evens below the yield strength. Generally, fatigue failures begin with a small crack, often developed at high-stress gradient area. To evaluate the cumulative damage in the design stage, the distribution of the stress rages and the total number of stress cycles N are usually used. A number of studies were performed by the International Association of Classification Societies (IACS) members in order to develop a unified requirement for fatigue design loads, but no conclusion has been made in this regard. Thus, the IACS (2006), provides the distributions of the stress ranges

usually from empirical functions for different types of ships. The stress cycles should be obtained by an accepted procedure in the American Society for Testing and Materials (ASTM) standard for cycle-counting method. Different procedures for cycle counting can be found in the literature ASTM (1985), for example, level-crossing counting, peak counting, simple-range counting, rainflow counting and their respective methods in each class. Although the rainflow counting method is not based on an exact physical concept to account for fatigue damage accumulation, it may well be expected to give a more realistic representation of the severity of load-time histories. Therefore, the rainflow cycle counting method proposed by Matsuishi et al. (1968) is the most widely accepted method in the engineering field for fatigue life prediction.

Once the stress cycles are obtained, the ship fatigue life assessment can be evaluated. High-cycle fatigue is recognizing as the fatigue failure of the ship structure that usually requires more than 10^4 cycles. For high-cycle fatigue life assessment of welded joints, the material behavior is generally described by the characteristic *S-N* curves approach. The characteristics *S-N* curves, also known as Whöler diagram, are available in different design codes for various structural details in the ship, and offshore structures. The Whöler curve shows a log-linear dependence between the stress cycle range $\Delta\sigma$ and the number of cycles to failure N as shown in Eq. 1.1

$$\log(N) = \alpha - m log(\Delta\sigma) \tag{1.1}$$

where the parameters $\alpha > 0$ and $m \geq 1$ depend on the properties of the material, structural details and the stress ratio R. For fatigue assessment of ship structures, α and m are obtained from fatigue tests and categorized based on the properties of structural details.

For the shipbuilding industry, *S-N* curves are widely used with a single slope and two slopes depending on the application. For low-stress amplitudes, the *S-N* curve exhibited a lower limit which implies that fatigue failures did not occur after high numbers of load cycles. This is called the fatigue limit. The fatigue limit is of practical interest for many structures which are subjected to millions of load cycles in service while fatigue failures are unacceptable. The design *S-N* curves are based on the mean-minus-two-standard-deviation curves for relevant experimental data. Thus associated with a 97.6% probability of survival. Some classification societies use 90%. Classification societies provide the material constants for the *S-N* curves depending on material and weld type, type of loading, geometrical configuration and/or environmental conditions (air or sea water). Examples of the *S-N* curves provided by the classification societies are shown in Fig. 1.2. These figures *S-N* curves used in the DNV-GL (2015) and BV (2016), where the magnitude of a stress range ($\Delta\sigma$) is plotted against the logarithmic scale of cycles to failure (N).

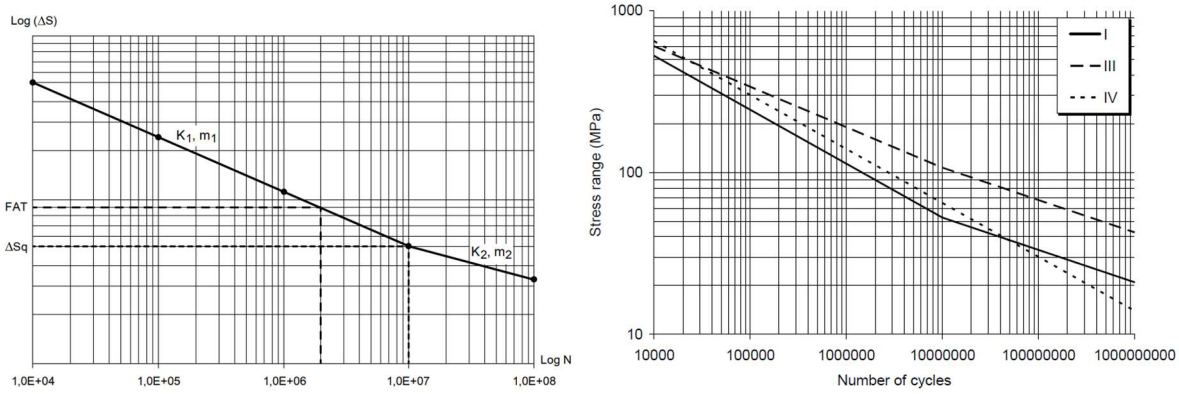

(a) BV (2016) **(b)** DNV-GL (2015)

Fig. 1.2 *S-N* curves of different structural details provided from various class rules.

When the cycle load level varies during the fatigue process, a cumulative damage model is often hypothesized. Fatigue damage accumulated during each stress cycle can be calculated through the *S-N* curve. Thus, in the evaluation of the total accumulated fatigue damage, a cumulative damage hypothesis is assumed.

Palmgren (1924) and Miner (1945) published the hypothesis which is now generally known as the Palmgren-Miner rule or the linear cumulative damage hypothesis. According to Palmgren (1924) applying n_i times a cycle corresponding to the ith block of constant stress amplitude $\boldsymbol{\sigma}_{a,i}$ in a sequence of a blocks and a corresponding fatigue life N_i is equivalent to consuming a portion of n_i/N_i of the fatigue life. Failure occurs when one-hundred percent of the fatigue life is consumed. Then, Miner (1945) introduced the idea that fatigue damage is the consequence of work absorbed by the material which was assumed to be proportional to the number of cycles. If the damage parameter is denoted by D, Eq. 1.2 shows the linear cumulative damage rule that states that failure would occur when:

$$D = \sum_{i=1}^{a} \frac{n_i}{N_i} = 1 \tag{1.2}$$

Moreover, although that the mean level of the imposed fatigue cycle is known to play an important role in influencing the fatigue behaviors of engineering materials, in this thesis this effect has not been considered for the fatigue analysis on ship structures. However, early studies can be found on the effect of the mean stress effects on fatigue life (Gerber 1874; Goodman 1899; Soderberg 1939; Smith 1942; Morrow 1968; Dowling 2004, among others).

1.1.4 Fatigue testing of ship welded joints

The assessment of the service durability of components and structures has become more important in maritime technology, with regards to the increasing trend toward light-weight constructions and greater demands concerning costs, product safety and reliability. In order to fulfill these demands, numerical and experimental methods must be applied for effective development and proof of designs. Material testing standards assist our understanding of how materials behave under fatigue

loading situations and provide the basis for improvements in designs. Fatigue loading in structural components is variable amplitude and not constant amplitude. However, extensive majority of the material testing is conducted at constant amplitude and all of the current testing standards on fatigue methodology deal only with constant amplitude loading (for example American Society for Testing and Materials – ASTM, Association Francaise de Noemalisation – AFNOR, British Standards Institution – Bsi, Institut fur Normung – DIN, European Committee for Iron and Steel Standardization – ECISS, and International Organization for Standardization – ISO) (Hopkins et al., 2005). Nonetheless, to understand correctly variable amplitude fatigue effects, constant amplitude fatigue behavior must first be understood.

In the ship design, higher frequent stresses due to vibrations induced by wave impact, called whipping, are typically not considered in design according to previous longitudinal strength assessment procedures (IACS 1978). However, the examination on a large ore carrier shows that the wave-induced vibration shares between 41-73% of the total fatigue damage (Storhaug et al. 2006). After that, similar results were reported on a large container ship (Storhaug et al., 2007) and an LNG carrier (Heggelund et al., 2010).

Therefore, recently, in order to have a better understanding of the high-frequency stress effects on the fatigue strength of ship welded joints, various researches have been conducted (Yamada 2006; Sumi et al. 2012; Kitamura et al. 2012; Gotoh et al. 2012; Fricke et al. 2012, 2014; Kahl et al. 2015; Osawa et al. 2013, 2015a, 2015b). To investigate the behavior of the crack propagation under variable amplitude loading containing different frequency components, studies compared the classic *S-N* approach with the re-tensile plastic zone generating (RPG) load criterion that can emulate load sequence effect on the fatigue life (see Sumi et al. 2012; Kitamura et

al. 2012). They stated that the higher frequency component with smaller amplitude superimposed on the first-order wave has no significant effect, but only the enlargement effect of the total amplitudes is effective. A similar finding was reported by Gotoh et al. (2012) that performed fatigue tests with stress containing superimposed stresses and noted that the RPG load criterion based on fracture mechanics was superior in considering load sequence effects on the fatigue life compared to that evaluated by the traditional *S-N* approach.

Another approach can be found in the literature in which fatigue tests were carried out using simplified stress histories with superimposed stress cycles with different frequencies in order to simulate the low-frequent wave loading and higher frequent whipping stresses (see Fricke et al. 2012, 2014; Kahl et al. 2015). The principal outcome was that almost the whole fatigue damage is caused by the low-frequent stress cycles enlarged by whipping, whereas the additional small whipping cycles can be neglected. Also, the commonly accepted approach using rainflow counting and Palmgren-Miner rule is appropriate to evaluate the fatigue assessment for ship-typical stress histories considering the low-frequent stress cycles enlarged by whipping.

Osawa et al. (2013) proposed to perform fatigue tests with a special fatigue testing machine using motors with eccentric mass which emulate the high frequency superimposed wave loading effect on out-of-plane gusset welded joints. The results confirmed that for both springing and whipping superimposed loading tests, the fatigue lives can be estimated with acceptable accuracy by using the rainflow counting method. The results show that the enlargement effect of the total stress range has a dominant influence on fatigue strength under the conditions chosen.

Moreover, Sumi et al. (2014) and Osawa et al. (2015a) stated that further researches are still needed for the occurrence probability of vibratory responses, such

as whipping, to improve the fatigue strength assessment of marine structures. Also, examine fatigue testing that emulates the intermittent occurrence is needed.

1.2 Problem Statement

Since the first publications on the wave-induced vibrations, valuable investigations in the numerical simulations, scaled tests, and in-service full-scale measurements have been made. As a ship is getting longer, it is more easily exposed to wave-induced vibrations due to its low natural frequency. The underestimation of the fatigue load can lead to frequent maintenance, contributing to the decrease of the profit for the ship owners and questioning the reputation of the operators. The influence of wave-induced vibrations on the structural strength highly depends on types, sizes, and operational conditions of ships. It is well known that whipping is not constant in real ships. The occurrence of whipping greatly depends on an operational condition. A voluntary speed reduction can minimize an occurrence of slamming by a reduction of relative vertical motion of the bow flare.

The existing numerical methods considering ship responses in waves have been validated against experimental data, compared with other computational programs and applied on different designs, but still, there are no consents for a methodology that can reliably predict the whipping and springing response for a general design. Further, various studies have proposed techniques to consider the occurrence probability for slamming induced vibrations. However, it is unclear the effect of the vessel operation, such as voluntary and involuntary speed reduction or course change. Hence, some uncertainties exist regarding the real fatigue damage under typical stress histories containing wave loads and wave-induced vibrations. On the other hand, practical procedures are needed for the design of ship structures, and

fatigue testing provides a valuable understanding of how the material behaves under wave loads and wave-induced vibrations.

Many researchers reported the increase in the fatigue damage evaluated by RainFlow Cycle Counting (RFCC) taking account of whipping, but the validity of RFCC for those stress waveforms has not been fully verified yet. The characteristics of whipping vibration can be simulated by Non-Linear Hydro-Elasticity Analyses (NLHEA). The validity of RFCC should be examined by carrying out fatigue tests with stress histories which emulate the characteristics of the simulated whipping vibration. However, most of the investigations have focused on simplified testing conditions due to the limitation in the conventional hydraulic-type fatigue testing machines leading to unrealistic stress histories to emulate the occurrence of whipping. For these tests, it is needed to develop a fatigue testing apparatus which can apply whipping superimposed stress waveform in high speed and low cost.

The objective of this thesis is to presents a fatigue assessment method for ship structures considering the stochastic characteristics of the whipping vibration. This research focus on the clarification of the characteristics of whipping waveform; the development of a fatigue testing system for whipping superimposed loadings; and the verification of RFCC for those cases.

1.3 Framework of the Thesis

The background and motivation were covered in this chapter. The present thesis is structured as follows:

Chapter 1 briefly gives a background on the fatigue assessment of ship structures, uncertainties in fatigue life prediction, the actual procedures for fatigue testing of ship's welded joints and their challenges. A review of literature on the

whipping vibration and the wave environmental description is also conducted. The challenges, objective and structure of this thesis are also addressed.

Chapter 2 describes preliminary methodologies and theories of RFCC, NLHEA, weather routing, and storm wave load modeling. These are the basic background of the works in this doctoral thesis.

Chapter 3 presents a description of the main assumptions and calculation conditions for a series of NLHEA.

Chapter 4 shows a detail description of the proposed methodology for slamming and whipping prediction. As results, the characteristics of whipping waveform experienced by the target ship, which follows weather routing, can be simplified as a) the slamming impact occurs once in every 4 to 5 primary wave (PW) cycles; b) the maximum stress range due to slamming impact can be comparable to the PW stress range; c) the whipping superimposed waveform show approximately similar waveform regardless of significant wave height. Based on these results, the 'reference whipping superimposed waveform' has been proposed.

Chapter 5 provides detail information about fatigue testing experiments. An electric exciter (EE)-driven plate bending vibration (PBV) fatigue testing machine, which can apply various whipping loads is newly developed. The developed machine can apply the 'reference waveform' to out-of-gusset welded joint specimens with good linearity between load and strain at high speed. It is found that the fatigue life of welded joints subject to constantly and intermittently whipping superimposed loadings can be predicted with fair accuracy by RFCC. It is also shown that RFCC leads to conservative estimates, and it is likely that the fatigue damage up to the failure of intermittently superimposed cases is larger than that of constantly superimposed cases under conditions chosen.

Chapter 6 summarizes the contributions and major findings of the study. Suggestions for future work are also given.

Finally, the publications submitted during the doctoral course are listed.

Chapter 2 Basic Theoretical Background and Models

This chapter briefly describes some preliminary methodologies and theories, as the basis of the work in this thesis. First, the generals of the rainflow cycle counting method (RFCC) for fatigue analysis on ship structures is given. Then, the fatigue damage accumulation approach is explained. Section 2.3 describes the numerical computation of the hydrodynamic loads on ships. After that, the heavy weather avoidance concept is introduced. The last subsection briefly introduces the established statistical storm wave model partially considered in this thesis.

2.1 RainFlow Cycle Counting Method - RFCC

The mechanical stress cycles cause fatigue in materials. These stresses may result from vibration, shock, or thermal gradients within the material. Usually, fatigue life models (Basquin's law, Engelmaier's model, Coffin-Manson) require the information about the load cycles, for example, amplitude and the cyclic mean of the load cycle. This will lead to the assumption that the load conditions are constant. However, structures experience complex load patterns that can be parameterized in a single cyclic mean and amplitude. The transformation of complex load histories to a set of simple stress reversals can be achieved through "cycle counting".

The rainflow cycle counting method, also known as the pagoda-roof method, originally proposed by Matsuishi et al. (1968) is widely recognized and standardized with various other counting algorithms as found in the literature (ASTM 1985). Matsuishi et al. (1968) developed this counting method by relating the stress reversal cycles to streams of rainwater flowing down a Pagoda. Assume that a stress time history is composed of a sequence of peaks and troughs. Then,

- The time history is turned clockwise 90°, and the time axis in vertically downwards with the lines connecting the peaks are imagined to be a series of pagoda roofs (see Fig. 2.1). Rain is injected at each point of stress reversal in order and flows by gravity subject to the following rules:
- For rain moving toward the left and down, the flow disappears if it comes opposite to a reversal point farther to the right than, or equal to, the one from which it started.
- For rain moving toward the right and down, the flow disappears if it comes opposite to a reversal point farther to the left than, or equal to, the one from which it started.
- The flow disappears to avoid meeting rain from a roof above. The rainflow finish when reaches the end of the time history.

Figure 2.1 shows an example of the rainflow cycle counting method. The rainflow starts from A (trough), B (peak), C (trough), and so on, respectively. The first rainflow, starting from A, drops down at B and stops, because the following trough C is more negative than A. Thus, the segment A-B is identified as a half cycle. The next rainflow starting at B stops at C since the next cycle D is more positive than B. Then, B-C is counted as another half-cycle. For the example in Fig. 2.1 a total of 6 half-cycles are shown. The six half-cycles are A-B, B-C, C-D, D-G, G-H, and H-I. Additionally, the only full cycle is path E-F.

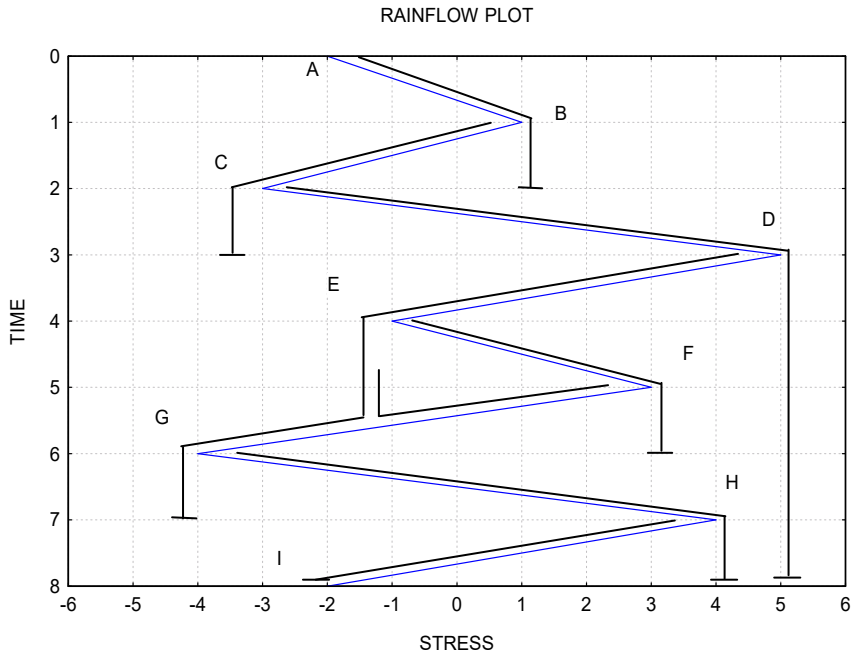

Fig. 2.1 Rainflow cycle counting method.

2.2 Fatigue Damage Accumulation Approach

In this study, a linear cumulative damage hypothesis is assumed. The fatigue damage accumulation is given by the Palmgren-Miner law, which defines the damage produced on a generic material as the fraction of spent life (in terms of energy) for the particular load level as presented in section 1.1.3. The relationship between $\Delta\sigma$ and N is approximated by the Basquin's law given in the following form as,

$$\Delta\sigma = \begin{cases} CN^{-m};\ \Delta\sigma \leq C \cdot (10^7)^m \\ C'N^{-m'};\ \Delta\sigma > C' \cdot (10^7)^{m'} \end{cases} \tag{2.1}$$

with parameters given in Table 1. N: predicted number of cycles to failure for stress range $\Delta\sigma$, $\Delta\sigma$: stress range, m: the negative inverse slope of the S-N curve.

Table 2.1 Properties of *S-N* employed in this research.

S-N Curve	$N \leq 10^7$		$N > 10^7$	
	C (MPa)	*m*	*C'* (MPa)	*m'*
	1.1494e+04	-3.3333e-01	1.3405e+03	-0.2000e-01

2.3 Analysis of Hydrodynamic Loads

The prediction of wave-induced motions and loads is of vital importance for the design of marine structures. Recently, focusing on the seakeeping problem, ship motions and loads analysis, theoretically, can be evaluated using a wide variety of techniques ranging from two-dimensional (2D) strip theory, three-dimensional (3D) panel theory to extremely complex fully nonlinear unsteady Reynolds Averaged Navier Stokes (RANS) computations (Hirdaris et al. 2014). Although that the computational fluid dynamics (CFD) tool, which is on the bases of solving RANS equations has been incorporated into the methodology of hydroelasticity, the immensity of time cost still makes it stay at an early stage and far from most practical engineering applications (Jiao et al. 2019). Therefore, the potential flow theory constitutes an invaluable tool in the prediction of ships hydroelastic responses.

In this research, the structural responses are evaluated by a direct motion-load simulation system shell stress oriented dynamic analysis code (SSODAC) originally proposed by Iijima et al. (2008). The methodology has been validated by conducting a tank test with a hydroelastically scaled model (Iijima et al. 2009). Further, the validity has been confirmed comparing with other numerical simulation codes (Fukasawa et al. 2011; Takami et al. 2017). Moreover, this numerical code can take into account the wave-induced vibrations and it has been used to examine the effect of the wave-induced vibrations on the fatigue damage for various applications including ships and offshore structures (Iijima 2011; Iijima et al. 2011).

Generally, rigid body motions of ships can be represented by Euler's equation. Rigid body motions of ships including translational and rotational motions can be expressed by references to its center of gravity as presented in Eq. 2.2.

$$\boldsymbol{M}\ddot{\mathbf{a}} = \boldsymbol{F}(\boldsymbol{a},\dot{\mathbf{a}},\ddot{\mathbf{a}},t) \tag{2.2}$$

where **M** is a mass matrix, **a** is a displacement vector, and **F** is a force vector. This equation may be extended to describe the motion of flexible modes by applying the modal method. Then, the vector represents a generalized coordinate vector consisting of the coordinates of rigid body motions and flexible modes. Nonlinear load properties can be accounted for by integrating the pressure up to the instantaneous surface of waves. A frequency-domain three-dimensional (3D) panel method based on linear potential theory is employed to evaluate the pressure field (Iijima et al. 2008). For adopting the potential theory, such assumptions as inviscid, incompressible, and irrotational fluid have been made. The fluctuating potential around the ship must satisfy the Laplace equation and boundary conditions. The boundary conditions are a kinematic and kinetic condition at the free surface, radiation condition at infinity, sea bottom condition, and hull surface condition. Then, a simplification is made on the condition with a forward speed by introducing the so-called encounter frequency correction (Papanikolaou et al. 1992). Then, the boundary condition on the free surface becomes identical to the free surface condition with zero forward speed and encounter frequency ω_e. In this manner, Green function with zero speed is extended to forward speed case. Once the potential around the ship is obtained, the hydrodynamic pressure is given in by using Bernoulli's theory. The impact loads are also evaluated and accounted for in the present calculations. They are evaluated on 2D strips and integrated by using a classical von Karman's momentum theory (The von Karman 1929).

The motions and structural deformation are evaluated by using the modal superposition. In this research, the vertical bending moment is evaluated by using the modal superposition, and the stress is obtained by dividing by the sectional modulus. It is expected that the stress value converges even when we consider the first few modes of deformation if we refer to the stress at deck side where the effect of local pressure distribution is negligible.

2.4 Heavy Weather Avoidance

Maritime trades are highly dependent on the environmental conditions experienced by the vessel in her sailing. The great-circle route (GCR) is known as the minimum distance route between two points measured on the surface of a sphere. When planning, usually it is assumed that the ship navigates without course change, but the ship speed is reduced according to the ship speed performance curve. However, several factors affect this assumption and the operational performance of the ship during sailing, e.g. meteorological conditions (waves, wind, current), vessel traffic, ship performance, ship response, the experience of the shipmaster, among others. Therefore, weather routing plays an important role in various transportation systems (Soares et al. 2015). Ship weather routing may be defined as the development of an optimum sea-route planning of ocean voyages based on forecast of weather, ship's individual characteristics and sea conditions for a demanding sailing route (Mao et al. 2009; Sen et al. 2015; Simonsen et al. 2015; Vettor et al. 2016). The principal benefits of the ship weather routing systems are primarily in time and cost reductions while increasing safety and crew comfort. Other factors are considered such as the minimum greenhouse gas emissions, risk, etc. The savings in operating costs are derived from reductions in-transit time, fuel consumption, cargo

and hull damage, heavy weather encounters, and more efficient scheduling of maintenance activities.

Ship and cargo characteristics have a significant influence on the application of ship weather routing. Ship size, speed capability, and type of cargo are an important consideration in the route selection process prior to sailing and the surveillance procedure while underway. Furthermore, environmental factors of importance to ship weather routing are elements of the atmosphere and ocean that may produce a change in the status of a ship transit. In ship routing, consideration is given to wind, seas, ice, ocean current and fog. Although all of the environmental factors are important for route selection and surveillance, in optimum routing is normally considered if the effects of wind and seas can be optimized. In weather routing, three methods are mainly considered in the development of numerical tools: the isochrones method (James 1957; Hagiwara 1989; Tamaru et al. 1999; Szlapczynska et al. 2007), dynamic programming (Lundgren et al. 2010; Shao et al. 2012) and calculus of variations (Haltiner et al. 1962; Perakis et al. 1989). An isochrone is defined as a line on a map or diagram connecting places from which it takes the same time to travel.

In this research, a weather routing algorithm based on analyzing the isochrones, called minimum time route (MTR), is considered based on Tamaru (2016). The isochrone methods can be summarized as follows:

- Isochrones are constructed with a given time limit from the departure point. The isochrones have different physical length, in nautical miles, due to the variance in resistance for the different ship headings.
- The engine power is assumed constant and the velocity will vary with resistance.

- New isochrones are again constructed at the endpoints for the previous isochrones.
- The isochrones are constructed in the same manner until the destination is reached.
- When the first isochrone meets the destination point, the optimal route has been found.

The MTR method is optimized by a spatiotemporal distribution of sea states to decide the minimum time between two destinations. An example of the isochrones construction is presented in Fig. 2.2. The relationship between ship speed loss, significant wave height, and the relative heading angle are considered in the model, and the spatiotemporal sea state data was generated from Japan Weather Association (JWA) hindcast data.

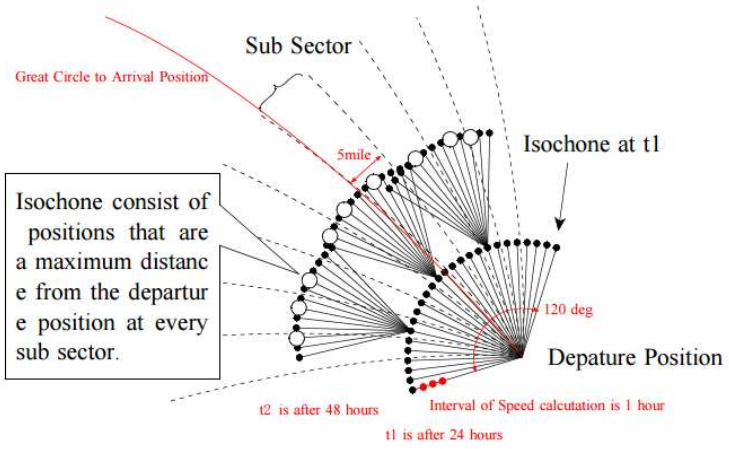

Fig. 2.2 Construction of isochrones according to Tamaru (2016).

2.5 Statistical Storm Wave Load Model

The wave environment description aims to determine the environmental conditions in which a ship or offshore structure may experience during its service

life based on past observations. Short-sea sequence and its modeling have been the focus of extensive researches due to the importance of the fatigue assessment and extreme analysis of ship structures. Ocean waves are described as a sequence of sea states (stationary periods). Then, for each sea state, the wave elevation is described as a random process. Generally, the short-sea state is characterized by the significant wave height *Hs* and the mean zero-up cross period *Ts* and is assumed their duration from 30 minutes to various hours. Classification societies provide the environmental information in the form of wave scatter (*Hs,Ts*) diagram and fitter distribution of seas states (for example DNV-GL 2014). The wave scatters reflect the long-term distribution of waves encountered by all ships sailing at these specific areas. However, it has been reported that due to the increasing use of systems to help the ship navigation, e.g. weather routing systems, the vessel can avoid harsh wave conditions without difficulties by optimizing the sailing path. Therefore, the effect of weather routing can be significant and the assumed wave conditions can differ from the wave environment encountered by the ships (Olsen et al. 2005; Mao 2010a; Mao et al. 2013).

Furthermore, to provide more realistic wave information for ship design and operation various statistical wave models have been developed to model wave environments along arbitrary shipping routes (for example Tomita et al. 1995; Baxevani et al. 2009; Minoura et al. 2004, 2006) based on a large database of wave environment records from various wave data sources, i.e., buoy data, onboard observations, satellite measurements, and hindcast data, etc. These wave models can be used to generate wave conditions encountered along a ship's actual sailing routes. Then, that generated wave information can be useful for ship fatigue design and extreme loading predictions.

For the safe and reliable assessment of the fatigue life of ship, the first-generation storm model (1G-storm model) was proposed by Tomita et al. (1995) to emulate real random significant wave height time histories and examine fatigue crack growth behavior under random loading, based on collected wave data of ships that sailed on the Pacific Ocean. The model presumes that the wave oceanography phenomena is possible to divide mainly into two conditions: calm sea and storm conditions as in Fig. 2.3. Furthermore, sailing in calm sea condition the encountered sea state history can be modeled as a time-independent random process, and in the storm condition the significant wave height increase over time and reaches a maximum value at one point only before decreasing gradually. Thus, encountered significant wave height in a storm condition is a time-dependent process. These two conditions appear alternately in random order as in Fig. 2.3. Kawabe (2002) proposed a modified version of the 1G-storm model. This model considered the correlation between *Hs* and *Ts* by using the joint probability of *Hs* and *Ts*, also known as wave scatter diagram. Both of Tomita and Kawabe model is derived from a single wave scatter diagram by using a trial and error manner. Further, the 3G-storm model that applies automatic storm configuration, consider the fluctuation of storm duration on the short-sea history and generate equivalent sea state history from the data with various observation period was proposed by Prasetyo et al. (2012).

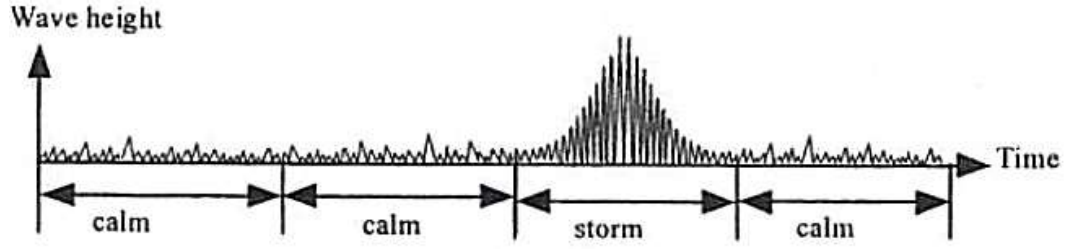

Fig. 2.3 Idealized encountering wave condition (Tomita et al. 1995).

Let Hs_{avg} be the H_s for the whole ship life average, Hs_{ext} is the maximum *Hs* that occurs once in the whole ship's lifetime, and $Hs_{max}^{(i)}$ is the maximum *Hs* in *i*-th storm class $S^{(i)}$. Thus, the storm is classified based on $Hs_{max}^{(i)}$ and its range between Hs_{ext}

to Hs_{avg}. First, the generation of *Hs* time history needs a "storm profile" configuration. Details can be found in Prasetyo (2013). The storm profile is the sea state information consisting of the significant wave height sequence and the occurrence probability of storms with various maximum wave heights. The storm profile is configured based on assumptions such as the ship's target design life is 25 years, the duration of the storm is varied with 3.998 days' average and 1.822 days' deviation, and is composed by:

- the probability density of the storm, $P_{storm,}$ and calm sea, P_{calm};
- the probability density of the H_s in a calm sea, $P_{calm}(Hs)$;
- the probability density of the *i*-th storm class $S^{(i)}$, $P_{storm}{}^{(i)}$;
- the H_s profile for each storm class $n(Hs)^i$.

The long-term distribution of *Hs* is assumed to follow the Weibull distribution and joint probability distribution of *Hs* and *Ts* is refitted by obeying the conditional of the lognormal distribution of *Ts* given *Hs* (Wan et al. 1995). Thus, the parameters of the Weibull distribution (shape parameter X_{wb}; scale parameter m_{wb}) are identified from wave measurement along the ship routes. The *Hs* profile in a storm $n(Hs)^i$ is determined based on the assumption that this profile is distributed by the following the tail of the Weibull distribution and $n(H_s, H_{s\_max}{}^{(i)})$ is unity:

$$n\left(H_{s,j}\right)^i = n\left(H_{s,j}\right)^{i,0} + n_{add}\left(H_{s,j}\right)^i \tag{2.3}$$

$$n_{add}\left(H_{s,j}\right)^i = \left(\frac{H_{s,j}^{m_{wb}-0.65}}{x_{wb}}\right) * \Delta_{ss} * e^{-\left[\frac{H_{s,j}^{m_{wb}-0.65}}{x_{wb}}\right]} \tag{2.4}$$

where, $n(H_{s,j})^{i,0}$ is the initial $n(H_s)^i$, Δ_{ss} is the difference between total initial $n(H_s)^i$ with that of the number of short sea in a 3.5 days storm. Based on long term H_s distribution $n(H_s)$ and $n(H_s)^i$, the *i*-th storm class density, $N(i)$, is determined by

satisfying the condition that: (a) $N^{(i)} \leq N^{(i+1)}$, (b) all H_s distributions with $H_s > H_{s\_avg}$ are completely used. Since the severest storm class $S^{(1)}$, $N^{(1)}$ is unity, and existing long term H_s distribution after used with $S^{(1)}$ $n(H_s)^{1'}$ are $n(H_s)$ - $N^{(1)} \times n(H_s;\ H_s = H_{s\_max}^{(i)} \sim \ldots)^i$. The density for the 2nd severe storm class $S^{(2)}$, $N^{(2)}$ is $n(H_s;\ H_s = H_{s\_max}^{(2)})^{1'}$. By repeating this procedure, the following storm classes (i=3,4,...) can be determined.

The *Hs* history in position *p* and at time *t*, *Hs*(*p*,*t*), is modeled by using the storm profile configuration as described above. The position *p* and the time *t* are related to the existing wave data point (herein called "point") and season. For the chosen point and season, random *Hs* is generated as follows:

- Decide between the calm and storm sea condition by random number selection, considering the occurrence probability of storm seas and calm seas, P_{calm} and P_{storm}.
- For a calm sea condition, a random sequence of *Hs* is generated by obeying $P_{calm}(Hs)$.
- For a storm sea condition, decide the storm class by random number selection. The variation of the duration of the storm, d_{var}, is chosen so it fits the single Normal distribution. For the storm class $S^{(i)}$, generate a crescendo-decrescendo sequence of *Hs* as presented in Table 2.2.

Table 2.2 Significant wave height waveform in the *i*-th storm class.

j	Hs	Num. of repeat	
		*	**
j_{end}	$H_{S,ext}$–i–j_{end}+1	0.5 $N_{jend,i}$	Int(0.5 $N_{jend,i}$)
j_{end}-1	$H_{S,ext}$–i–j_{end}	0.5 $N_{jend-1,i}$	Int(0.5 $N_{jend-1,i}$)
⋮	⋮	⋮	⋮
2	$H_{S,ext}$–i–1	0.5 $N_{2,i}$	Int(0.5 $N_{2,i}$)
1	$H_{S,ext}$–i	$N_{1,i}$=1	$N_{1,i}$=1
2	$H_{S,ext}$–i–1	0.5 $N_{2,i}$	$N_{2,i}$–Int(0.5 $N_{2,i}$)
⋮	⋮	⋮	⋮
j_{end}-1	$H_{S,ext}$–i–j_{end}	0.5 $N_{jend-1,i}$	$N_{jend-1,i}$ –Int(0.5 $N_{jend-1,i}$)
j_{end}	$H_{S,ext}$–i–j_{end}+1	0.5 $N_{jend,i}$	$N_{jend,i}$–Int(0.5 $N_{jend,i}$)

*. For $N_{j,i}$ is the even-number case. **. For $N_{j,i}$ is the odd-number case.

- Once *Hs* is determined, the mean period *Ts* is determined by random number selection using the conditional probability of *Ts* given *Hs* proposed in Wan et al. (1995), as presented in Eq. (2.5):

$$p(T_S|H_S) = \exp\left(-\frac{(ln(T_S)-\mu)^2}{2\sigma^2}\right)\alpha(T_S,H_S) \tag{2.5}$$

$$\alpha(T_S,H_S) = \frac{1}{\sqrt{2\pi}T_S\sigma}, \quad \mu = E[\ln(T_S)\,|H_S], \quad \sigma^2 = var(\ln(T_S)\,|H_S)$$

where *p(Ts|Hs)* is the conditional probability density for *Ts* given *Hs*. The joint probability distribution *p(Hs,Ts)* is calculated by Eq. (2.6):

$$p(Hs,Ts) = p(Hs)p(Ts|Hs) \tag{2.6}$$

A sequence of the storm and calm sea conditions are generated by sampling with replacement. Figure 2.4 shows an example of a time history of significant wave height with variable storm duration generated by storm model simulation.

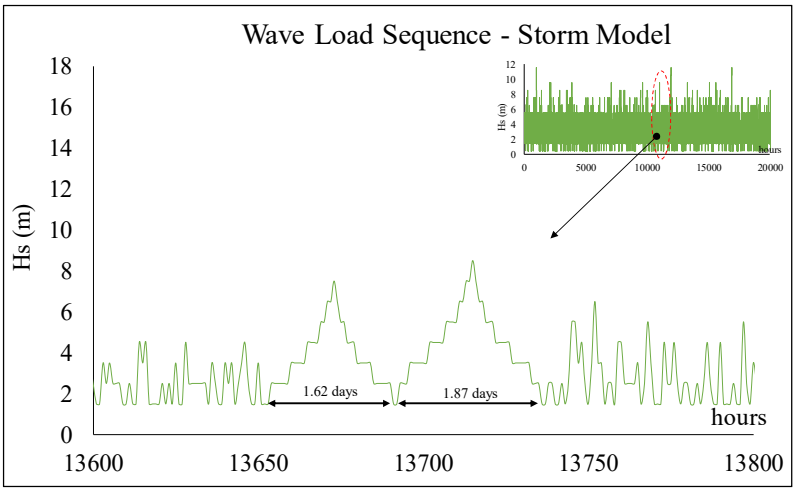

Fig. 2.4 Significant wave height time history with variable storm duration generated by storm model simulation.

Chapter 3 Analysis Conditions

Nowadays the ship routes are motivated by the time of delivery, trade request and fuel consumption. Occasionally, the routes can be modified using weather routing systems due to heavy weather conditions. Generally, in the design stage, the environmental conditions for ships and marine structures are supposed to be continuously operating in the North Atlantic Ocean. However, this conservative assumption can be mitigated by the fact that the crew may modify the route according to the meteorological forecast condition.

A description of the assumptions and calculation conditions for a series of nonlinear hydro-elastic simulations are presented in this chapter. Then, the short sea conditions for the non-linear hydro-elastic analysis (NLHEA) are chosen. Finally, the numerical model and the main particulars of the subject ship for the nonlinear hydro-elastic simulations are introduced. Assumptions concerning the numerical simulations are also presented.

3.1 Oceanographic Data Source

Fatigue is dominated by loads of relatively low amplitude but high frequency of occurrence. Moreover, ship performance (e.g. maneuvering and seakeeping) degrades under various environmental factor, mainly driven by waves (wind, tide, and current conditions) due to hull resistance and undesirable vessel motions. Therefore, it of vital importance a reliable description of the oceanographic conditions that the marine structure will be exposed. The classification society rules provide representative environmental conditions for ship design as standard loads (e.g. DNV-GL 2014). Hence, the relationship between the design loads and sea states actually experienced by ships appear to be poor.

Alternatively, other sources of oceanographic data are available, i.e. buoy, visual observations, instrumental observation, hindcast data, among others. The most well-known onboard observation data in the marine industry is the Global Wave Statistics – GWS (Hogben et al. 1990). Oceanographic data from the buoy, wave radar and satellite are considered as instrumental measurements and are operated by various organizations, i.e. National Oceanic and Atmospheric Administration – NOOA, universities, oil companies, research institutes, space agencies, etc. Weather satellite is widely used to monitor weather and climate of the earth. Some of them are capable to generate radar images ranging from small sea areas to several kilometers.

Recently, hindcast data are available to access to the long-term history of accurate measurements of extreme storm generated winds, waves, currents and storm surge to estimate the probability distribution for design loads on ships or marine structures (Cardone et al. 1976; Ward et al. 1978; ISSC 2012, 2015). The hindcast refers to atmospheric and ocean response models for a historical period (typically several decades-long) in order to develop the specification of climate and extremes for an application. Wave hindcasting is considered adequate for generating a reasonable representation of the waves climate since surface waves are generated by the wind.

The comparison of the different wave data sources is presented in Fig. 3.1. The probability density function (PDF) of the significant wave height, *Hs*, for the North Atlantic is shown. The latitude and longitude ranges for the hindcast data are as follows: 30ºN ~ 60ºN and 80ºW ~ 10ºE. *Hs* data are provided from the Japanese Weather Association (JWA) hindcast, Europe Centre for Medium-Range Weather Forecasts (ECMWF) hindcast, the recommendation No. 34 of the International Association of Classification Societies (IACS) for the North Atlantic, and the recommendation of DNV-GL (2014) for the North Atlantic.

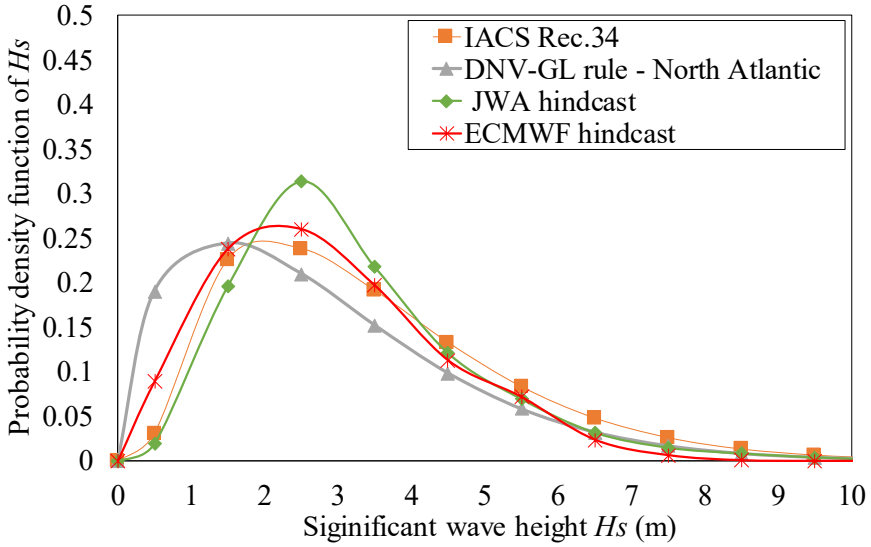

Fig. 3.1 Probability density function of *Hs* from different sources.

In Fig. 3.1 it is shown that the *Hs* probability density function of all sources almost agree with each other for waves larger than 4m. The PDF recommended for the North Atlantic given by the DNV-GL is smaller than that of the JWA and ECMWF hindcast in the low-mid region (0.5 m < *Hs* < 4 m), while JWA shows larger PDF than that of ECMWF. The above comparison shows that the differences between the JWA and ECMWF hindcast are not significant. Therefore, JWA hindcast data[3] is selected as a source wave data, which correspond to the longest environmental data examined in this research.

3.2 Wave Environments

The loads in the ship design process have to be representative of the environmental and operational conditions encountered through the entire life of the ship, ensuring the integrity of the hull structure.

[3] JWA hindcast data is used by permission from the Research Initiative on Ocean-Going Ship (RIOS) Osaka University.

This section is, therefore, structured to present the procedure to select the short sea conditions for the NLHEA based on a statistical storm wave model simulation. First, the working sea area considered is presented. After that, a detail explanation of the differences in the short sea characteristics due to ship operation based on weather routing is given, including the effect of weather routing on fatigue damage. The short sea sequences generated by storm model simulation. Finally, the short sea conditions for the numerical NLHEA are given.

3.2.1 Sailing area

The wave scatters diagrams are recognized as the summarized description of the average wave environment in a specific region. Typically, are presented as the joint probability distribution of *Hs* and *Ts* during the time period they are encompassing. The wave scatter diagrams are assembled for marine routes in the North Atlantic Ocean between Bishop Rock (Lat. 50° N, Long. 5° W) and Boston (Lat. 35° 30’ N, Long. 72° 40’ W) adopting the short sea sequences from Tamaru’s weather routing algorithm (Tamaru 2016). Japan Weather Association (JWA)’s hind-cast data on the North Atlantic Ocean is chosen as the source data (see sec. 3.1). The North Atlantic area is Lat. 30° N ~ 60° N, Long. 80° W ~ 10° E. Hindcast data were calculated from January 2000 to December 2009 with the time interval of 2 hours. The gridpoint interval is 2.5 degrees in latitude and longitude directions. Figure 3.2 shows the JWA hindcast area in the North Atlantic Ocean.

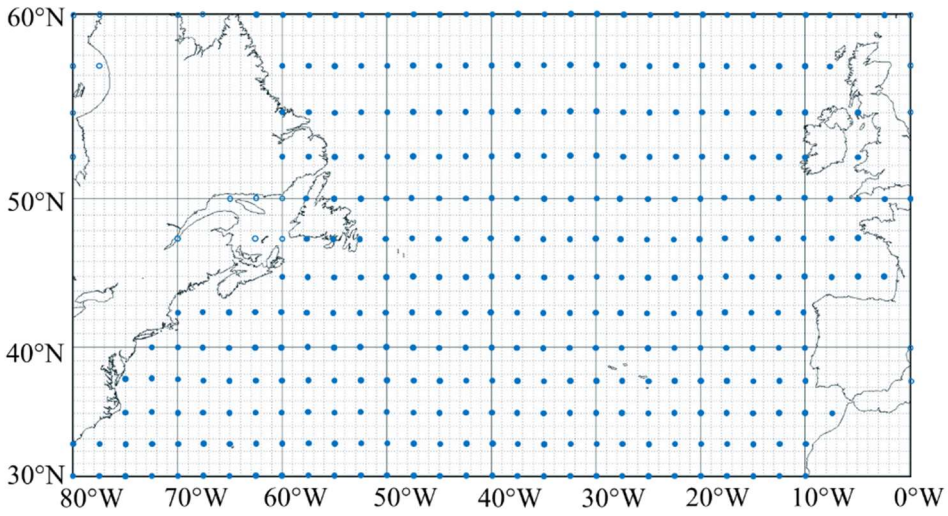

Fig. 3.2 JWA hindcast area in the North Atlantic Ocean.

3.2.2 Marine routes

In order to examine the effect of weather routing on fatigue damage, it is assumed that 10 years of voyage routes are simulated based on the JWA hindcast data. The sea state (significant wave height *Hs*, mean period *Ts* and wave direction θ) sequence experienced by the ship is determined by those at the nearest JWA hindcast data grid point. Figure 3.3 presents examples of the westbound/eastbound minimum time routes – MTRs (black lines) between Europe and the West coast of the United States (US). In addition, the great circle routes – GCRs are presented for the same routes (red lines). The criteria for route selection reflect a balance between the captain's desired levels of safety, speed, comfort, and considerations of operations such as fleet maneuvers, towing, fishing, etc. While sailing the captain evaluate course changes or speed reductions according to his judgment. In Fig. 3.3 it is observed that the eastbound voyages nearly follow the great-circle route compare to that seen in the westbound voyages. In the westbound routes, it is inferred that the larger changes in the ship course around the great-circle route are to avoid heavy weather conditions that could exceed the safety levels. The changes in the forward speed associated with various heading angles sailing in the MTR routes are presented in Fig. 3.4.

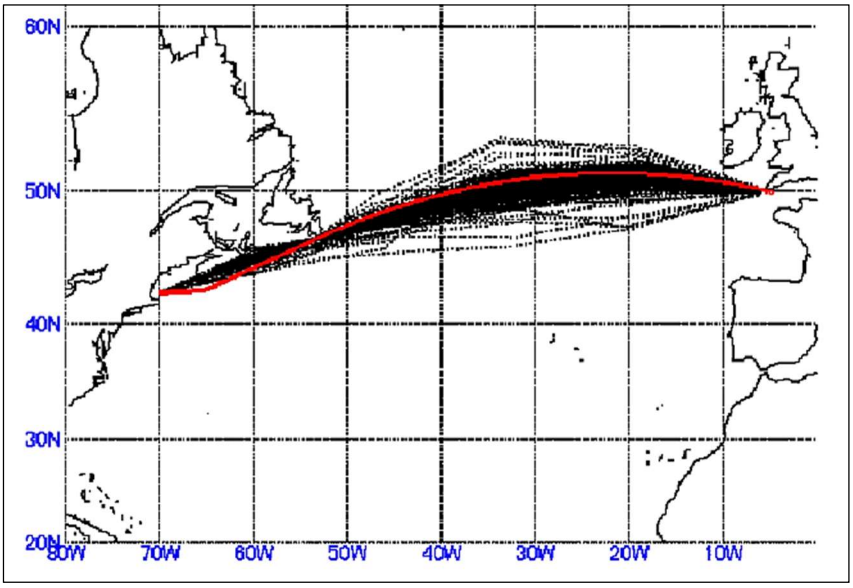

a) Eastbound voyages

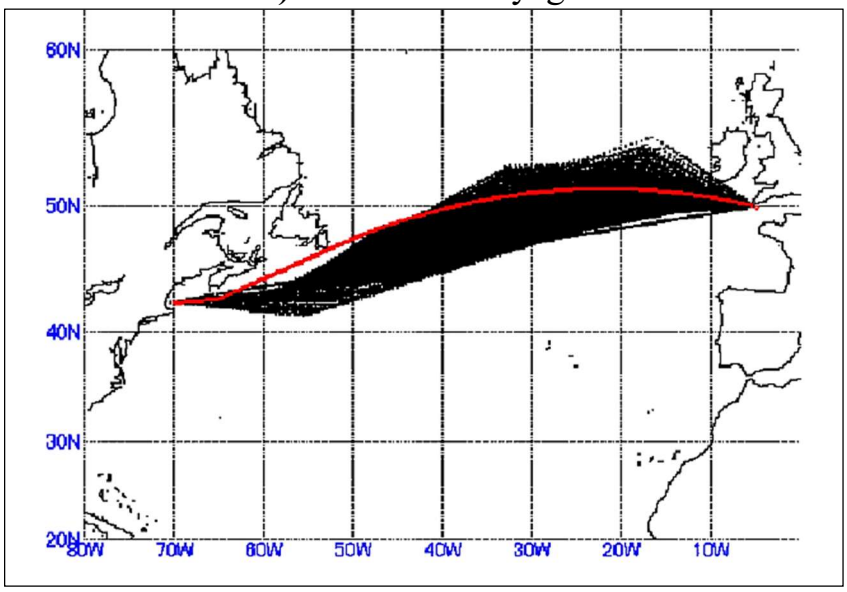

b) Westbound voyages

Fig. 3.3 An example of minimum time routes between the US west coast and Europe. Adapted from Tamaru 2016.

According to Tamaru (2016), Fig. 3.4 represents the average ship performance curve examined from various operational ship data obtained from ship records, interviews with shipmasters, log-books for similar container ship size (6000 TEU). All vessels considered in the examination used weather routing systems to avoid severe sea conditions. The main criteria for speed reduction and/or change of ship

headings according to the shipmaster's judgment were to avoid loss of cargo and crew seasickness. It is observed from Fig. 3.4 that the ship speed progressively decreases while Hs is increasing (involuntary speed reduction, mainly due to added resistance). Then, according to the shipmaster's judgment, based mainly on the frequency of slamming, bow acceleration, propeller racing and/or water on deck, for waves larger than 6 m the operational limit is relevant and the ship speed start to continuously decrease. It is noted that the average performance curve considering operational judgment (Fig. 3.4) is in relatively good agreement with findings reported by Prpić-Oršić et al. (2014), where stated that all shipmasters that participated in the study, according to their judgment, indicated that heavy weather conditions start when significant wave height reaches 6-8 meters. For smaller waves, the involuntary speed reduction due to added resistance in waves and wind determines the reduction in ship speed at full engine power. It is considered that the ship cannot have an effective forward speed sailing with waves over 12 m. Ships found in such extreme conditions are exposed to the high risk of structural damages or losing cargo. Therefore, the captains, as a rule, try to avoid any heavy weather by changing the ship course or waiting for the storm to pass (Prpić-Oršić et al. 2014).

A sample of the changes in the significant wave height of the sea state encountered each hour on each route are shown in Fig. 3.5 and Fig. 3.6. It is observed in Fig. 3.5 that the wave height exceeds 6 m several times in the GCR (Bishop Rock – Florida) voyages compared to that in the MTR for the same period. This is considered because as observed in Fig. 3.3*b* (westbound voyages) the captain tends to divert from a specified course more often compared to that eastbound voyages. In addition, in the US west coast – Bishop Rock voyage shown in Fig. 3.6, the wave height remains below 6m most of the time.

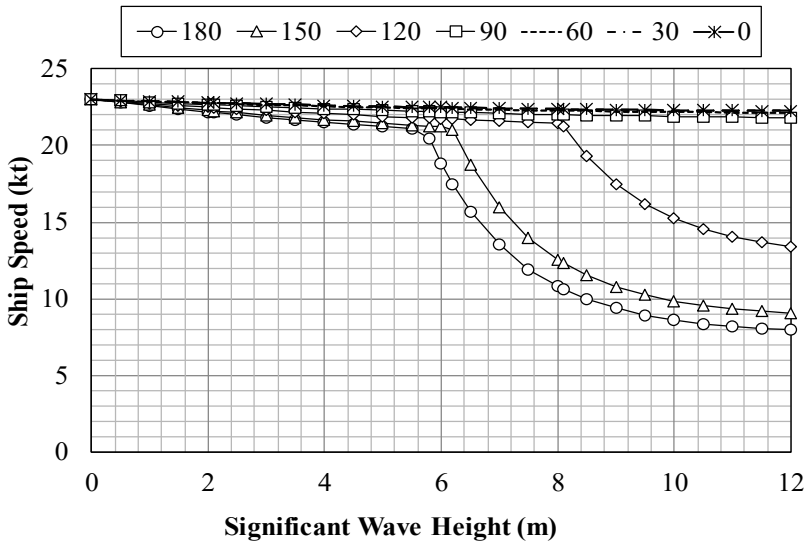

Fig. 3.4 The ship performance curve of the target ship (Tamaru 2016).

Furthermore, the changes in ship speed on each route are presented in Fig. 3.7 and Fig. 3.8. It is assumed that for the GCR, the ship strictly sails following the great-circle route considering the ship performance curve presented in Fig. 3.4. It is understood from Fig. 3.7 and 3.8 that the ship speed decreases greatly at the timing when the wave height rises on the GCR, while the ship speed slightly decreases in the MTR. This is because the ship speed is greatly reduced when encountering a high wave height, but by maneuvering so that the ship speed is partially reduced by changing the relative angle between the ship and the wave from the head waves to the oblique waves. In the MTR, navigation time is shortened because navigation is performed to avoid high wave height and not reducing the ship speed.

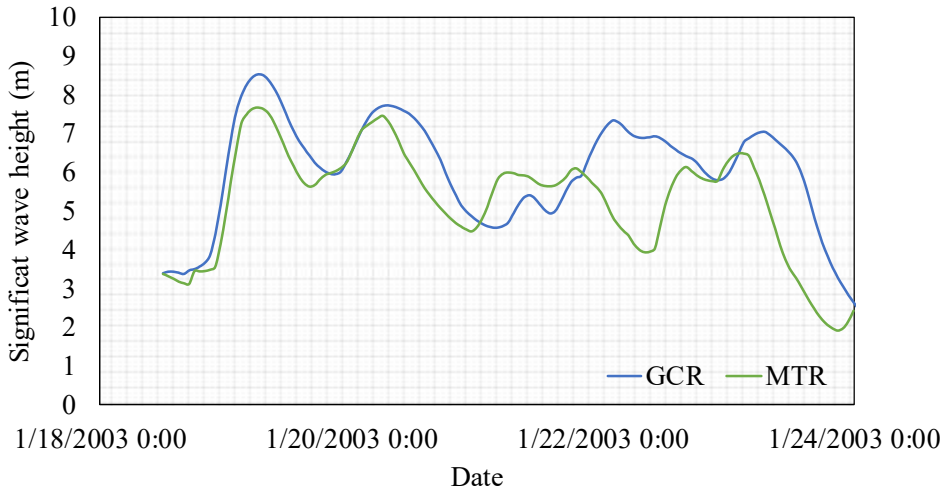

Fig. 3.5 Change in wave height every one hour in a Bishop Rock to Florida voyage (From January 18th, 2003).

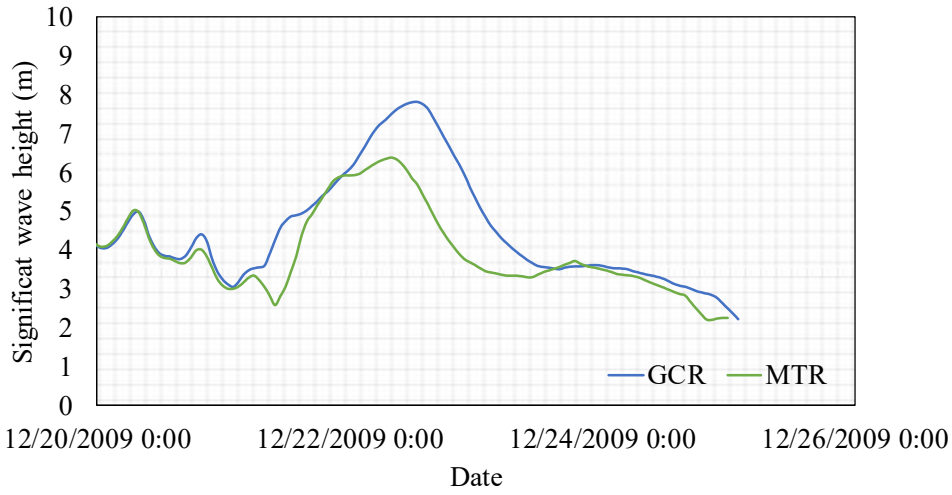

Fig. 3.6 Change in wave height every one hour in a Florida to Bishop Rock voyage (From December 20th, 2009).

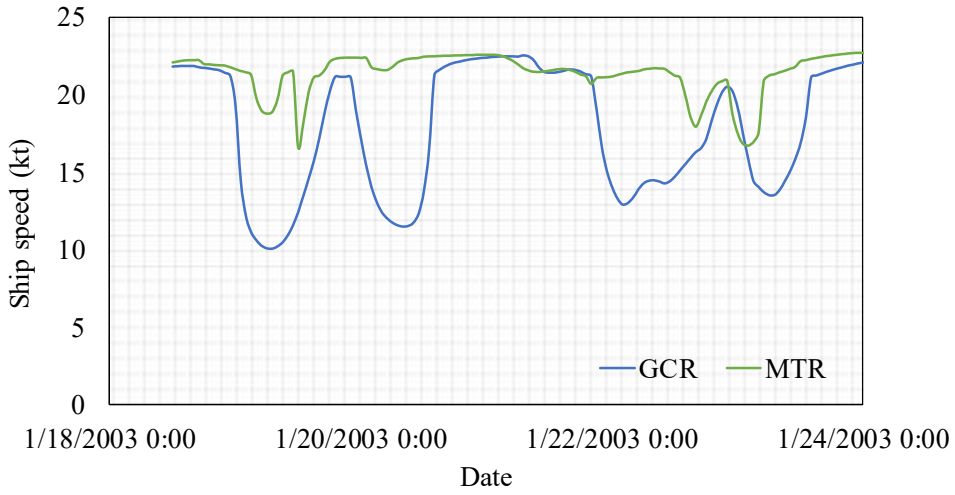

Fig. 3.7 Change in ship speed every one hour in a Bishop Rock to Florida voyage (From January 18th, 2003).

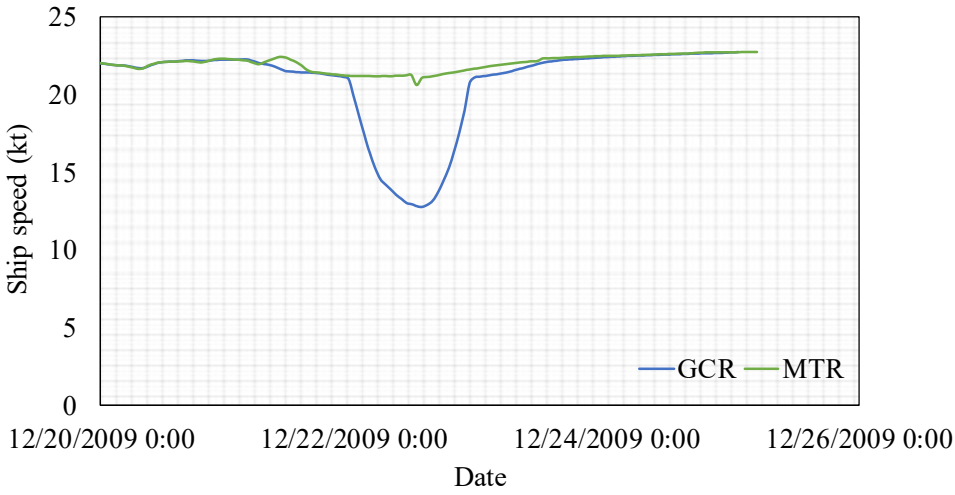

Fig. 3.8 Change in ship speed every one hour in a Florida to Bishop Rock voyage (From December 20th, 2009).

Scatter diagrams are summarizing the wave climate and are typically representing the joint probability of (*Hs*, *Ts*) combinations during the time period they are encompassing. In this thesis, the wave scatter diagrams have been computed summing up all the sea states encountered in each route. The wave scatter diagrams obtained for the GCR and MTR routes are presented in Fig. 3.9 and Fig. 3.10, respectively. It is observed that on the GCR, it is likely that the ship encounters

severe sea state with large waves, for example, 16.5 m waves. However, such severe seas are found a few times during the total ship life. On the other hand, in the MTR due to the avoidance of heavy weather conditions, it is observed in the wave scatter that the severest seas found are with 11.5 m waves. This shows that from the operational perspective on the MTR, the head seas are avoided to minimize the reduction of the ship speed. This also could be confirmed from operational data on the MTR routes.

Hs (m)\Ts (s)	4	5	6	7	8	9	10	11	12	13	14	15	16	17	18
0.5	0	23	12764	74135	81025	32951	6603	1318	334	86	19	15	0	1	3
1.5	0	0	1277	52494	117286	91889	45916	15709	4229	1239	415	117	32	23	3
2.5	0	0	0	628	35354	73170	51467	30363	11566	3400	865	225	61	22	1
3.5	0	0	0	0	289	21996	46764	28052	15065	5441	1374	278	75	14	5
4.5	0	0	0	0	0	250	14467	26710	13235	5241	1931	516	99	19	12
5.5	0	0	0	0	0	0	268	10181	13394	5419	1797	840	170	39	7
6.5	0	0	0	0	0	0	1	417	6968	6331	1756	661	192	80	12
7.5	0	0	0	0	0	0	0	2	683	3987	2108	574	245	59	35
8.5	0	0	0	0	0	0	0	0	16	779	1995	690	194	44	7
9.5	0	0	0	0	0	0	0	0	0	62	729	854	270	46	8
10.5	0	0	0	0	0	0	0	0	0	0	72	543	346	82	1
11.5	0	0	0	0	0	0	0	0	0	0	2	132	283	121	17
12.5	0	0	0	0	0	0	0	0	0	0	0	7	101	112	27
13.5	0	0	0	0	0	0	0	0	0	0	0	1	28	89	17
14.5	0	0	0	0	0	0	0	0	0	0	0	0	2	24	15
15.5	0	0	0	0	0	0	0	0	0	0	0	0	0	1	24
16.5	0	0	0	0	0	0	0	0	0	0	0	0	0	0	3

Fig. 3.9 Wave scatter diagram obtained for GCR.

Hs (m)\Ts (s)	4	5	6	7	8	9	10	11	12	13	14	15	16	17	18
0.5	24	310	13093	73170	80513	32423	6304	1233	285	77	18	16	0	1	3
1.5	0	133	1906	52475	116196	91302	45995	15859	4264	1209	408	119	42	21	2
2.5	0	2	84	1026	35628	71764	50810	30401	11750	3461	841	231	63	18	1
3.5	0	0	1	57	459	21121	45041	27664	15101	5591	1412	298	61	17	5
4.5	0	0	0	3	25	292	14047	26134	13145	5638	2208	612	123	28	10
5.5	0	0	0	0	0	8	318	9754	12814	5278	1947	880	285	42	11
6.5	0	0	0	0	0	0	3	383	5107	4341	1386	614	304	83	16
7.5	0	0	0	0	0	0	0	3	547	2409	1283	413	251	61	30
8.5	0	0	0	0	0	0	0	0	5	447	1044	394	204	53	10
9.5	0	0	0	0	0	0	0	0	0	26	448	468	222	51	3
10.5	0	0	0	0	0	0	0	0	0	0	59	287	223	43	8
11.5	0	0	0	0	0	0	0	0	0	0	2	31	132	59	9
12.5	0	0	0	0	0	0	0	0	0	0	0	0	0	0	0
13.5	0	0	0	0	0	0	0	0	0	0	0	0	0	0	0
14.5	0	0	0	0	0	0	0	0	0	0	0	0	0	0	0
15.5	0	0	0	0	0	0	0	0	0	0	0	0	0	0	0
16.5	0	0	0	0	0	0	0	0	0	0	0	0	0	0	0

Fig. 3.10 Wave scatter diagram obtained for MTR.

3.2.3 Weather routing effect

For the realistic modeling of encountered wave conditions, herein is presented a more advanced statistical storm wave model called “4G-storm model”, that considers the occurrence probability distribution of the wave direction to evaluate a

ship's stress response. It means that the change of relative heading angle during the sailing period can be simulated. This 4G-storm model is based on the statistical model proposed by Prasetyo (2013). First, the wave scatters diagram for the GCR and MTR voyage routes are assembled. Then, following the 3G-storm model simulation procedure presented in section 2.5, the sea state sequences are generated. Figure 3.11 shows the significant wave height time history with variable storm duration generated by storm model simulation in the GCR and MTR routes. It is observed that the storm model can well describe the variations of the significant wave height in arbitrary routes. In addition, it is noted that the severe waves are found in the GCR compare to that in the MTR for the same period.

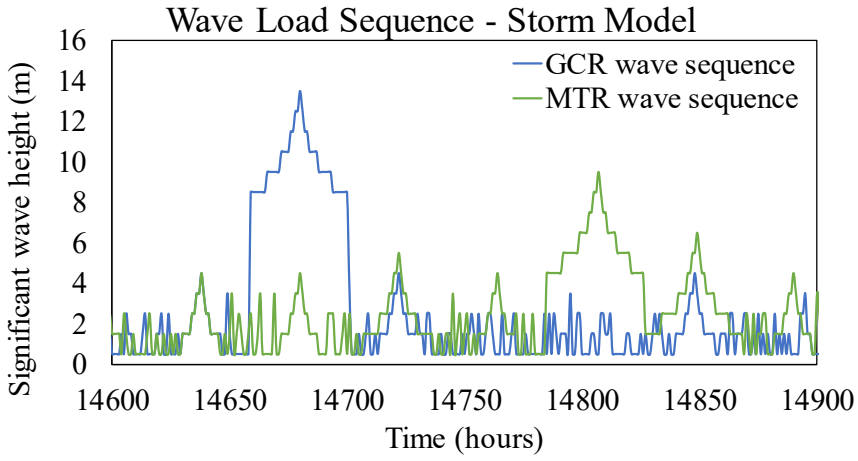

Fig. 3.11 Significant wave height time history with variable storm duration generated by storm model simulation in the GCR and MTR routes.

Moreover, for the structural stress computation, the heading angle of the ship could be determined considering the occurrence probability distribution of the wave direction. Assume that θ, α, and χ is the wave direction, the ship's heading angle, and relative heading angle. The classical ship's fatigue design procedures assume that the relative headings angle has an equal probability of occurrence when evaluating the stress response. This approximation is called 'all-headings model'. Concerns arise that this assumption might deteriorate the fatigue strength calculation

of ship structural members for being inadequate to reflect the changes in the operational conditions, e.g. relative heading changes during heavy weather avoidance. In the 4G-storm model, the stress response is calculated considering the relative headings angle occurrence probability. Herein this model is called 'real-headings model'. θ is determined by random number selection considering θ's occurrence probability f_θ, and χ is calculated by Eq. (3.1) each time.

$$\chi = \alpha - \theta \tag{3.1}$$

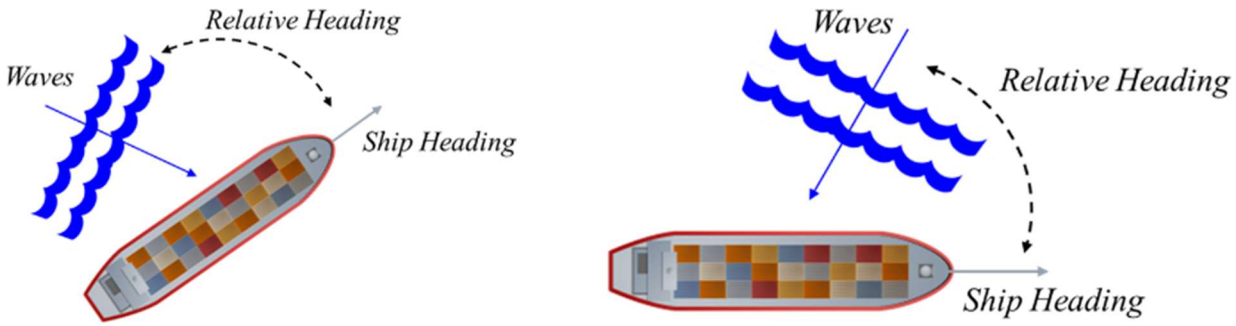

Fig. 3.12 Relative heading.

Ships are under constant impact of waves that influence with a particular relative angle each time. In order to consider the stochastic variations of the relative angle in the stress response evaluation, the real-heading model is considered in this calculations (Eq. 3.1). f_χ is the χ occurrence probability determined by analyzing the generated χ sequence. Let $f_{\chi,AH}$ be the f_χ derived from all-headings model, and $f_{\chi,RH}$ be that derived from the hindcast's wave direction. Figure 3.13 and Fig. 3.14 show the comparison of $f_{\chi,AH}$ and $f_{\chi,RH}$ in the GCR and MTR voyages, respectively. It is shown that $f_{\chi,AH}$ is nearly uniform, while $f_{\chi,RH}$ shows substantial variations. Both routes shows sharp peaks around χ=330 deg This is due to the large variance in the ship's heading angle in these routes and the strong directivity of the wave direction on these routes.

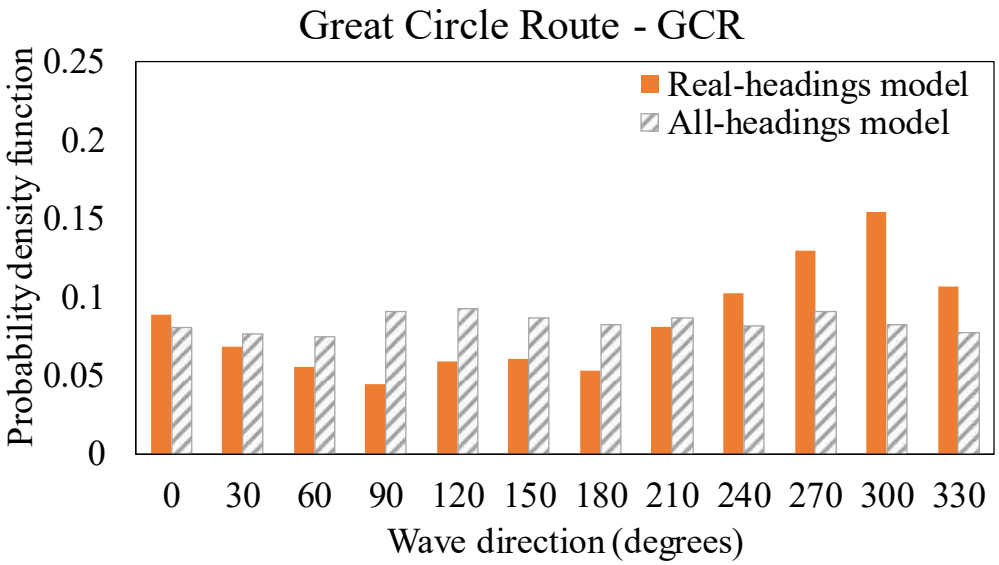

Fig. 3.13 Probability density function of the variation of the relative angle in the GCR voyages.

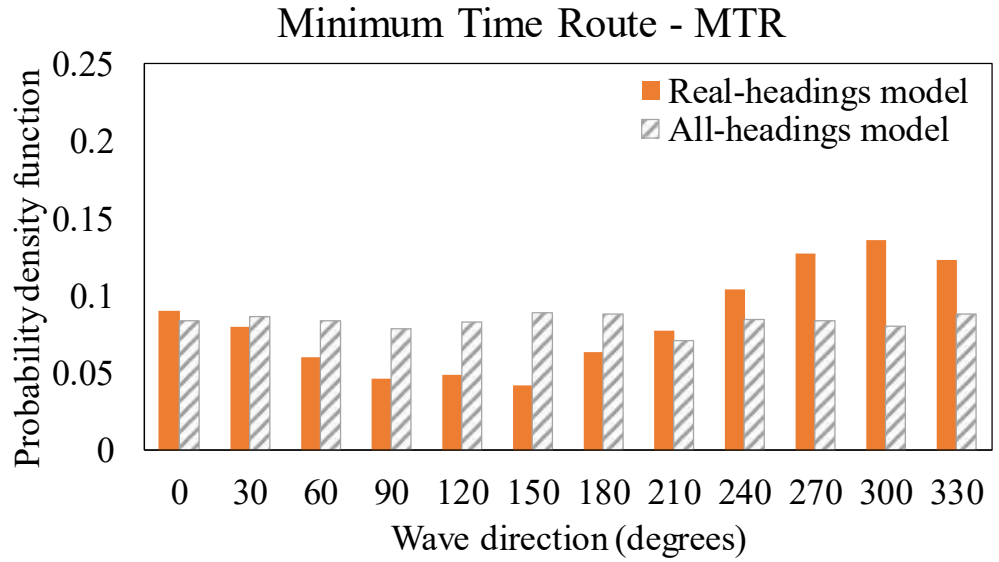

Fig. 3.14 Probability density function of the variation of the relative angle in the MTR voyages.

Once the waves environments are generated, a ship's structural stresses in a specific sea state can be estimated by combining the wave spectrum and transfer function of stresses (RAOs) at various regular wave conditions (Fricke et al. 2002). $\Delta\sigma_{HS}$ denotes the hotspot stress range. Once sequences of (Hs,Ts,θ) is given, $\Delta\sigma_{HS}$ sequence can be generated by following linear spectrum analysis. The RAO for this study is given in appendix 1 (see Fig. A1.1). Let $P_{EX,\Delta\sigma}$ be the stress range's

exceedance probability. Let $P_{EX,\Delta\sigma|GCR}$ and $P_{EX,\Delta\sigma|MTR}$ be $P_{EX,\Delta\sigma}$ of storm model stress sequences for GCR and MTR routes. A comparison of $P_{EX,\Delta\sigma|GCR}$ and $P_{EX,\Delta\sigma|MTR}$ is presented in Fig. 3.15. It is shown that the difference in the encountered wave condition shows that the difference in the stress exceedance probability becomes visible around $\Delta\sigma_{HS}$ > 150MPa, and the difference becomes slightly larger with the increase in $\Delta\sigma_{HS}$. Even though considerable differences in the wave statistics were found between the GCR and MTR routes, a partial explanation for the small differences in the exceedance probability is given by the relative heading angle randomness and the variation in stress response amplitude operator associated with the relative angle (shown in Fig. 3.13 and Fig. 3.14). Additionally, the storm model does not rely on a precise description of the routes and the way the storm is distributed along the ship route. This means that this model is very useful at the design stage where the stresses are calculated at the ship design speed.

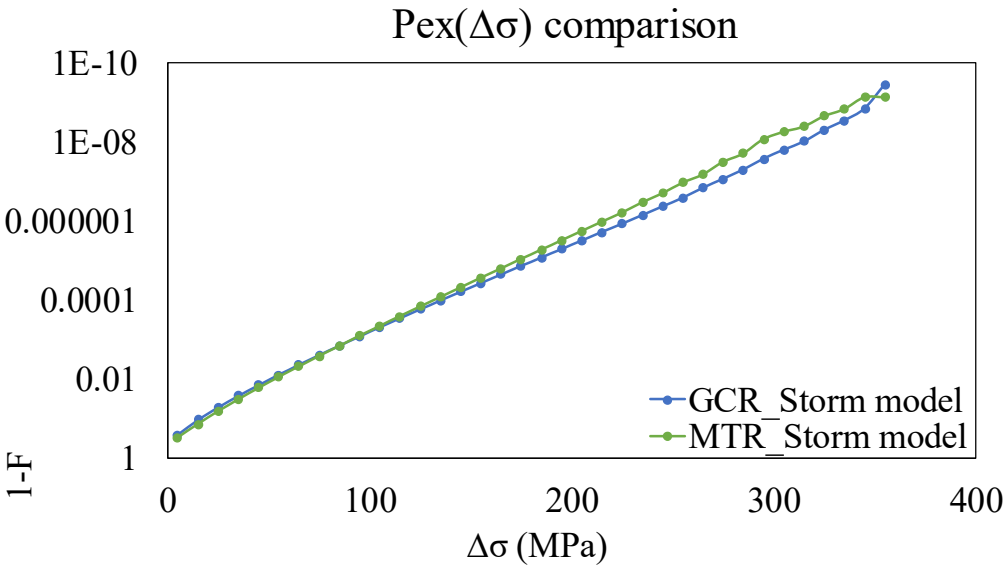

Fig. 3.15 The comparison of stress range's exceedance probability, $P_{EX,\Delta\sigma}$, generated by storm model simulation for GCR and MTR routes.

After evaluating the stresses response, the effect of the weather routing on the cumulative fatigue damage is evaluated by the Palmgren-Miner rule. It is considered that the total damage experienced by the structure may be expressed by the

accumulated damage from individual load cycles at different stress levels. Further, it is assumed that the cumulative damage is calculated for a butt weld in the upper deck for 10 years, $D_{10years}$. The cumulative fatigue damage of the target welded joint for a given sequence is calculated by the Eq. 2.1. The thickness effect is not considered and the mean stress is assumed to be zero.

Table 1 shows the cumulative fatigue damage results over 10 years. It is observed, that the cumulative damage in the MTR is about 15% smallest than that found in the GCR. This means weather routing systems optimize a route contributing to reducing the total accumulated fatigue damage, by considering proper operational conditions, such as ship's speed and course in order to avoid severe weather conditions (see Fig. 3.7 and 3.8).

Table 1 Comparison of the cumulative fatigue damage

Item	Storm Model	
Route	GCR	MTR
$D_{10years}$	0.3694	0.3223
L_f (years)	27.07	31.03

As shown above, the optimum sea-route planning of ocean voyages based on the forecast of weather has become imperative for ship operations, especially for its contribution to the safety in navigation, cost reductions and more efficient maintenance coordination's. Therefore, the short conditions for the NLHEA are chosen based on the short seas experienced by the target ship on the MTR voyages which considers a more realistic representation of the operational profile of ocean-going ships, as presented above.

The NLHEA is evaluated for various conditions, including short seas, heading angles, and ship speeds. The sea states are describing by the combinations of *Hs* and *Ts*. For the purpose of fatigue and the development of a probabilistic model for whipping occurrence, 73 sea states in head seas (180 deg) and 30 sea states in oblique

seas (120 deg) are examined. It is important to select these states to cover the dominating fatigue damage from both the conventional wave frequency and high-frequency loading. The selected target sea states and vessel speeds are listed in Fig. 3.16 and 3.17 for head seas and oblique seas, respectively.

Short-term sea states evaluated - 6500 TEU Container - Head seas (180deg)													
Vs (kt)	Hs (m)	Ts (sec)											
		4.5	5.5	6.5	7.5	8.5	9.5	10.5	11.5	12.5	13.5	14.5	15.5
0	12.5												
8	11.5					*	*	*	*	*	*		
9	10.5					*	*	*	*	*	*		
9	9.5					*	*	*	*	*			
11	8.5					*	*	*	*	*	*		
13	7.5				*	*	*	*	*	*	*	*	
19	6.5				*	*	*	*	*	*	*	*	
21	5.5					*	*	*	*	*	*		
21	4.5					*	*	*	*	*	*		
22	3.5					*	*	*	*	*	*		
22	2.5	*	*	*	*	*	*						
23	1.5	*	*	*	*	*	*						
23	0.5												

Fig 3.16 Examined sea states and ship speeds in head seas.

Short seas evaluated - 6500 TEU Container - Oblique seas (120deg)													
Vs (kt)	Hs (m)	Ts (sec)											
		4.5	5.5	6.5	7.5	8.5	9.5	10.5	11.5	12.5	13.5	14.5	15.5
8	12.5												
15	11.5									*	*	*	
15	10.5								*	*	*		
17	9.5								*	*	*		
21	8.5						*	*	*				
21	7.5						*	*	*				
22	6.5						*	*	*				
22	5.5						*	*	*				
22	4.5				*	*	*						
22	3.5		*	*	*								
22	2.5		*	*	*								
23	1.5												

Fig 3.17 Examined sea states and ship speeds in oblique seas.

3.3 Subject Ship and Numerical Model

A 6000 TEU class container ship is selected as the target ship in this research. The total displacement is about 110,000 tons. The main particulars of the ship are L x B x D – d (L – length, B – breadth, D – depth, and d – draught) = 280 x 42.5 x 25.5 – 14 m. The hydrodynamic mesh model has 3004 nodes and 2820 elements on the surface of the hull. For the structural modeling, the whole ship is discretized into 24 beam elements. The sectional properties of the beam are given based on the mass and rigidity distribution of a prototype ship. Figure 3.18 shows the panel model for the 6000 TEU class container ship adapted in this study from Iijima et al. (2019).

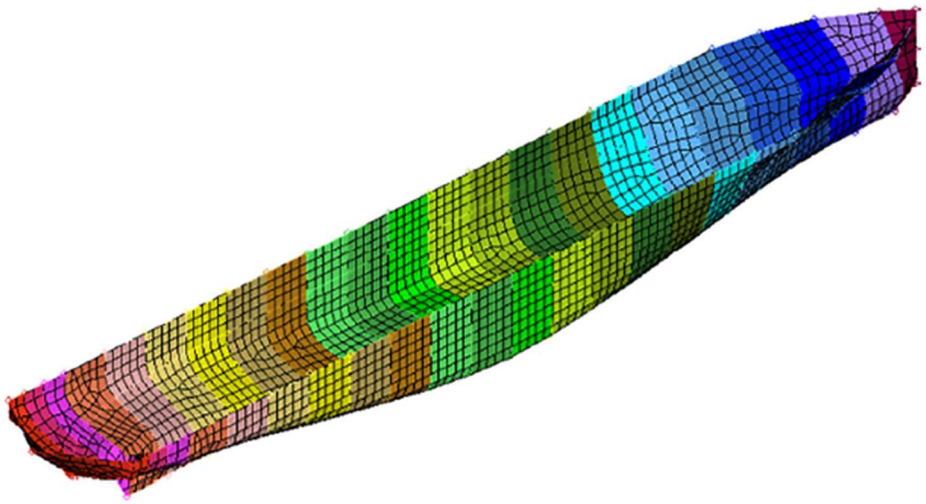

Fig. 3.18 Panel model for 6000TEU class container ship. Adapted from (Iijima et al. 2019).

Table 2 shows a summary of the first three natural frequencies of the ship. The first natural frequency of the ship corresponds to the two nodded vertical bending mode. The lowest natural frequency (dry mode) is found at 0.747 Hz. It is also to be noted that the accuracy of the results may be degraded for the higher modes due to the assumption of Bernoulli–Euler beam and the element subdivision number 24 of the whole ship. However, in the following simulations, the dominating contributions come from the first to the third modes, and the accuracy of the eigenvalue-analysis

results up to the third is believed to be sufficient. Even though it is commonly known that the lowest natural frequency of container ships is the torsional mode, the antisymmetric modes including the torsion are out of the scope of the present research.

Table 2 Summary of natural frequencies

Mode	Frequency (Hz)	Note
1	0.7467	2 node VB
2	1.6159	3 node VB
3	2.6574	4 node VB

The numerical method employed in this research explains the hydro-elastic vibration characteristics to a certain extent considering the following:

1. Only the symmetric modes are the subject of this research. In general, it is considered that the shell FE model is necessary to represent the symmetric and antisymmetric modes. The beam representation adopted in the present research may is not sufficient for modeling the antisymmetric modes (Iijima et al. 2009).
2. The recommended sea spectra assumed is given by the ISSC (International Ship and Offshore Structures Congress) spectral formulation for fully developed seas.
3. The ship forward speed is constant. Is set to the maximum achievable speed considering voluntary and/or involuntary ship speed. The ship performance curve adopted in this research is presented in Fig. 3.4.
4. It is assumed that the target ship always navigates in head seas (180 deg) or oblique seas (120 deg).
5. The ship's structural damping is not clear. It is assumed less than 2% critical damping for the respective flexible modes.

6. The assessment of the stresses is at the deck of the amidships section.

3.4 Summary

In this chapter, it is presented the conditions for the NLHEA which include various short seas, heading angles, and ship speeds. The conditions are chosen based on the effect of the weather routing on the fatigue cumulative damage examined by 4G-storm model simulation. Finally, a description of the numerical model of the target ship and main assumptions for a series of NLHEA are given. The results of the NLHEA are converted into deck stress for the amidships section and adopted in chapter 4 to demonstrate the principles of the proposed probabilistic model for whipping occurrence.

Chapter 4 Principles of the Probabilistic Model for Whipping Occurrence

In this chapter, a description of a methodology proposed to examine the characteristics of the hull vibration superimposed stress waveform (HVSSW) is given. The stochastic characteristics of HVSSW experienced by 6000 TEU class container ship deck longitudinal are examined based on the results of a series of NLHEA for various conditions (short seas/heading angles/ship speeds). The application of the proposed model is verified with an onboard record measured in a 9000 TEU class container carrier. Finally, the characteristics of whipping HVSSW experienced by the target ship are simplified to define a representative HVSSW for high-frequency effect fatigue tests.

4.1 Slamming Impact Detection Methodology

Slamming occurrence and severity for different operating conditions (wave height, encounter frequency, speed, and heading) are essential to consider safe environmental conditions for ship operators and in providing long-term estimates of structural load statistics (Magoga et al. 2014). As presented in chapter 1, recent studies have focused on the effect of whipping vibration on extreme load and fatigue damage accumulation. However, these studies did not necessarily clarify the relation between the occurrence probability of a slamming induced vibration and sea state, vessel operation (voluntary or involuntary speed reduction) or course change. Given that no universally accepted criterion for identification of slamming event exists in the open literature, the topic is definitively open to further discussion and improvement. Model tests or full-scale measurements for the slamming loads are not practical for all of the ships in different sea states (Wang et al. 2017). Hence, it is

more reasonable to examine the slamming occurrence based on numerical simulations.

This section presents the development of the slamming impact detection methodology. The results of the numerical simulation are used to detect a whipping event. All the vertical bending moments (VBM) has been converted into deck stress for the amidships section. The primary wave (PW), also known as wave-frequency, the response is obtained bypass filtering the HVSSW time histories to include only the energy at frequencies in the primary wave range. The upper cutoff frequency is 0.30 Hz. After the primary wave stress is obtained, by high-pass filtering the original signal the hull vibration (HV) stress component is obtained. The upper cutoff frequency for PW stress filtering is the same as the lower cutoff frequency for HV stress filtering. Responses above 1.0 Hz are also removed. Figure 4.1 shows an example of HVSSW, HV and PW stress time histories experienced by 6000 TEU class container ship (Hs=6.5m, Ts=10.5s, head waves). It is noted that hogging condition is positive, with slamming in sagging.

Once the hull vibration stress waveform (the blue line in Fig. 4.4) is obtained, let 'peak stress' $\sigma_{HV\text{-}PK}$ and 'valley stress' $\sigma_{HV\text{-}VL}$ be the peak and valley of the i-th HV waveform, and 'peak-valley range' $\Delta\sigma_{PK}$ be the difference between $\sigma_{HV\text{-}PK}$ and $\sigma_{HV\text{-}VL}$ (see Fig. 4.2). To neglect the smallest stress ranges, the only $\Delta\sigma_{PK}$ whose ratio is larger than 0.20 is considered. The slamming peaks are detected according to the following procedure:

a) Create sequence lists of $\sigma_{HV\text{-}PK}$, $\sigma_{HV\text{-}VL,}$ and $\Delta\sigma_{PK}$ (the orange line in Fig. 4.4). and calculate the standard deviation of $\Delta\sigma_{PK}$, s_{Rng}.

b) Let $\Delta\sigma_{CREST}^{i}$ be the crests of the i-th $\Delta\sigma_{PK}$ sequence's skyline. Detect $\Delta\sigma_{CREST}^{i}$ from the sequence of $\Delta\sigma_{PK}$ by Savitzky-Golay filtering (Savitzky et al.

1964) (kernel k=2 and half-width n=3). The i-th $\Delta\sigma_{CREST}{}^{i}$ is considered if $\Delta\sigma_{CREST}{}^{i+1}$ - $\Delta\sigma_{CREST}{}^{i} > 0$ (see Fig. 4.3).

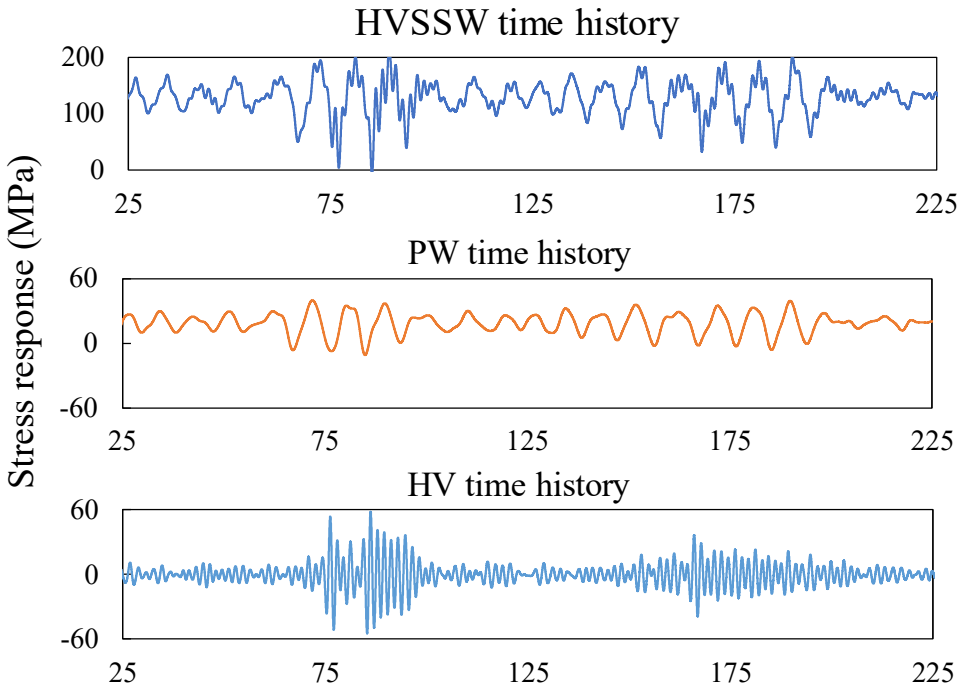

Fig. 4.1 An example of HVSSW, HV and PW stress signals experienced by 6000 TEU class container ship (Hs=6.5m, Ts=10.5s, head waves).

c) A threshold T_{HRES} is established in Eq. 4.1 to extract the $\Delta\sigma_{PK}$ as a whipping vibration due to the slamming impact. Remove $\sigma_{HV\text{-}PK}$ from the sequence according to Eq. 4.2 (the green dashed line in Fig. 4.4):

$$T_{HRES} = a \times s_{Rng} \tag{4.1}$$

$$\Delta\sigma_{PK\text{-}VL,Rng} > T_{HRES} \tag{4.2}$$

where a is a non-dimensional factor. The remaining sequence of $\Delta\sigma_{PK}$ (the red marks in Fig. 4.4) gives the sequence of the slamming stress ranges. For T_{HRES} in procedure step c), a=1.5. The a parameter was chosen as an appropriate indicator so the frequency ratio of the hull vibration to the period of the hull vibration superimposed stress waveform nearly become identical to the reported in the Toyoda et al. (2012).

d) The sequence of the times at which $\sigma_{HV\text{-}PK}$ occurs responsible for the $\Delta\sigma_{PK\text{-}VL,Rng}$ in the remaining list gives the sequence of the slamming occurred times. The sequence is examined each short-sea duration t_{ssdur} (in seconds).

The importance of considering the $\Delta\sigma_{PK}$ instead of the $\sigma_{HV\text{-}PK}$ to recognize the whipping vibration is to minimize the uncertainties associated with the recognition of a spike load of a whipping event, especially in the lower *Hs*.

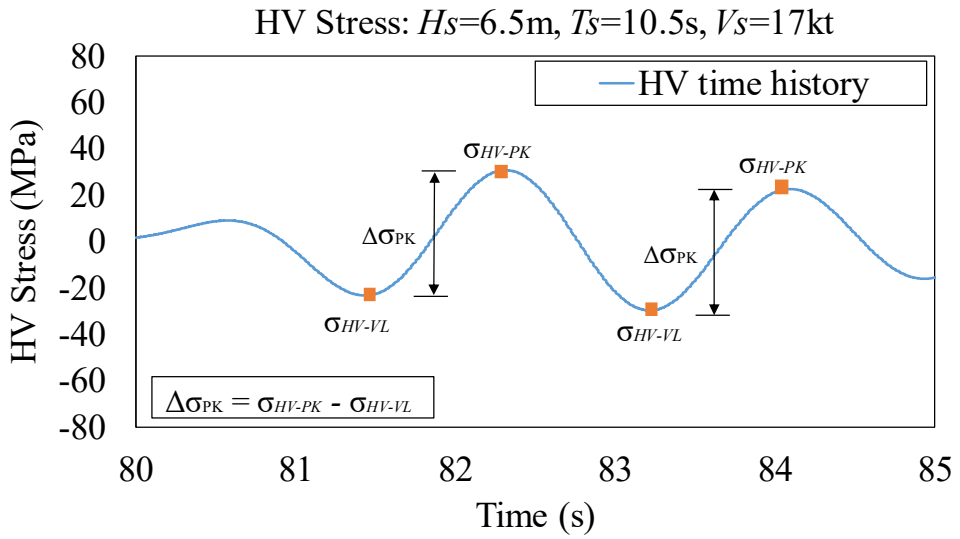

Fig. 4.2 An example of the "peak-valley range" stress calculation procedure.

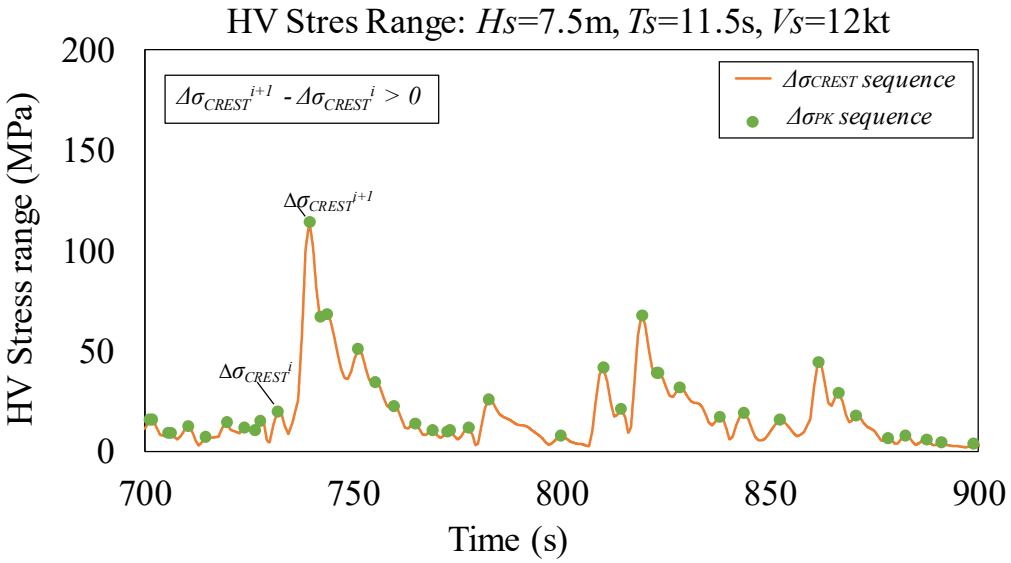

Fig. 4.3 An example of the "crests" selection procedure from the "peak-valley sequence".

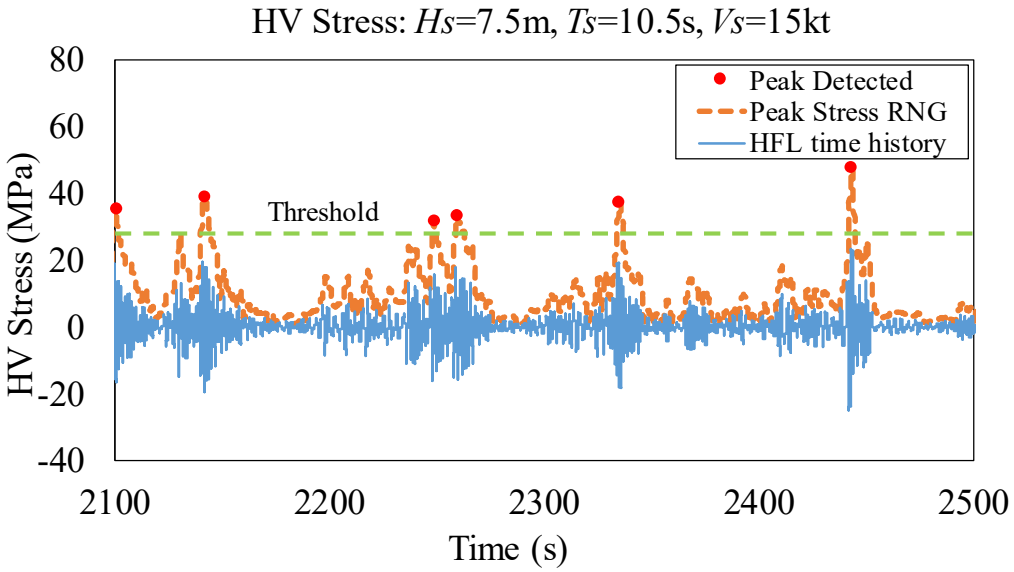

Fig. 4.4 An example of slamming impact detection procedure.

4.2 Occurrence Frequency of Whipping Vibration

The occurrence frequency of whipping vibration is examined by counting the number of slamming impact in the hull vibration stress component during t_{ssdur}. Let n_{slm}, f_{PW} and f_{slm} be the numbers of slamming impact, the frequency of the primary wave cycles and the frequency of the slamming impact during each t_{ssdur}. n_{slm} is determined once the ΔS_{PK} sequence is obtained. The average f_{slm} is determined as the ratio of n_{slm} to t_{ssdur}. Then, the average f_{PW} can be approximated by the inverse of T_S. The dimensionless coefficient of whipping interval C_{wh} is given by Eq. (4.3):

$$C_{wh} = f_{slm} / f_{PW} \tag{4.3}$$

It is noticed that slamming occurs more frequently when C_{wh} is increasing. If the C_{wh} coefficient reaches 1.0, slamming occurs every primary wave.

4.3 Numerical Simulation Results

The whipping characteristics (occurrence frequency of whipping vibration, slamming impact stress range and the effect of the whipping vibration on the fatigue cumulative damage) are investigated using NLHEA. Different short sea conditions, ship speeds, and wave conditions (head waves – 180 deg and oblique waves – 120 deg) are evaluated. Table 4.1 and Table 4.2 shows the sea states examined in head and oblique waves, respectively. It is considered that the target ship follows the performance curve presented in Fig. 3.4. Samples of the numerical results time histories of HVSSW for head wave are presented in Fig. 4.5 and Fig. 4.6, while for oblique waves samples are shown in Fig. 4.7 and Fig. 4.8.

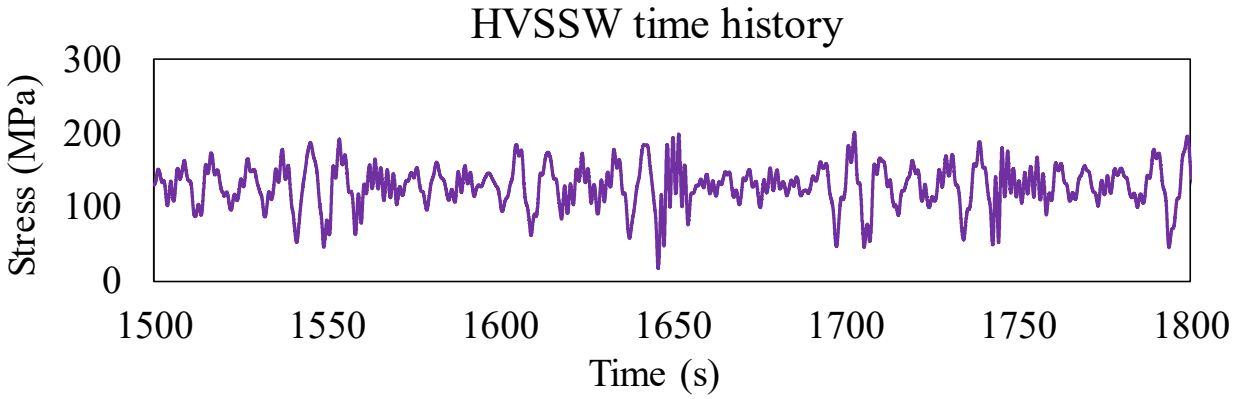

Fig. 4.5 An example of HVSSW experienced by the 6000 TEU class container ship (*Hs*=5.5 m, *Ts* =10.5 s, *Vs*= 21 kt, head waves).

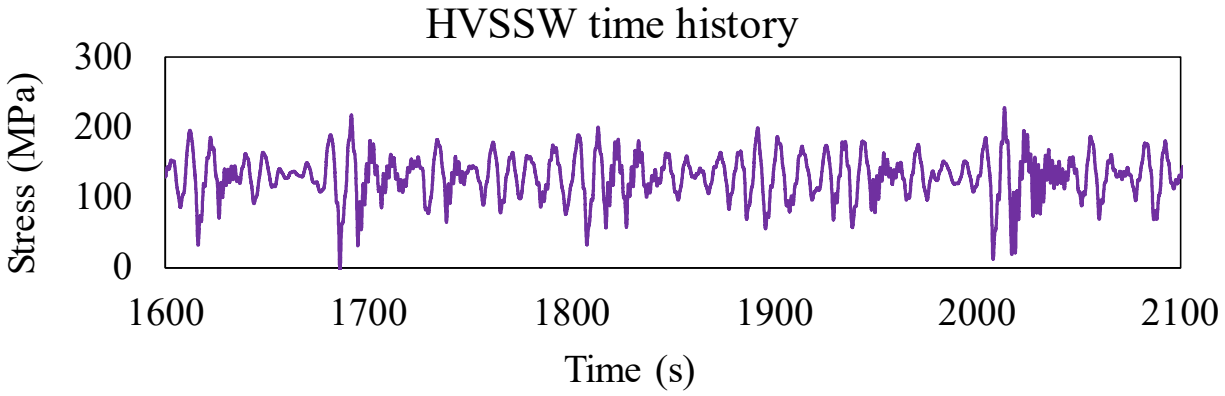

Fig. 4.6 An example of HVSSW experienced by the 6000 TEU class container ship (*Hs*=7.5 m, *Ts* =11.5 s, *Vs*= 13 kt, head waves).

Table 4.1 Sea states evaluated in head wave condition.

Sea State No.	Hs (m)	Ts (s)	Vs (kt)	Sea State No.	Hs (m)	Ts (s)	Vs (kt)
1	1.5	4.5	22	36	6.5	12.5	19
2	1.5	5.5	22	37	6.5	13.5	19
3	1.5	6.5	22	38	6.5	14.5	19
4	1.5	7.5	22	39	7.5	7.5	13
5	1.5	8.5	22	40	7.5	8.5	13
6	1.5	9.5	22	41	7.5	9.5	13
7	2.5	4.5	22	42	7.5	10.5	13
8	2.5	5.5	22	43	7.5	11.5	13
9	2.5	6.5	22	44	7.5	12.5	13
10	2.5	7.5	22	45	7.5	13.5	13
11	2.5	8.5	22	46	7.5	14.5	13
12	2.5	9.5	22	47	8.5	8.5	11
13	3.5	8.5	22	48	8.5	9.5	11
14	3.5	9.5	22	49	8.5	10.5	11
15	3.5	10.5	22	50	8.5	11.5	11
16	3.5	11.5	22	51	8.5	12.5	11
17	3.5	12.5	22	52	8.5	13.5	11
18	3.5	13.5	22	53	9.5	8.5	9
19	4.5	8.5	21	54	9.5	9.5	9
20	4.5	9.5	21	55	9.5	10.5	9
21	4.5	10.5	21	56	9.5	11.5	9
22	4.5	11.5	21	57	9.5	12.5	9
23	4.5	12.5	21	58	10.5	8.5	9
24	4.5	13.5	21	59	10.5	9.5	9
25	5.5	8.5	21	60	10.5	10.5	9
26	5.5	9.5	21	61	10.5	11.5	9
27	5.5	10.5	21	62	10.5	12.5	9
28	5.5	11.5	21	63	10.5	13.5	9
29	5.5	12.5	21	64	11.5	8.5	8
30	5.5	13.5	21	65	11.5	9.5	8
31	6.5	7.5	19	66	11.5	10.5	8
32	6.5	8.5	19	67	11.5	11.5	8
33	6.5	9.5	19	68	11.5	12.5	8
34	6.5	10.5	19	69	11.5	13.5	8
35	6.5	11.5	19				

Table 4.2 Sea states evaluated in oblique wave condition.

Sea State No.	Hs (m)	Ts (s)	Vs (kt)
1	2.5	5.5	22
2	2.5	6.5	22
3	2.5	7.5	22
4	3.5	5.5	22
5	3.5	6.5	22
6	3.5	7.5	22
7	4.5	7.5	22
8	4.5	8.5	22
9	4.5	9.5	22
10	5.5	9.5	22
11	5.5	10.5	22
12	5.5	11.5	22
13	6.5	9.5	22
14	6.5	10.5	22
15	6.5	11.5	22
16	7.5	9.5	21
17	7.5	10.5	21
18	7.5	11.5	21
19	8.5	9.5	21
20	8.5	10.5	21
21	8.5	11.5	21
22	9.5	11.5	17
23	9.5	12.5	17
24	9.5	13.5	17
25	10.5	11.5	15
26	10.5	12.5	15
27	10.5	13.5	15
28	11.5	12.5	15
29	11.5	13.5	15
30	11.5	14.5	15

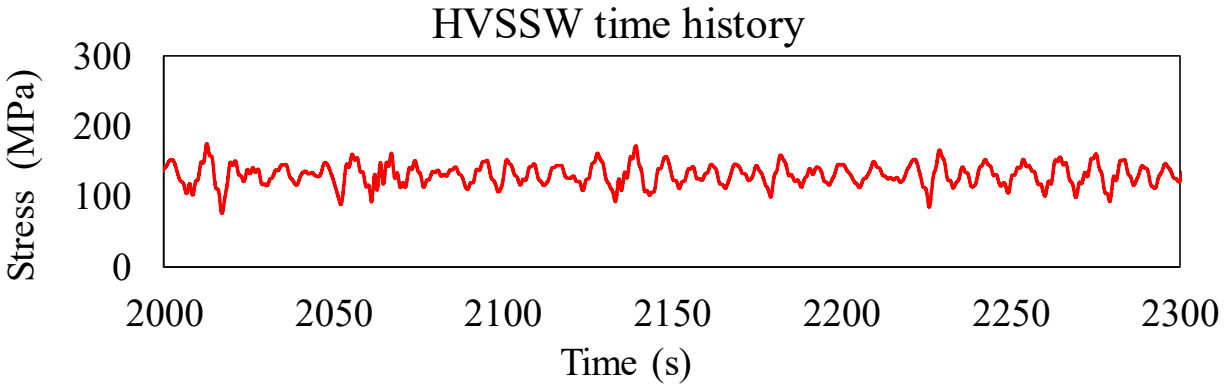

Fig. 4.7 An example of HVSSW experienced by the 6000 TEU class container ship (*Hs*=5.5 m, *Ts* =10.5 s, *Vs*=21 kt, oblique waves).

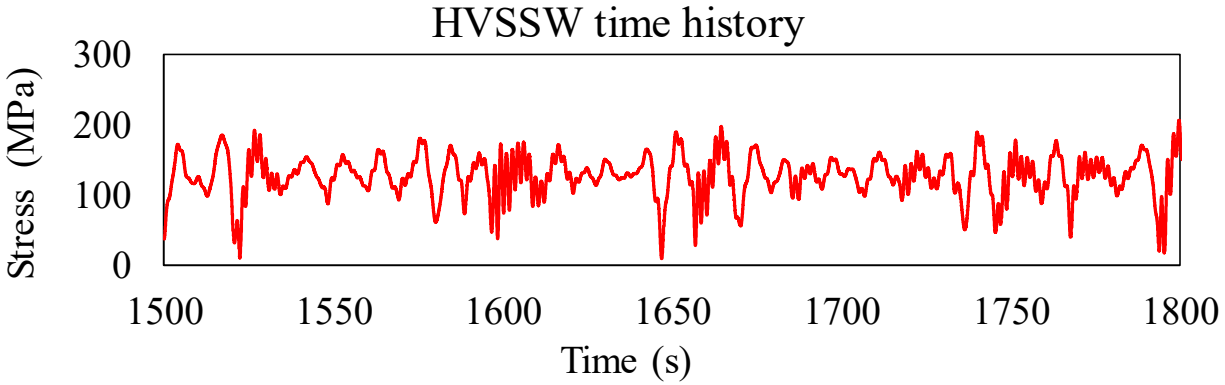

Fig. 4.8 An example of HVSSW experienced by the 6000 TEU class container ship (*Hs*=11.5 m, *Ts* =13.5 s, *Vs*=15 kt, oblique waves).

4.3.1 Occurrence frequency of whipping vibration

The statistical prediction of the whipping vibration can be achieved by assuming that the phenomenon is a sequence of events occurring in time. It may often be necessary to know the time or cycles to the primary wave interval between successive slam impacts or the time elapsed before the next severe impact occurs.

Figure 4.9 shows the calculated C_{wh} in head sea conditions for various short seas. Results are plotted by different color/mark for each ship speed *Vs*. In Fig. 4.9, presented data includes data for *Vs* beyond the performance curve of the target ship (Fig. 3.4), which is not experienced in actual practice. *Hs* increases from left to right for each *Vs*. It is shown that C_{wh} ranges from 0.16 to 0.60, and it becomes smaller as

Hs becomes larger. Also, it is noted that C_{wh} increases with *Vs*. These results show that the variations of C_{wh} are more sensitive to the changes in *Vs* than that found for *Hs*.

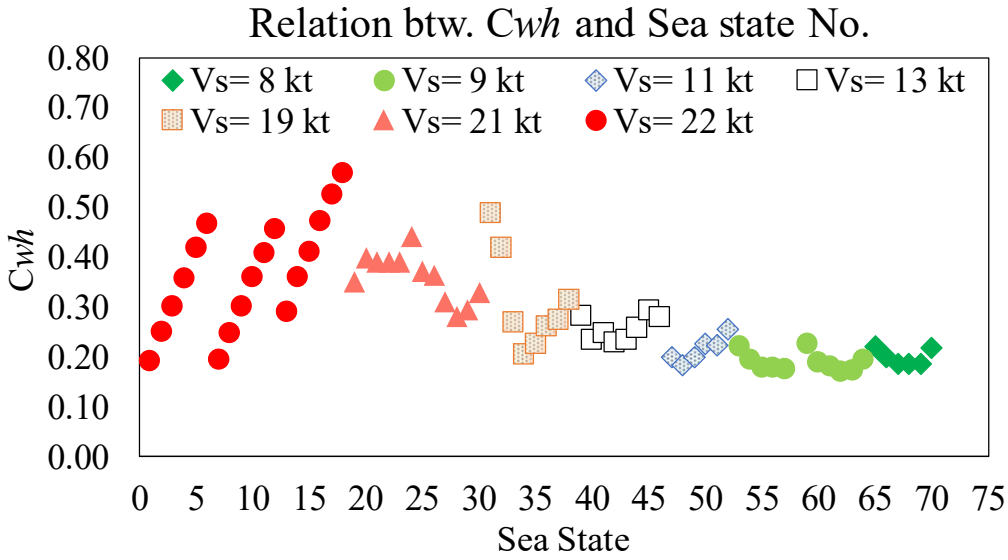

Fig. 4.9 The variation in the coefficient of whipping interval C_{wh} for short sea with various significant wave heights and ship speeds– head seas–.

Let 'limit speed' $V_{\lim}(Hs)$ be the maximum *Vs* achievable for a given *Hs*, which can be determined by the performance curve (Fig. 3.4). The voluntary (mainly as a result of operational judgment from the captain) and involuntary (mainly due to added resistance) speed reduction is considered in this analysis. Let $C_{wh,\lim}$ (*Hs*) be C_{wh} for $V_{\lim}(Hs)$. The relation between *Hs* and $C_{wh,\lim}$ (*Hs*) is shown in Fig. 4.10. In this figure, it is shown that $C_{wh,\lim}$ (*Hs*) has a decreasing tendency with the increase in *Hs*, and it ranges between 0.18 and 0.35 for cases with *Hs* >5.5m. This means that it can be approximated that a slamming impact happens once in every 3 to 5 primary wave under conditions chosen. Moreover, it is considered that the high $C_{wh,\lim}$ (*Hs*) with *Hs* < 4.5m is the result of the linked effect of whipping and springing, where an important role plays the sea states with shorter since the linear or higher-order harmonics of wave loads are more likely to meet the natural frequency of the structure.

Furthermore, Fig. 4.11 shows the changes of $C_{wh,\lim}$ (H_S) with the increase of the ship speed for head waves condition. It is noted that: a) $C_{wh,\lim}$ (H_S) gradually increase with an increase if ship's forward speed; b) $C_{wh,\lim}$ (H_S) shows slight increase with an increase of $V_{\lim}$(H_S) between 8-11 kt; and c) $C_{wh,\lim}$ (H_S) shows a linear increasing tendency with an increase of $V_{\lim}$(H_S) between 11-22 kt. Similar findings are reported in the available literature in terms of the vertical bending moment and pitch motion (Iijima et al. 2019).

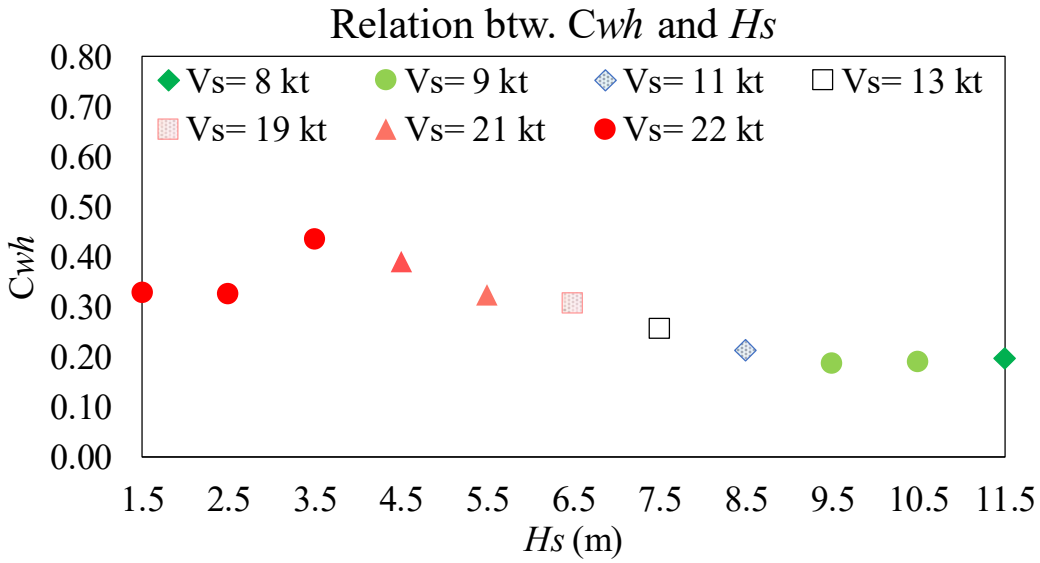

Fig. 4.10 The relation between significant wave height H_S and coefficient of whipping interval at the limit speed $C_{wh,\lim}$ (H_S) –head seas–.

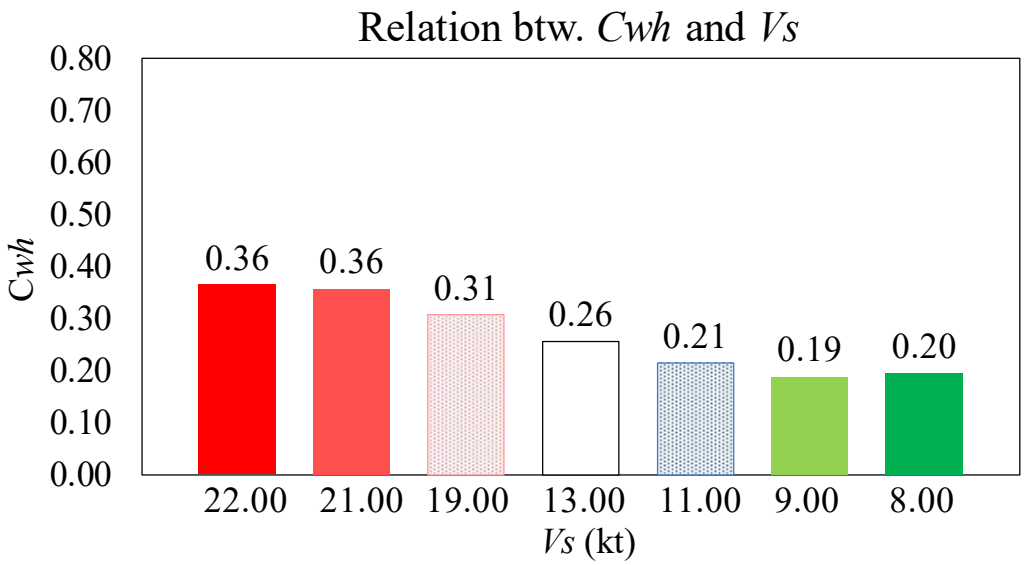

Fig. 4.11 The relation between the maximum V_S achievable for a given *Hs*, $V_{\lim}(Hs)$, and coefficient of whipping interval at the limit speed $C_{wh,\lim}$ (*Hs*) –head seas–.

The occurrence frequency of whipping vibration for a wave encountering angle of 120 deg are presented herein. The effects of the hull vibrations are expected to be larger when the ship sails in head waves. As can be seen in Fig. 4.12, similar to the results in head seas, with the increase of the ship forward speed, the relative velocity of the wave surface and ship's bow increase. Then, the slamming loads become more frequently. The results show that the target ship experienced more frequently whipping vibrations per regular waves under the influence of 4.5m waves at a ship speed of 22 kt. A similar tendency is reported from the fatigue damage perspective (Iijima et al. 2011). Figure 4.13 presents the relation between *Hs* and coefficient of whipping interval at the limit speed $C_{wh,\lim}$ (*Hs*) in oblique waves. It is noted that $C_{wh,\lim}$ (*Hs*) decreases with the increase of *Hs*, while the average $C_{wh,\lim}$ (*Hs*) is around 0.23. This suggest that, in oblique wave condition, a slamming impact happens once in every 4 to 5 primary waves regardless of the variations of *Hs*. This outcome shows the importance to consider the effect of the slamming impact not only in head sea waves but also from oblique seas. However, it is unclear whether similar tendency

result appears for a beam or following seas, and additional study should be done in order to clarify the probability of occurrence of whipping vibration.

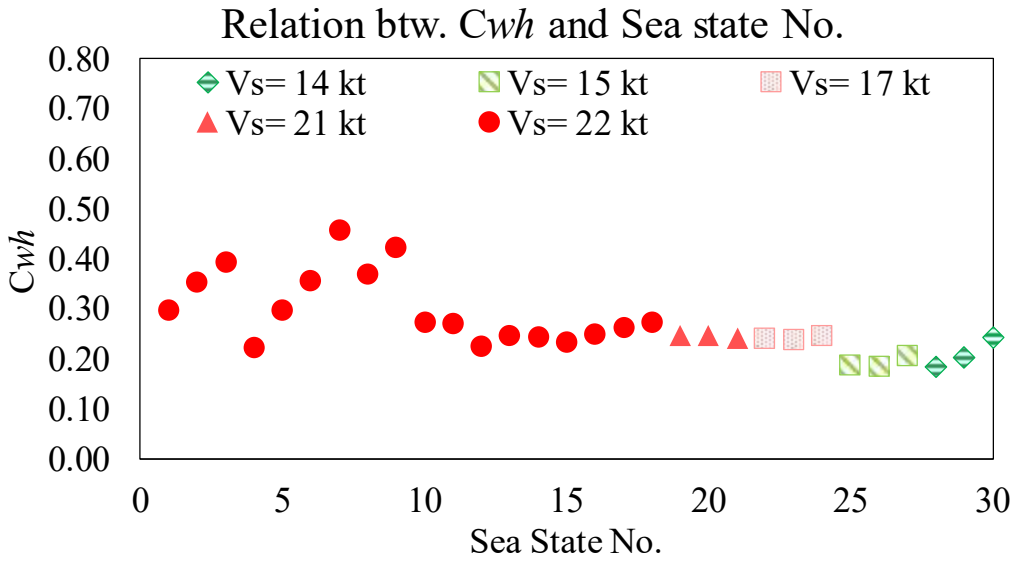

Fig. 4.12 The variation in the coefficient of whipping interval C_{wh} for short sea with various significant wave heights and ship speeds– oblique seas–.

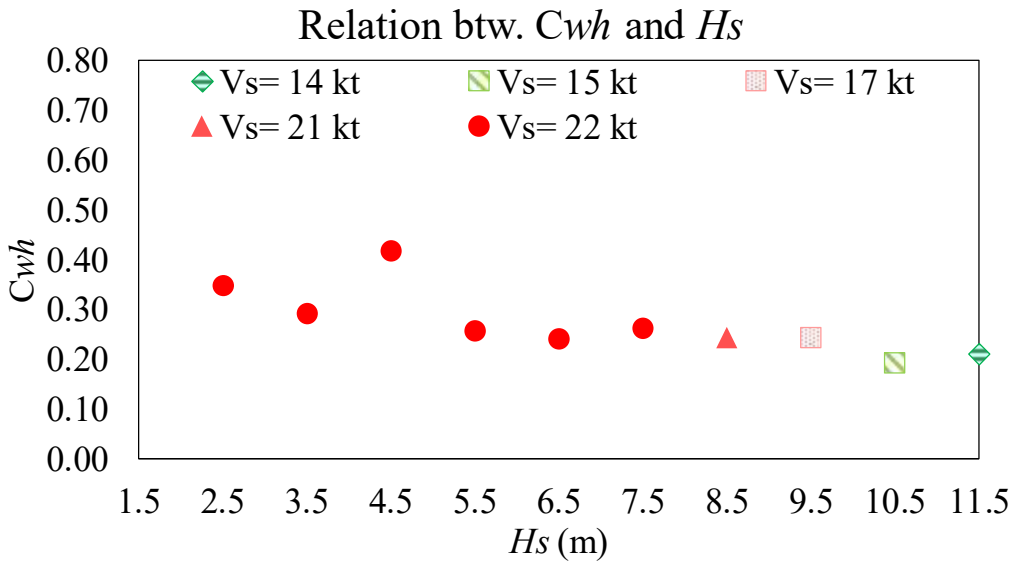

Fig. 4.13 The relation between significant wave height *Hs* and coefficient of whipping interval at the limit speed $C_{wh,\mathrm{lim}}$ (*Hs*) –oblique waves–.

4.3.2 Slamming impact stress range

For estimating the magnitude of the slamming impact, let $\Delta\sigma_{PW}$ be the stress range of the primary wave stress waveform, and $\Delta\sigma_{PK,\mathrm{lim}}$, and $\Delta\sigma_{PW,\mathrm{lim}}$ be the average values of $\Delta\sigma_{PK}$ and $\Delta\sigma_{PW}$ for $V_{\mathrm{lim}}(H_S)$. $\Delta\sigma_{PK}$ is analyzed in the slamming detection

analysis of section 4.1, and $\Delta\sigma_{PW}$ is calculated as the range of the low-pass filtered stress. The variation of the slamming peak stress range $\Delta\sigma_{PK}$ for short sea with various significant wave heights and ship speeds under a head wave is presented in Fig. 4.14. The relation between H_S and $\Delta\sigma_{PK,lim}$ is shown in Fig. 4.15, and that between H_S and $\Delta\sigma_{PW,lim}$ is shown in Fig. 4.16. In all figures, H_S increases from left to right for each V_S.

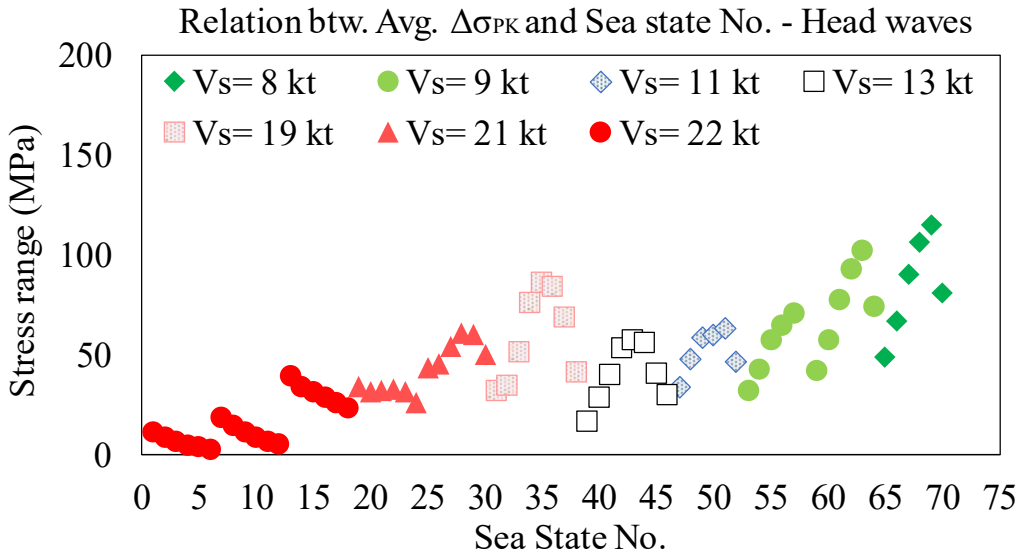

Fig. 4.14 The variation of the slamming peak stress range $\Delta\sigma_{PK}$ for short sea with various significant wave heights and ship speeds –head seas-.

Figure 4.14 shows that $\Delta\sigma_{PK}$ ranges between 25-120 MPa, while the $\Delta\sigma_{PK}$ levels constantly increase with the increment of *Hs*. Along with the changes with *Hs*, it is noted variations during each constant *Vs*. These variations correspond to the variations on *Ts* during each constant *Vs*. For more severe sea states, the slamming of the ship's fore end and, occasionally, of the aft end can induce whipping with higher amplitude than those occurring during springing events (Liao et al. 2015).

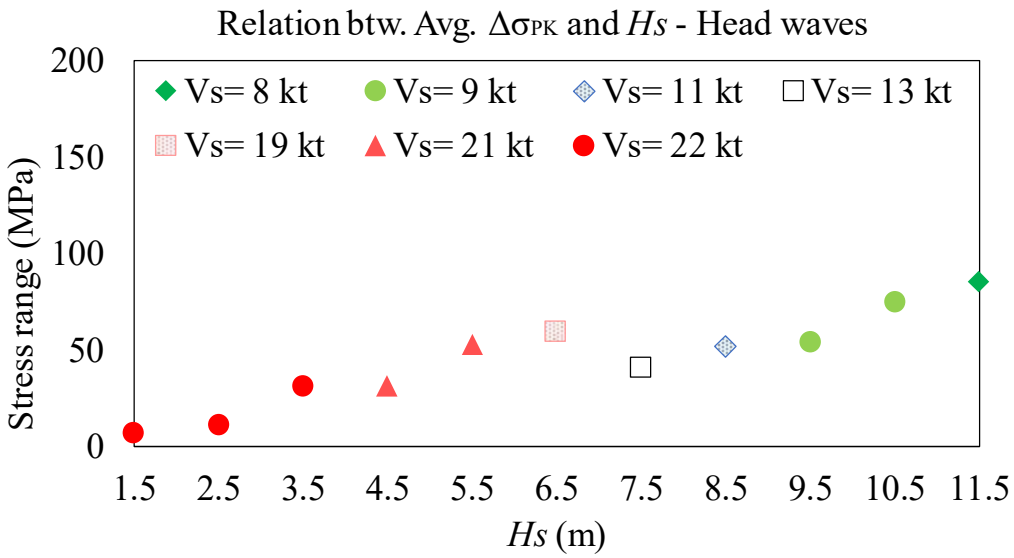

Fig. 4.15 The relation between significant wave height H_S and slamming peak stress range at the limit speed $\Delta\sigma_{PK\_lim}$ (Hs) –head seas-.

Furthermore, in Fig. 4.15 it is shown that $\Delta\sigma_{PK,lim}$ is almost linearly in proportion to Hs. It is reasonable that $\Delta\sigma_{PK}$ increases for larger significant wave heights since the nonlinear loads are more important in high waves. Similar to the findings in ΔS_{PK} results, $\Delta\sigma_{PW,lim}$ is found to change almost linearly in proportion to Hs (see Fig. 4.16), and the $\Delta\sigma_{PW,\text{lim}}$ ranges between 55-245 MPa. In addition, the ratio of $\Delta\sigma_{PK,\text{lim}}$ to $\Delta\sigma_{PW,\text{lim}}$ ranges from 0.4 to 0.7. However, the ratio of $\Delta\sigma_{PK}$ to $\Delta\sigma_{PW}$ (not the average) can be up to 1.0 in some cases, as shown in Fig. 4.17. Finally, $\Delta\sigma_{PK}$ stresses for Hs < 4.5m is about 75% lower than those found for higher waves, for example, Hs=9.5 m. This means, that even though $C_{wh,\text{lim}}$ (H_S) shows a high frequency of slamming impact for lower H_S (i.e. Hs < 4.5m) the results show that the stresses are relatively lower compared to those found in the higher waves.

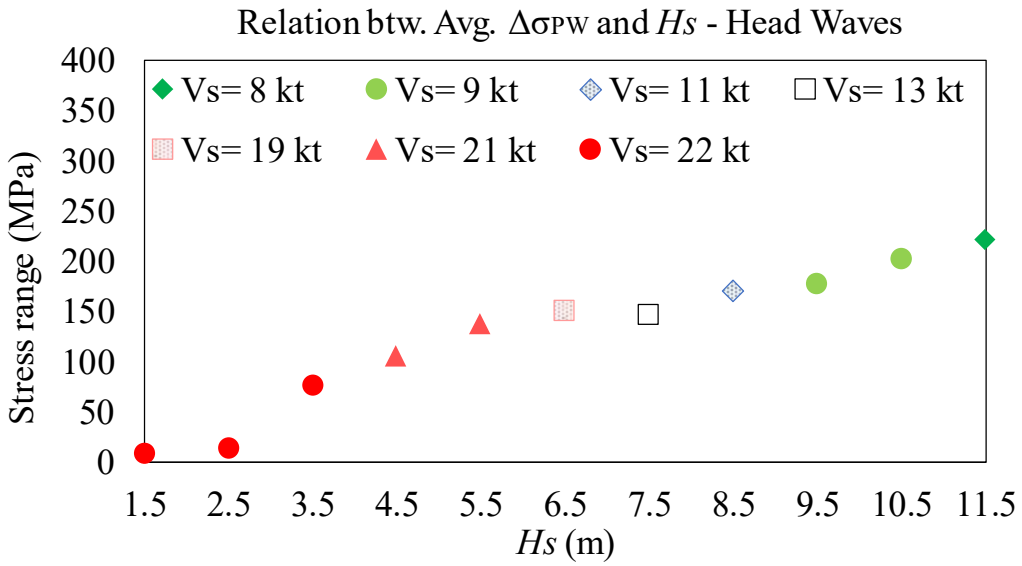

Fig. 4.16 The relation between significant wave height H_S and primary stress range at the limit speed $\Delta\sigma_{PW,lim}$ (H_S) –head seas-.

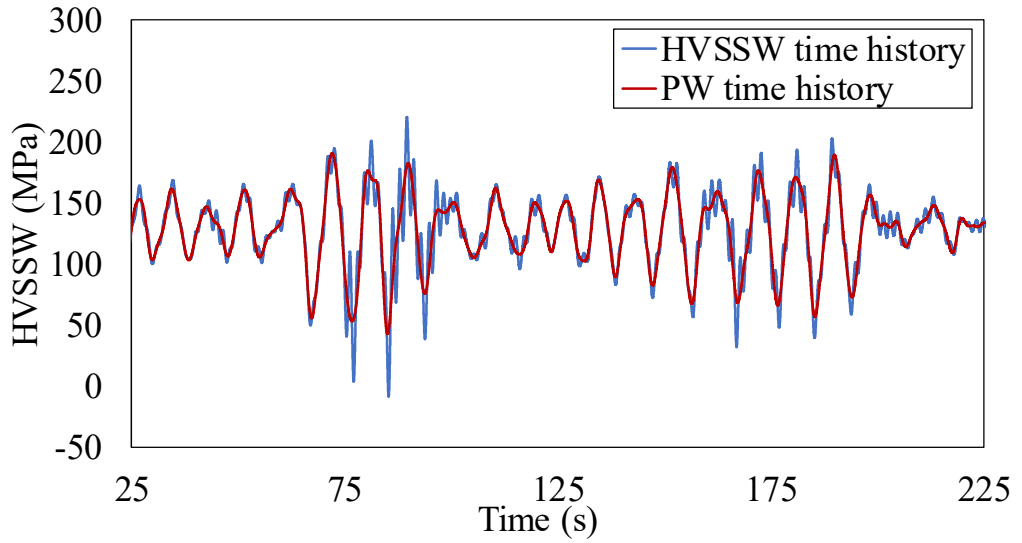

Fig. 4.17 An example of HVSSW and primary wave comparison experienced by 6000 TEU class container ship (*Hs*=6.5m, *Ts* =10.5s, head waves).

The stress range results of the slamming peak stress range and that of the primary wave stress waveform are presented for oblique waves -120 deg- from Fig. 4.18 to Fig. 4.20. As mentioned previously, it is expected that the ship stresses when the heading angle tends to be oblique, becomes lower than that for head seas. The variation of the slamming peak stress range $\Delta\sigma_{PK}$ for short sea with various significant wave heights and ship speeds is presented in Fig. 4.18. *Hs* increases from

left to right, while the *Vs* decreases from left to right. It is observed that $\Delta\sigma_{PK}$ constantly increase with an increment of *Hs*. Further, the variations of $\Delta\sigma_{PK}$ increase while increasing *Hs*. Figure 4.19 introduces the relation between H_S and slamming peak stress range at the limit speed $\Delta\sigma_{PK\_lim}$ (H_S) for oblique waves. It is noted that the average distribution of the per sea state in oblique seas – 120deg seems to follow a similar tendency founded in the head sea cases. $\Delta\sigma_{PK\_lim}$ (H_S) increase has small variations for *Hs* < 4.5 m, while the stresses remain below 10 MPa. Moreover, $\Delta\sigma_{PK\_lim}$ (H_S) almost linearly increase for *Hs* > 5.5 m. Further, the results show that the variations on the slamming peak stress range are more sensitive to the changes on *Hs* than that of *Vs*. Furthermore, it is observed that the average stress levels are comparable to those found in the head wave cases, ranging between 5-135 MPa. Finally, the relation between H_S and primary wave stress range at the limit speed $\Delta\sigma_{PW\_lim}$ (H_S) –oblique waves- is presented in Fig. 4.20. It is observed that equivalent stress ranges to that observed in the slamming peak stress range are found.

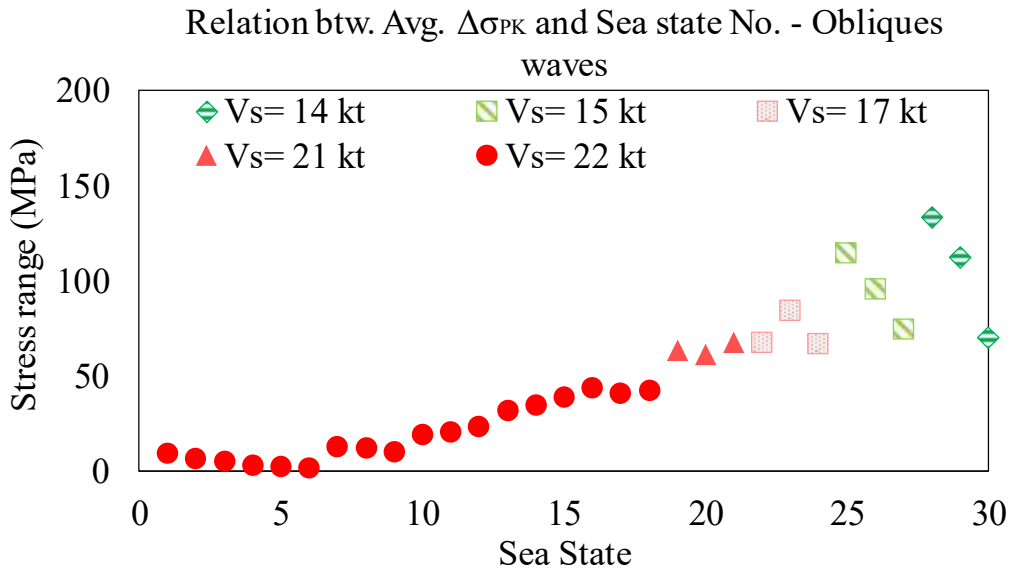

Fig. 4.18 The variation of the slamming peak stress range $\Delta\sigma_{PK}$ for short sea with various significant wave heights and ship speeds –oblique seas-.

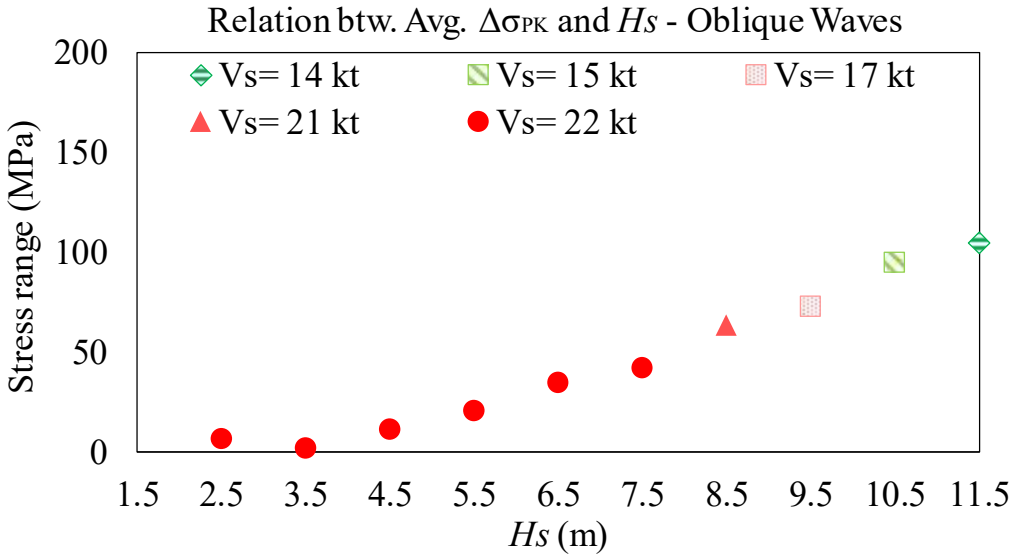

Fig. 4.19 The relation between significant wave height H_S and slamming peak stress range at the limit speed $\Delta\sigma_{PK\_lim}$ (H_S) –oblique waves-.

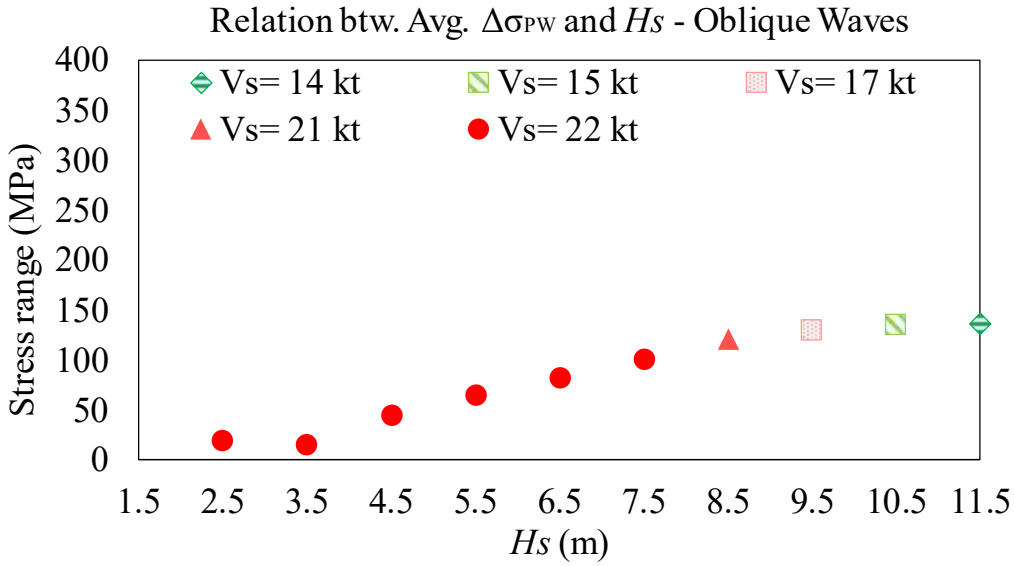

Fig. 4.20 The relation between significant wave height H_S and primary wave stress range at the limit speed $\Delta\sigma_{PW\_lim}$ (H_S) –oblique waves-.

4.3.3 Effect of the whipping vibration on the cumulative damage

The effect of the wave-induced vibrations on fatigue damage is measured by the C_{vib} factor:

$$C_{vib} = \frac{D_{\mathrm{HVSSW}}}{D_{PW}} \tag{4.4}$$

where D_{HVSSW} is the fatigue damage from the stress including the primary wave and hull vibration components while D_{PW} is the fatigue damage due to the primary wave stress. The factor is defined by the respective short-term sea state. The ship design life is assumed to be 20 years. The cumulative fatigue damage calculations are based on the recommendation given by DNVGL-CG-0129 (DNVGL 2015) (see Appendix 2). First, the results for head wave condition are presented. It is considered that this assumption may overestimate the effect of the hull vibrations, since the effect of the wave-induced vibrations is considered to the largest in head waves. The variations of the C_{vib} for short sea with various significant wave height and ship speeds in head waves is presented in Fig. 4.21. The results show that the variations of the C_{vib} per each Hs are larger for Hs < 6.5 m than that for Hs > 7.5 m. The C_{vib} varies between 1-13. Figure 4.22 shows the scatter diagram distribution of factor C_{vib} for the respective short sea. Small quantities are represented in green, whereas larger values are shown in red. As stated above, the resulting vibration due to resonance phenomenon, springing, may increase the fatigue damage even in moderate sea states. It is considered that C_{vib} shows larger variation for Hs < 6.5m since the forward speed may contribute to the springing phenomenon, especially in head seas where the forward speed increases the wave encounter frequency to the level of the hull girder Eigen frequency.

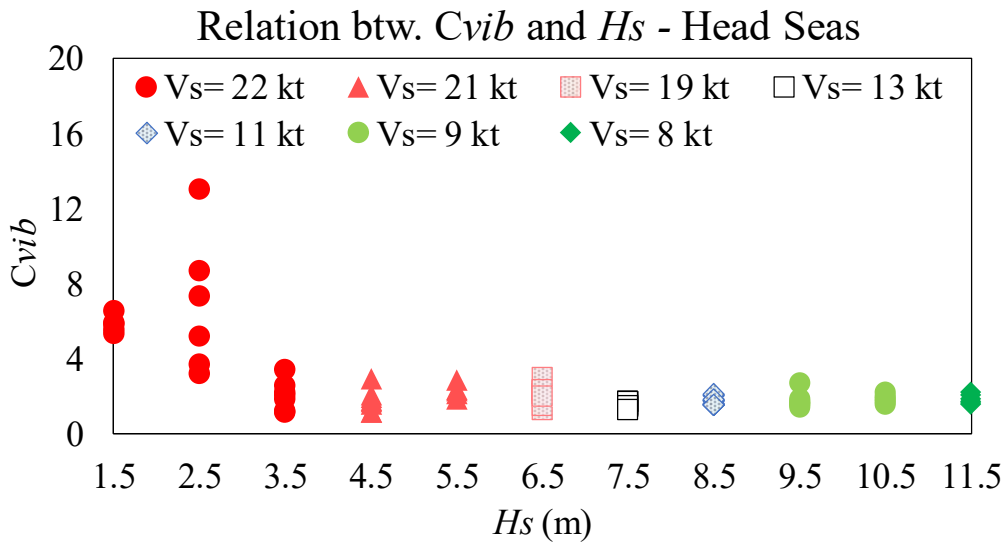

Fig. 4.21 The variations of the C_{vib} for short sea with various significant wave height and ship speeds -head waves-.

Figure 4.23 shows the fatigue damage contributions from the respective short sea, obtained for HVSSW stress. It is noticed that the largest contributions come from mild to rough sea states with significant wave height larger than 6.5 m. In addition, Fig. 4.23 shows that although high C_{vib} are presented in the low significant wave height region (Hs < 4.5 m), the contribution of those seas states to the HVSSW fatigue damage is considerably small compared to that found for mid-high waves (Hs > 5.5 m). Furthermore, Fig. 4.24 presents the fatigue damage contributions from the respective short sea, obtained for the primary wave stresses. Based on these results, it is reasonable that the fatigue damage contribution for the respective short-term sea is higher for larger significant wave heights since the nonlinear loads are more important in high waves as shown in Fig. 4.14.

Cvib per Short Sea in Head Waves													
Vs (kt)	Hs (m)	Ts (sec)											
		3.5	4.5	5.5	6.5	7.5	8.5	9.5	10.5	11.5	12.5	13.5	14.5	15.5
0	12.5													
8	11.5						1.61	1.69	1.94	2.13	2.29	1.76		
9	10.5						1.60	1.63	1.88	2.06	2.26	1.75		
9	9.5						1.48	1.48	1.62	1.70	1.79			
11	8.5						1.60	1.65	1.76	1.79	1.84	1.57		
13	7.5					1.50	1.53	1.59	1.71	1.74	1.73	1.51	1.32	
19	6.5					3.02	2.14	2.15	2.30	2.40	2.38	2.01	1.56	
21	5.5						2.93	2.38	2.34	2.32	2.19	1.91		
21	4.5						2.99	2.14	1.94	1.86	1.75	1.59		
22	3.5						6.51	3.44	2.59	2.26	2.09	1.89		
22	2.5		13.04	8.71	7.37	5.23	3.78	3.23						
22	1.5		6.61	5.98	5.97	5.90	5.63	5.42						
23	0.5													

Fig. 4.22 The variations of the C_{vib} for short sea with various significant wave height and ship speeds -head waves-.

Fatigue damage contribution from each short-term sea, obtained for HVSSW in head waves.													
Vs (kn)	Hs (m)	Ts (sec)											
		3.5	4.5	5.5	6.5	7.5	8.5	9.5	10.5	11.5	12.5	13.5	14.5	15.5
0	12.5													
8	11.5						8.58E-04	1.58E-03	2.29E-03	2.57E-03	2.53E-03	1.58E-03		
9	10.5						6.29E-04	1.17E-03	1.74E-03	1.96E-03	1.98E-03	1.24E-03		
9	9.5						3.98E-04	7.47E-04	1.05E-03	1.14E-03	1.10E-03			
11	8.5						3.46E-04	7.16E-04	1.01E-03	1.07E-03	1.02E-03	6.74E-04		
13	7.5					7.71E-05	2.58E-04	5.55E-04	8.00E-04	8.56E-04	7.86E-04	5.19E-04	4.10E-04	
19	6.5					1.42E-04	3.63E-04	8.31E-04	1.32E-03	1.55E-03	1.44E-03	1.02E-03	5.48E-04	
21	5.5						3.24E-04	5.53E-04	8.11E-04	9.21E-04	8.45E-04	6.65E-04		
21	4.5						1.53E-04	2.29E-04	3.01E-04	3.28E-04	3.00E-04	2.55E-04		
22	3.5						1.42E-04	1.42E-04	1.50E-04	1.44E-04	1.27E-04	1.10E-04		
22	2.5		2.02E-06	1.41E-06	1.32E-06	1.51E-06	1.71E-06	1.73E-06						
22	1.5		1.02E-06	9.41E-07	9.47E-07	9.80E-07	1.01E-06	1.02E-06						
23	0.5													

Fig. 4.23 Fatigue damage contribution from each long-term sea state, obtained for HVSSW stress.

Fatigue damage contribution from each short-term sea, obtained for PW in head waves.													
Vs (kn)	Hs (m)	Ts (sec)											
		3.5	4.5	5.5	6.5	7.5	8.5	9.5	10.5	11.5	12.5	13.5	14.5	15.5
0	12.5													
8	11.5						5.34E-04	9.33E-04	1.18E-03	1.21E-03	1.10E-03	8.99E-04		
9	10.5						3.93E-04	7.20E-04	9.24E-04	9.50E-04	8.74E-04	7.05E-04		
9	9.5						2.69E-04	5.03E-04	6.49E-04	6.68E-04	6.13E-04			
11	8.5						2.16E-04	4.34E-04	5.73E-04	5.95E-04	5.52E-04	4.29E-04		
13	7.5					5.14E-05	1.69E-04	3.49E-04	4.68E-04	4.93E-04	4.55E-04	3.43E-04	3.10E-04	
19	6.5					4.68E-05	1.70E-04	3.87E-04	5.76E-04	6.44E-04	6.03E-04	5.08E-04	3.52E-04	
21	5.5						1.11E-04	2.32E-04	3.46E-04	3.98E-04	3.85E-04	3.48E-04		
21	4.5						5.12E-05	1.07E-04	1.55E-04	1.76E-04	1.71E-04	1.60E-04		
22	3.5						2.19E-05	4.13E-05	5.79E-05	6.35E-05	6.07E-05	5.79E-05		
22	2.5		1.5E-07	1.62E-07	1.797E-07	2.888E-07	4.516E-07	5.37E-07						
22	1.5		1.5E-07	1.58E-07	1.585E-07	1.662E-07	1.8E-07	1.87E-07						
23	0.5													

Fig. 4.24 Fatigue damage contribution from each long-term sea state, obtained for primary wave stress.

The variations of the C_{vib} for short sea with various significant wave height and ship speeds in oblique waves is presented in Fig. 4.25. The effect of the hull vibrations for encountering angle 120 deg is examined by the C_{vib} coefficient for each short sea and presented in Fig. 4.26. It is observed that the C_{vib} coefficient is almost comparable and in some cases higher than that observed in head seas. This is

partially explained because when there is an increment of the frequency of slamming events sailing at head seas, the master may change the ship heading to keep higher ship speed in oblique waves. For the target ship, in oblique waves, the ship speed tends to be higher sailing in higher waves than that found for head waves. For example, for 10.5 m waves, the ship speed in oblique seas is 15 kt and that in head waves is 8 kt. The increase in the ship speed increases the contribution of the non-linear loads and therefore it is reflected in the C_{vib} coefficient presented in Fig. 4.26 for oblique waves cases. This is observed in the fatigue damage accumulated during each short sea shown for HVSSW and primary wave component presented in Fig. 4.27 and Fig. 4.28.

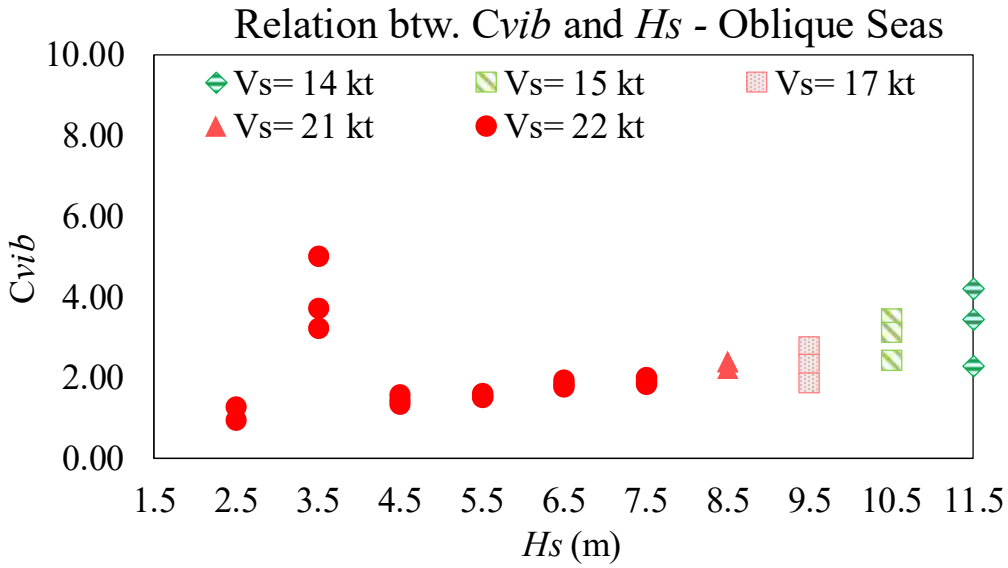

Fig. 4.25 The variations of the C_{vib} for short sea with various significant wave height and ship speeds -oblique waves-.

Cvib per Short Sea in oblique waves												
Vs (kt)	Hs (m)	Ts (sec)										
		4.5	5.5	6.5	7.5	8.5	9.5	10.5	11.5	12.5	13.5	14.5	15.5
0	12.5												
15	11.5									4.17	3.42	2.27	
15	10.5								3.42	3.11	2.39		
17	9.5								2.72	2.31	1.84		
21	8.5						2.40	2.23	2.40				
21	7.5						2.00	1.83	1.88				
22	6.5						1.77	1.81	1.93				
22	5.5						1.51	1.54	1.61				
22	4.5				1.56	1.44	1.33						
22	3.5		5.00	3.69	3.20								
22	2.5		1.26	0.95	0.95								
23	1.5												

Fig. 4.26 The variations of the C_{vib} for short sea with various significant wave height and ship speeds -oblique waves-.

Fatigue damage contribution from each short-term sea, obtained for HVSSW in oblique waves												
Vs (kn)	Hs (m)	Ts (sec)										
		4.5	5.5	6.5	7.5	8.5	9.5	10.5	11.5	12.5	13.5	14.5	15.5
8	12.5												
15	11.5									2.26E-03	1.44E-03	7.46E-04	
15	10.5								2.05E-03	1.31E-03	7.69E-04		
17	9.5								1.19E-03	7.32E-04	4.49E-04		
21	8.5						8.44E-04	7.78E-04	8.25E-04				
21	7.5						4.18E-04	3.76E-04	3.76E-04				
22	6.5						2.00E-04	2.13E-04	2.17E-04				
22	5.5						8.34E-05	8.60E-05	8.39E-05				
22	4.5				2.37E-05	2.38E-05	3.00E-05						
22	3.5		1.04E-06	1.21E-06	1.30E-06								
22	2.5		2.41E-06	1.58E-06	1.95E-06								
23	1.5												

Fig. 4.27 Fatigue damage contribution from each long-term sea state, obtained for HVSSW stress.

Fatigue damage contribution from each short-term sea, obtained for PW in oblique waves												
Vs (kn)	Hs (m)	Ts (sec)										
		4.5	5.5	6.5	7.5	8.5	9.5	10.5	11.5	12.5	13.5	14.5	15.5
8	12.5												
15	11.5									5.41E-04	4.23E-04	3.29E-04	
15	10.5								5.98E-04	4.22E-04	3.21E-04		
17	9.5								4.39E-04	3.17E-04	2.45E-04		
21	8.5						3.52E-04	3.50E-04	3.44E-04				
21	7.5						2.09E-04	2.06E-04	2.00E-04				
22	6.5						1.13E-04	1.17E-04	1.12E-04				
22	5.5						5.54E-05	5.59E-05	5.22E-05				
22	4.5				1.52E-05	1.66E-05	2.26E-05						
22	3.5		2.08E-07	3.28E-07	4.05E-07								
22	2.5		1.91E-06	1.66E-06	2.06E-06								
23	1.5												

Fig. 4.28 Fatigue damage contribution from each long-term sea state, obtained for primary wave stress.

4.4 Verification with Onboard Measurements

The main objective of this section is to verify the validity of the slamming impact detection methodology presented above applied to full-scale measurements. Herein are presented the characteristics of the whipping occurrence probability evaluated from onboard records measured in a 9000 TEU class container carrier. Records for 6 months, between October 2014 - October 2015, were examined while sailing in a worldwide trading route that includes the North Atlantic Ocean as shown in Fig. 4.29. The ship was equipped with a weather routing system to guide the ship's navigation in order to avoid harsh environments. The duration of each sea state measured data is 1-hour. The sampling frequency is 20 Hz. All strain measurements have been converted into deck stress for the amidships section. Examples of measured stresses are shown in Fig. 4.30 during a winter voyage and Fig. 4.31 during an autumn voyage. The primary wave response is obtained by pass filtering the HVSSW time histories to include only the energy at frequencies in the primary wave range with upper cutoff frequency 0.30 Hz. After the primary wave stress is obtained, by high-pass filtering the original signal the hull vibration stress component is obtained. The upper cutoff frequency for PW stress filtering is the same as the lower cutoff frequency for HV stress filtering, see Fig. 4.32. Responses above 1.0 Hz are also removed.

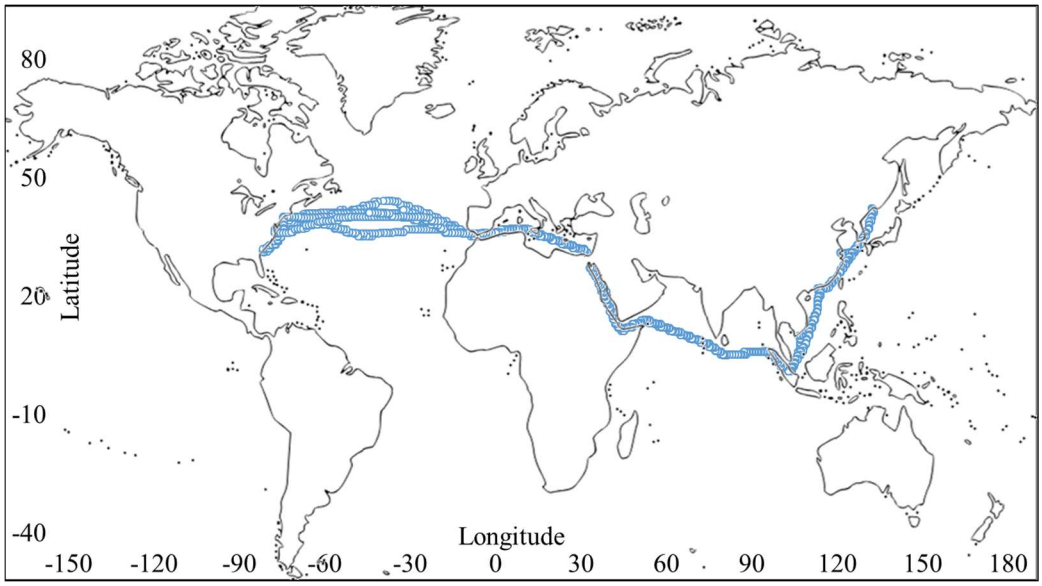

Fig. 4.29 Worldwide sailing route during the full-scale measurement campaign.

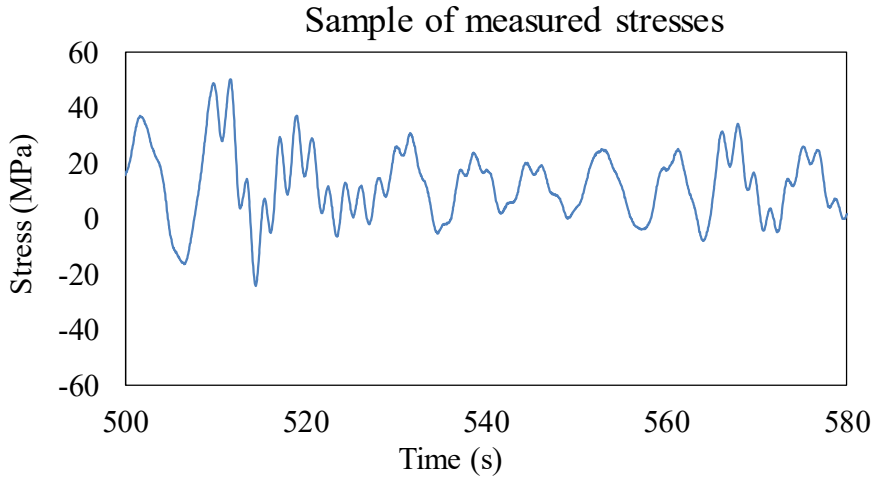

Fig. 4.30 An example of the measured stresses during a winter voyage.

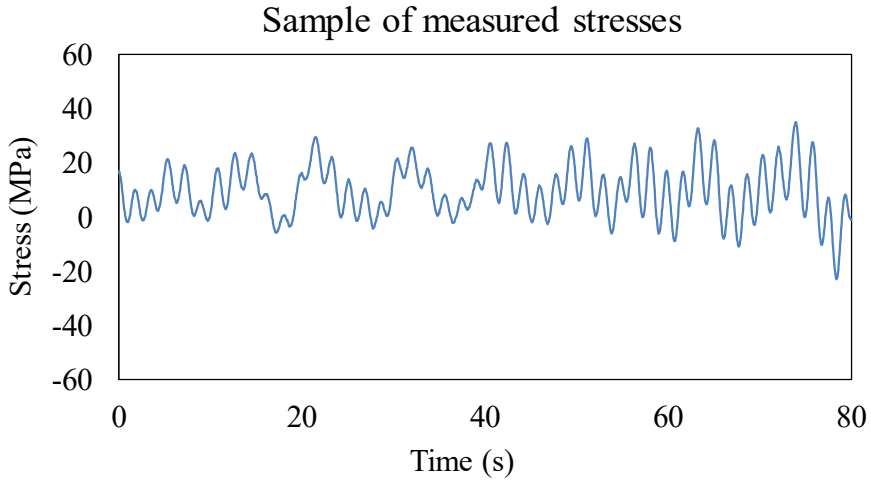

Fig. 4.31 An example of the measured stresses during an autumn voyage.

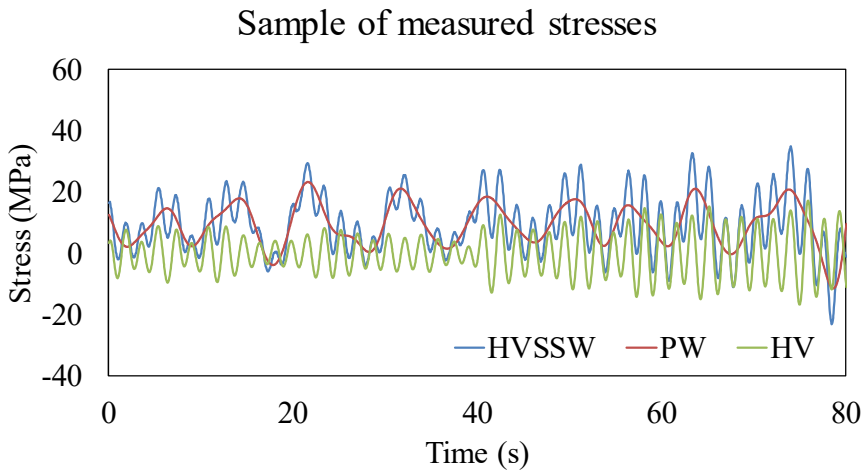

Fig. 4.32 Sample of HVSSW (blue line), HV (green line) and PW (red line) stress signals measured in the 9000 TEU class container ship.

4.4.1 Occurrence frequency of whipping vibration

The occurrence frequency of whipping interval is examined following the methodology presented in sections 4.1 and 4.2. The threshold variable a is set to1.5. First, C_{wh} is evaluated for each measured data. It is considered that the original measured data is organized in bins according to their wave height and wave period. For example, a measured data with wave height 4.7 m and wave period 8.3 s correspond to a bin with wave height 4.5 m and wave period 8 s, respectively. Then, the average C_{wh} is calculated for each Hs class. In this manner Fig. 4.33 is constructed. Figure 4.33 shows that C_{wh} slightly decreases for Hs < 3.5 m, while increase constantly for Hs ≥ 4.5 m. In general, while Hs increase the average C_{wh} becomes smaller. Further, C_{wh} varies between 0.20-0.40. In other words, the results suggest that the combined effect of the hull vibration components have much influence on the C_{wh} in the lower Hs range (Hs < 3.5 m). Moreover, it is found that the average C_{wh} imply that whipping may happen once every 3-5 primary waves. Finally, these results show the validity of the proposed methodology to evaluate the occurrence frequency of whipping vibration applied in onboard measurements.

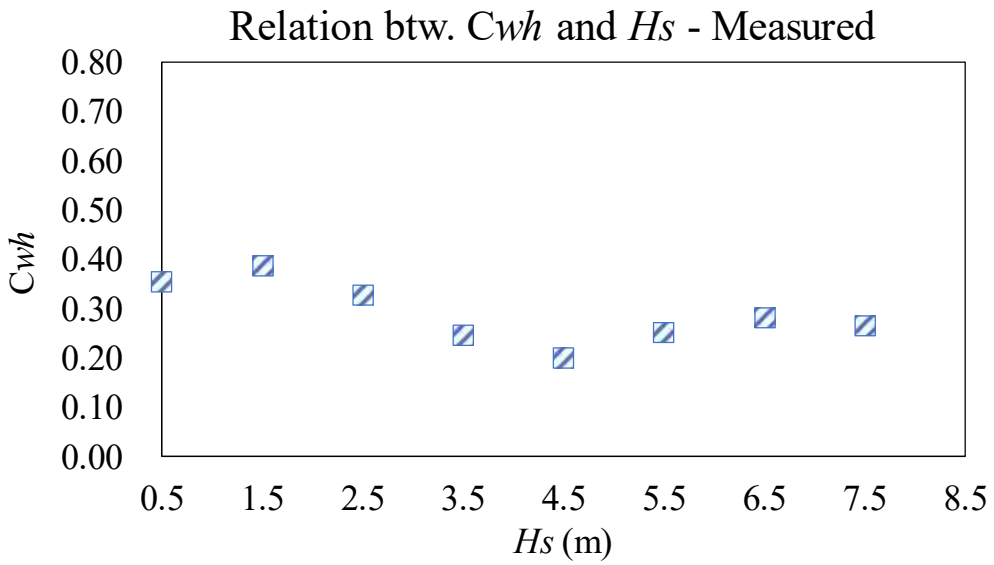

Fig. 4.33 The relation between significant wave height H_S and coefficient of whipping interval C_{wh}.

4.4.2 Slamming impact stress range

The relation between the significant wave height H_S and stress ratio, of $\Delta\sigma_{PK}$ and $\Delta\sigma_{PW}$, is presented in Fig. 4.34. The stress ratio $\Delta\sigma_{PK}/\Delta\sigma_{PW}$ shows the magnitude of the hull vibration stress component compared to that of the primary wave component. The stress ratio varies from 0.47 to 0.87. It is observed that the slamming impact stress ranges $\Delta\sigma_{PK}$ examined from the onboard measurements are nearly constant for waves Hs < 2.5 m, while it is almost comparable to $\Delta\sigma_{PW}$ for 4.5 m waves. After 4.5 m, the $\Delta\sigma_{PK}$ slightly decreases. This is explained to a certain extent by the variation of $\Delta\sigma_{PK}$ with Hs examined in the operational recorded data that shows that the heading angle changes tended to be oblique seas for waves larger than 4.5 m, preventing sailing in head sea condition while increasing the ship speed.

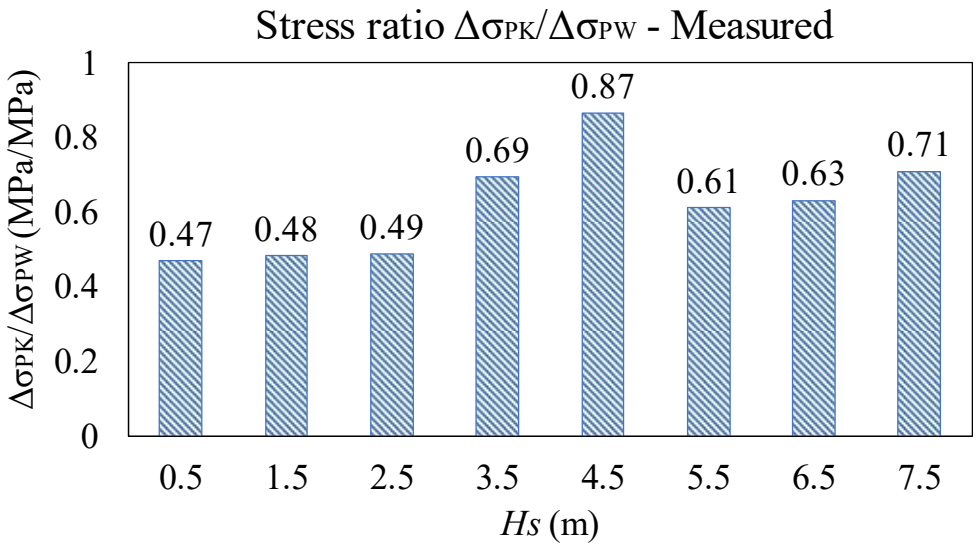

Fig. 4.34 The relation between the stress ratio of $\Delta\sigma_{PK}/\Delta\sigma_{PW}$ and *Hs* from onboard measurements.

4.4.3 Effect of the whipping vibration on the cumulative damage

The fatigue damage for the HVSSW and that for the primary wave are calculated based on the onboard records. Then, the C_{vib} factor is examined. Figure 4.35 shows the variations of the C_{vib} for short sea with various significant wave height from measurements. It is observed that the C_{vib} varies between 2-15. Although that C_{vib} means a larger contribution of the hull vibration to the total accumulated fatigue damage, it is observed from Fig. 4.36 and Fig. 4.37 that the cumulate damage for 1.5 m waves are considerably smaller than those found for waves larger, for example, 3.5 m. Additional to the hull vibration component contribution to the cumulative damage in low waves (springing and whipping), other high-frequency excitation sources may contribute to uncertainties in the measurements under low waves, such as noise, motors, etc.

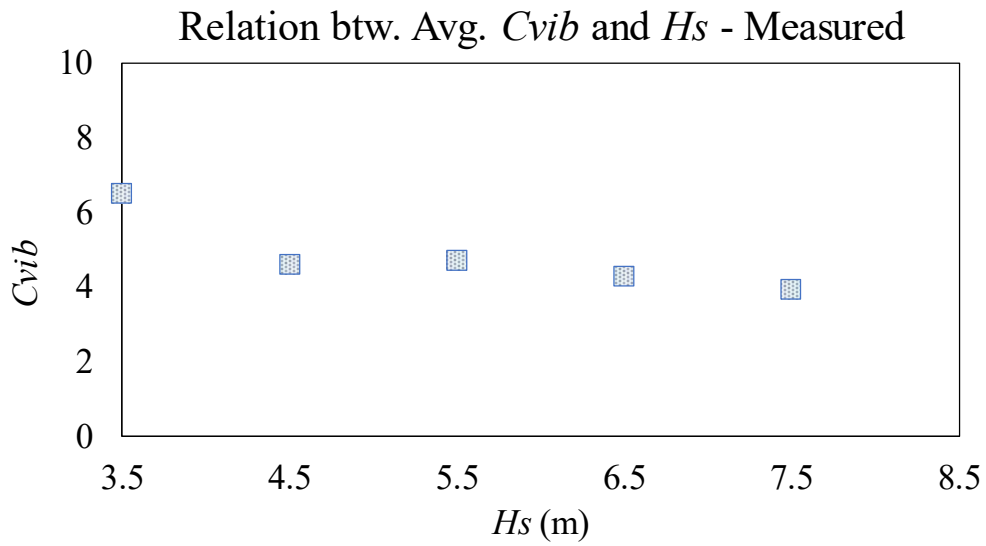

Fig. 4.35 The variations of the C_{vib} for short sea with various significant wave height.

Furthermore, the fatigue damage contribution from each sea state recorded, obtained for HVSSW and primary wave stress are presented in Fig. 4.36 and 4.37, respectively. The red-colored cells show the sea state with the highest fatigue cumulative damage, while the green color represents the smallest values. It is noted that the sea state that contributes the most to the total fatigue damage ranges between 3.5-6.5 m waves and 8-11 s wave periods. Furthermore, the contribution to the total damage for the sea states with waves below 2.5 m is much smaller than that sea states that contribute the most to the total cumulative damage. The same trend is observed for the damage contribution from each sea state, obtained for the primary wave stress presented in Fig. 4.37.

Total HVSSW damage per sea state - 9000 TEU class container carrier														
Hs (m)	Ts (sec)													
	2	3	4	5	6	7	8	9	10	11	12	13	14	15
8.5														
7.5									5.26E-06					
6.5								3.06E-07	7.32E-05	1.89E-04				
5.5								1.32E-04	1.54E-04	1.25E-04				
4.5						1.19E-07	4.17E-05	5.36E-04	2.88E-04	1.84E-04				
3.5						3.79E-05	3.11E-04	3.24E-04	1.72E-04	7.04E-05				
2.5					5.40E-06	2.17E-05	3.22E-05	7.60E-05	8.76E-05	1.48E-06	1.09E-06	1.09E-06	3.95E-07	1.75E-07
1.5			3.65E-10	8.12E-06	2.63E-05	3.06E-05	8.40E-06	6.16E-06	8.26E-06	1.39E-05	6.05E-07	2.39E-07		
0.5		6.07E-06	3.24E-05	2.03E-05	2.44E-05	1.99E-05	6.43E-06	7.16E-06	9.70E-08	6.51E-06	4.29E-08			

Fig. 4.36 Fatigue damage contribution from each sea state, obtained for HVSSW stress.

Total PW damage per sea state - 9000 TEU class container carrier														
Hs (m)	Ts (sec)													
	2	3	4	5	6	7	8	9	10	11	12	13	14	15
8.5														
7.5									1.40E-06					
6.5								1.78E-07	2.87E-05	2.36E-05				
5.5								2.09E-05	5.07E-05	1.48E-05				
4.5						3.96E-08	9.88E-06	1.16E-04	7.75E-05	2.83E-05				
3.5						5.65E-06	5.39E-05	6.44E-05	6.08E-05	9.36E-06				
2.5					1.38E-06	4.75E-06	9.11E-06	1.89E-05	2.10E-05	9.00E-07	5.90E-07	6.15E-07	3.16E-07	1.42E-07
1.5			4.82E-11	1.58E-07	1.38E-06	2.66E-06	3.35E-06	2.41E-06	2.23E-07	1.59E-06	3.31E-07	9.89E-08		
0.5		9.34E-11	1.68E-09	7.06E-08	3.70E-07	1.32E-07	1.83E-07	1.52E-07	6.11E-08	9.72E-11	2.76E-08			

Fig. 4.37 Fatigue damage contribution from each sea state, obtained for the primary wave stress.

4.5 Application of the Stochastic Characteristics of Whipping Vibration for HFE Fatigue Tests

From NLHEA results on slamming impact's occurrence frequency and its slamming impact stress range, the characteristics of whipping HVSSW experienced by the target ship (6000 TEU class container), can be simplified as follows when the ship follows weather routing which prevents the speed reduction:

- The slamming impact occurs once in every 4 to 5 primary wave cycles;
- The HVSSW show approximately similar waveform regardless of significant wave height;
- The maximum stress range due to slamming impact can be comparable to the primary wave stress range.

These findings are considered in the determination of a representative waveform for a fatigue test method for welded joints subjected to wave-induced loads with the whipping of being intermittent presented in chapter 5.

4.6 Summary

This chapter described the principles of the probabilistic model for whipping occurrence to examine the stochastic characteristics (amplitude ratio of hull vibration to the primary wave, the ratio of frequencies of hull vibration and primary

wave, slamming's occurrence interval, hull vibration decay time, etc.) based in NLHEA of a 6000 TEU class container ship. Then, the validity of the methodology is confirmed by examining the characteristics of the whipping occurrence probability evaluated from onboard records measured in a 9000 TEU class container carrier.

The relation of the occurrence frequency of whipping vibration, the magnitude of the slamming impact stress range, and the primary wave stress to the short sea with various significant wave heights, ship speeds, and wave condition are presented. Finally, the principal characteristics are designated to characterize a representative waveform for a fatigue test method for welded joints subjected to wave-induced loads with the whipping of being intermittent.

Chapter 5 Fatigue Testing considering Whipping Vibration

Detailed information of the new electric exciter (EE) driven plate bending vibration (PBV) fatigue testing machine which can carry out fast and low-cost fatigue tests of welded joints subject to high-frequency superimposed wave loading is given in this chapter. Then, the welded joint specimen and the location of the strain gages for the fatigue testing are shown. In section 5.3, the constant amplitude (CA) fatigue test results are presented to confirm the CA fatigue test results of the EE-driven PBV apparatus. After that, the conditions and results for constantly whipping superimposed fatigue tests are introduced.

Finally, the validity of the RFCC for real ship structure subject to HVSSW loading is examined by carrying out fatigue tests with stress histories which emulate intermittent occurrence of hull vibration.

5.1 Electric Exciter Driven PBV Fatigue Testing Machine

For fatigue tests of welded joints, conventional fatigue testing machines of closed-loop systems (for example hydraulic machines) are widely used. Drawbacks using these machines lies on the expensive initial and running costs. Further, when wave loads with high-frequency vibration are simulated, the running cost and testing time jump to unacceptable levels. This section shows the new fatigue testing machine, which can carry out fast and low-cost fatigue tests of welded joints subject to wave loads considering high-frequency hull vibration. The machine uses a digital controlled high-power EE and is designed for PBV type fatigue tests.

The PBV welded joint specimen is excited by a rod which connects the specimen and the exciter's driving shaft. The driving rod is attached to the specimen in the same position as the gravity center of the vibrator (motor with eccentric mass - EM)

for PW excitation in the EM-driven tests. A load cell is inserted between the exciter's driving shaft and the rod to measure the exciting force. Figure 5.1 shows the dimension of the testing machine and the set plan for fatigue loading tests. In Fig. 5.2 it is presented the EE-driven PBV testing machine developed for this research.

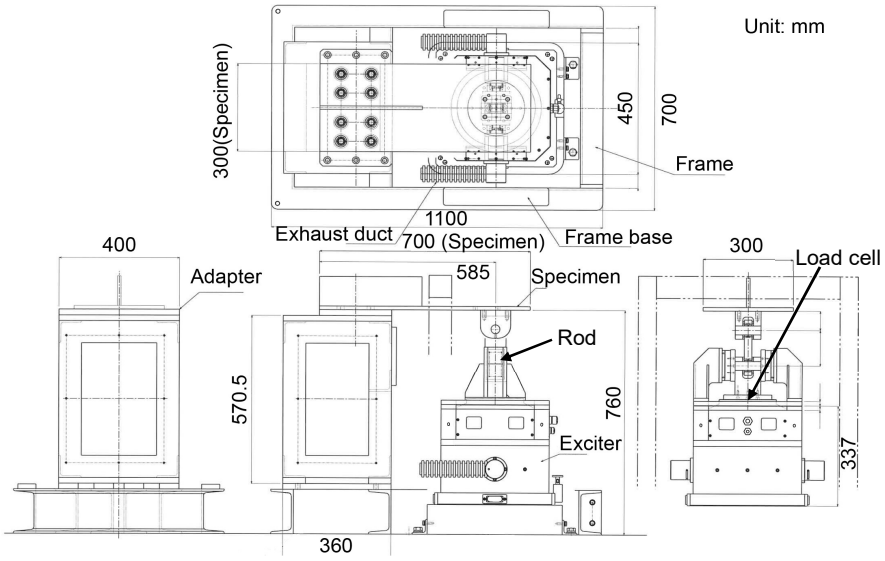

Fig. 5.1 Plans of the EE-driven PBV testing machine used in intermittently whipping superimposed loading tests.

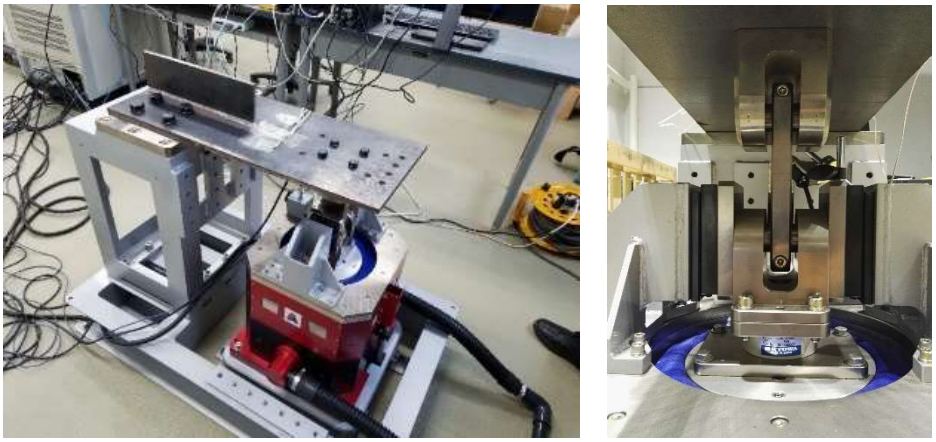

a) EE-driven PBV testing apparatus **b)** load cell

Fig. 5.2 Photos of the EE-driven PBV testing machine.

The main characteristics of the EE-driven PBV testing machine are:

- The excitation force is always proportional to the input current, and this makes the actuator load follow the input waveform precisely;

- User-defined arbitrary waveforms which include frequency element higher than 100 Hz with the nominal stress range larger than 200 MPa, which cause fatigue failure of the weld, can be applied;
- It is easy to apply stress waveform with arbitrary amplitude, which is analogous to the applied HVSSW;
- Excitation up to 3,920 N in a frequency range up to is 5 kHz can be applied.

5.2 Test Specimens

Fatigue tests are carried out for out-of-plane gusset welded joint specimens made from 12 mm-thickness AH32 ship structural steel plates. Size and shape of specimens are shown in Fig. 5.3. The left end of a specimen is fixed onto the frame base while the free end was excited by the EE (exciter). Fatigue cracks initiate at the weld toe near the main plate's centerline. The crack propagates along with the weld bead during a certain period, then turns and propagates into the main plate. Let $\Delta\sigma$ be the nominal bending stress range and N_b be the number of load cycles at which the crack propagation path turns into the main plate.

Plate surface strains are measured by 4 strain gages arranged at points Ch1~4 in Fig. 5.3. The responses of Ch1 and Ch2 include the local stress concentration due to the weld. Responses of Ch3 and Ch4 can be treated as the nominal bending strains.

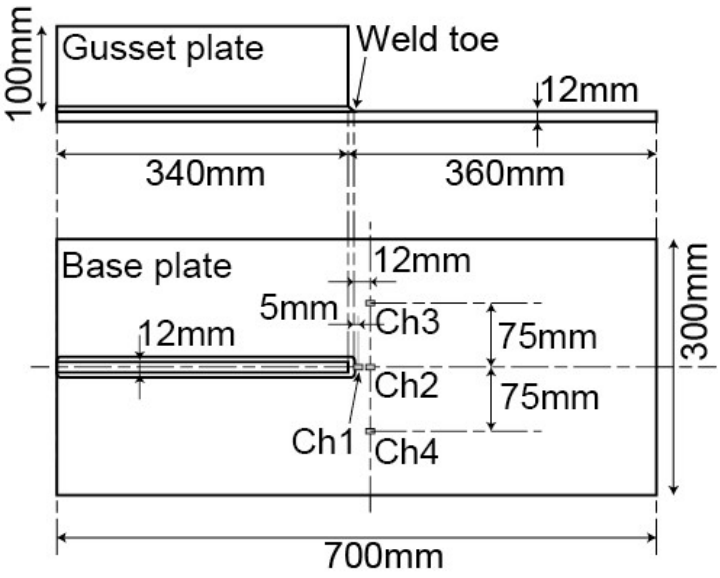

Fig. 5.3 The out-of-plane gusset welded joint specimen (unit: mm).

5.3 Constant Amplitude Fatigue Tests

CA fatigue loading is defined as fatigue under cyclic loading with a constant amplitude and a constant mean load. Sinusoidal loading is a classic example of CA fatigue loads applied in many fatigue tests. In previous chapters, it has been pointed out that ocean-going ships are subjected to variable-amplitude (VA) loading, which can be a rather complex load-time history, see for example Fig. 4.1.

The CA fatigue tests performed by using EM-driven PBV testing machines as reported in Osawa et al. (2014, 2015) are chosen as a reference for the CA fatigue test. Fig. 5.4 shows the changes in strain amplitudes with loading cycles measured in the CA test with $\Delta\sigma$=98.0 MPa.

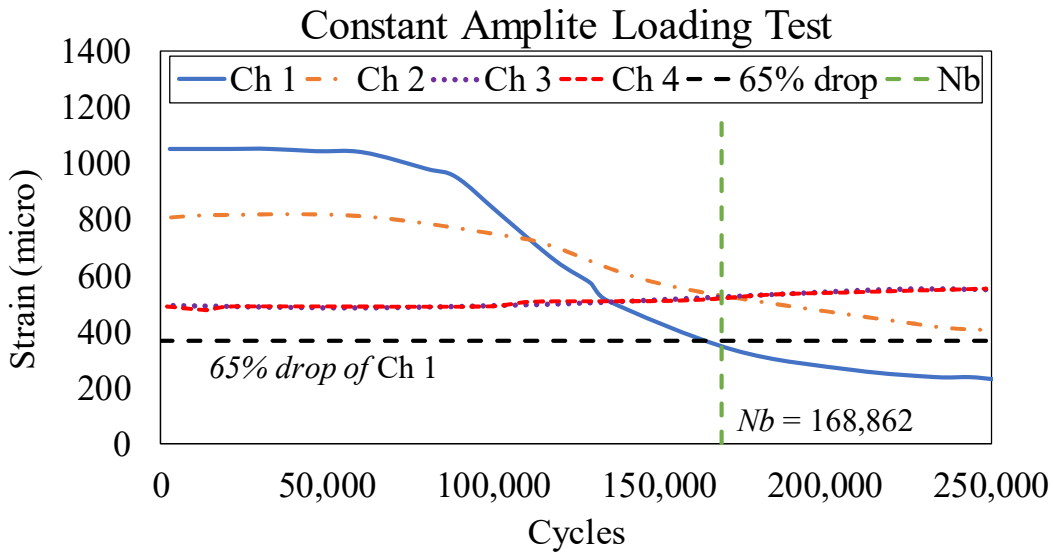

Fig. 5.4 Changes in strain amplitudes during a constant amplitude loading test (Δσ=98.0 MPa, EM-driven). Adapted from Osawa et al. (2015).

As it is shown in Fig. 5.4 strains affected by the local stress concentration (Ch1 and Ch2) decrease substantially with cycles after a certain period while nominal strains (Ch3 and Ch4) increase slightly. Δσ is determined from the initial strain amplitudes of Ch3 and Ch4. As observed in this figure, Ch1 strain amplitude showed about 65% drop at N_b (determined by visual inspection) in all constant amplitude tests reported in the literature (Osawa et al. 2015). The strain decline is caused by crack propagation and the decrease in ligament width. As Yamada et al. (2006) reported, the failure lives of welded joint specimens measured by conventional (hydraulic) fatigue testing apparatus almost agreed with the number of cycles to the 65% drop of host spot strain range measured in PBV fatigue tests. Further, the relationship between Δσ and N_b is approximated by Basquin's law,

$$\Delta\sigma = CN_b^m \tag{5.1}$$

where, C=3.443 x 10^3 MPa, and m= –0.293.

5.3.1 Fatigue test results

The CA EM-driven PBV fatigue test results are presented as an *S-N* plot in Fig. 5.5. In order to verify the CA fatigue test results of the EE-driven PBV test, results are also plotted in Fig. 5.5 as open round marks. It is observed that the EE-driven test results are within the variability range of EM-driven results. Therefore, *C* and *m* for EM-driven tests are adopted in fatigue damage calculation of EE-driven results. In the following, the CA EE-driven PBV fatigue test results are considered the reference results to examine the variability of the whipping superimposed fatigue tests.

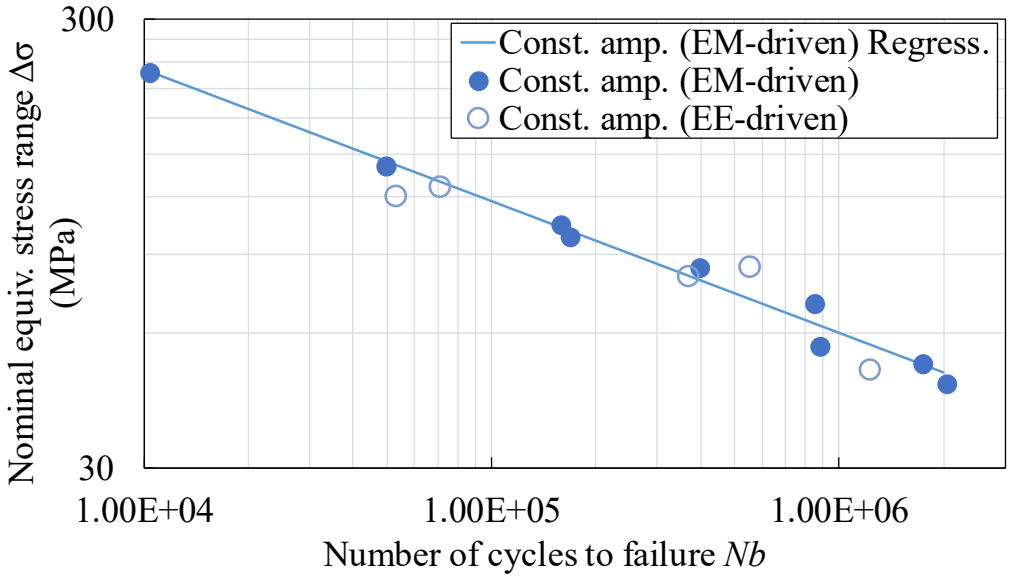

Fig. 5.5 Comparison of CA fatigue test results performed by EM- and EE-driven testing machines.

5.4 Whipping Superimposed Fatigue Tests

This section shows the results of the whipping superimposed loading tests performed by using the EE-driven testing machine developed in this study. The load is applied by performing Proportional-Integral-Differential (PID) control using the load cell's output as the process variable. It is needed to keep high linearity between the load (load cell's output) and the nominal strain (Ch3 or Ch4 strain gage's output)

because the nominal strain was treated as the loading signal in previous tests performed by the EM-driven machine. In order to verify the linearity, preliminary tests are carried out, and it is found that the high linearity can be achieved when the waveform does not include a frequency component higher than 20 Hz.

Furthermore, the characteristics of HVSSW numerical simulation shown in Section 4.5 experienced by the target 6000 TEU class container carrier are considered for the whipping superimposed fatigue testing conditions as shown in the next subsection. Moreover, the fatigue damage D_{rf} is calculated by modified Miner rule, that is, the fatigue limit is not taken into account. Equivalent stress range $\Delta\sigma_{eq,rf}$ is calculated by the equations below:

$$\Delta\sigma_{eq,rf} = C\left(\frac{N}{D_{rf}}\right)^{m} \tag{5.2}$$

where C and m are the coefficient and exponent of Eq. (5.1), and N is the number of PW cycles.

5.4.1 Testing conditions

In order to emulate the superimposed whipping waveform under the restriction condition for the frequency component, the drive force's waveform parameters listed in Table 5.1 are adopted. The 'damping time' in Table 1 is the number of PW in which the whipping wave's amplitude shows a 99% drop. The waveforms of setpoint (SP) signal (load) and that of measured nominal strain (Ch3 strain) are compared in Fig. 5.6. It is observed that good linearity between load and strain is established, and the waveform's characteristics are almost the same as those of the above mentioned simplified HVSSW. Hereafter, this strain waveform is called 'reference whipping superimposed waveform'.

Table 5.1 Waveform parameters of the reference whipping superimposed waveform.

Item	Primary wave - PW		Hull vibration - HV			Slaming intvl (cycle)	Damping time (cycle)	$\Delta\sigma_{eq,rf}$
	$\Delta\sigma_{PW}$ (Mpa)	Freq (Hz)	$\Delta\sigma_{HV}$ (Mpa)	Freq (Hz)	Phase diff (x π rad)			
Whipping	2.5	4	2.5	16	0.27	5	12	116.8

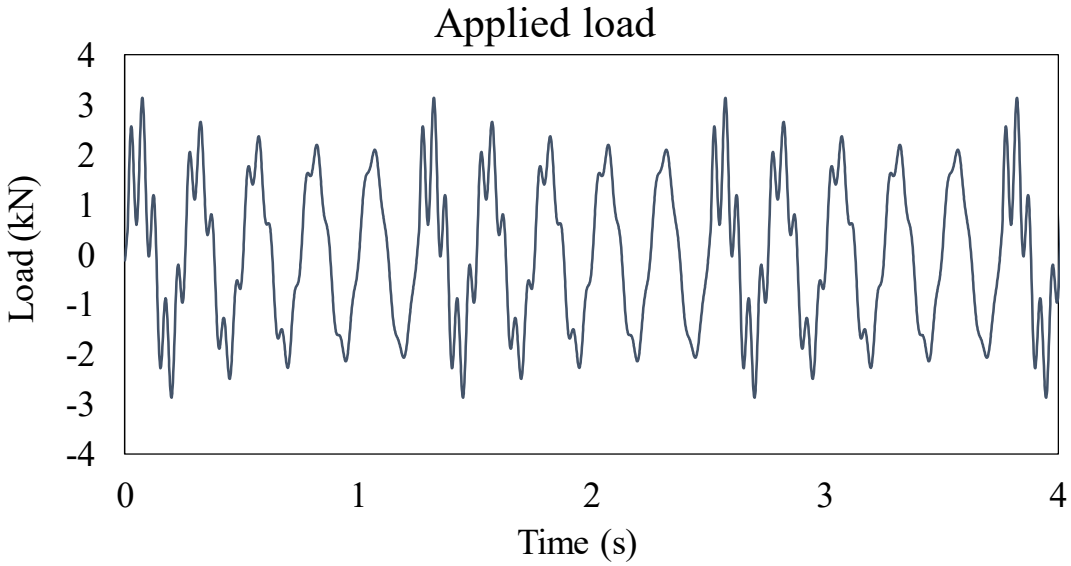

(a) The setpoint waveform for the applied load, herein called 'reference whipping superimposed waveform'.

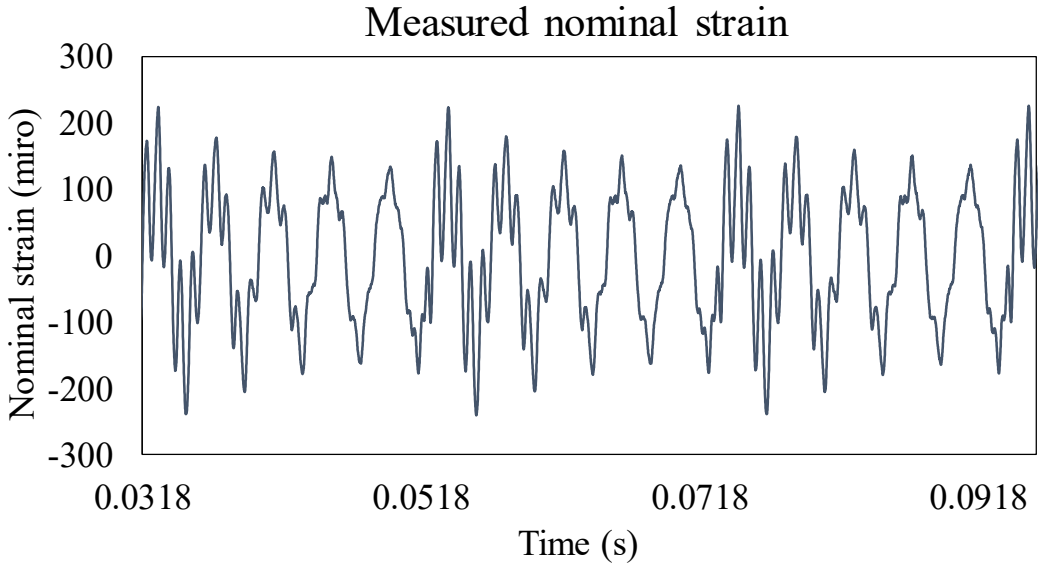

(b) Measured nominal strain waveform

Fig. 5.6 Load (a) and nominal strain (b) waveforms of reference whipping superimposed load.

5.4.2 Constantly whipping superimposed loading tests

Constantly whipping superimposed loading fatigue tests are carried out by using stress waveforms proportional to the reference waveform shown in Fig. 5.6. The loading conditions are listed in Table 5.2. In these tests, the number of PW cycles, N_{PW}, is treated as N. The measured failure lives (N_b), fatigue damages D_{rf} and equivalent stress range $\Delta\sigma_{eq,rf}$ is shown in Table 5.2.

Table 5.2 Loading conditions, fatigue lives and accumulated damage of constantly whipping superimposed loading tests.

test ID	Primary wave - PW		Hull vibration - HV			Slaming intvl (cycle)	Damping time (cycle)	$\Delta\sigma_{eq,rf}$ for SUP cycles	Nb (cycle)	Nc (cycle)	D_{rf}	$\Delta\sigma_{eq,rf}$ for whole life (MPa)
	$\Delta\sigma_{PW}$ (MPa)	Freq (Hz)	$\Delta\sigma_{HV}$ (MPa)	Freq (Hz)	Phase diff (x π rad)							
CW-1	85.90	4	85.90	16	0.27	5	12	116.80	152,280	28,180	1.523	118.03
CW-2	51.54		51.54					70.08	440,020	154,080	0.824	72.23
CW-3	68.72		68.72					93.44	602,660	205,700	2.296	88.95
CW-4	77.31		77.31					105.12	159,020	22,920	0.921	100.55

Table 5.2 shows that the damage up to failure DUF (D_{rf} up to N_b) for constantly whipping superimposed loadings ranges from 0.824 to 2.296, and the average is around 1.391. These constantly whipping superimposed EE-driven PBV fatigue test results are presented as an S-N plot of $\Delta\sigma_{eq,rf}$ and N_b by open triangular marks in Fig. 5.7. This figure also indicates the reference CA S-N curve (solid line).

Results from the EM-driven PBV testing machine, as reported in Osawa et al. (2014, 2015), are similar to those found here for the EE-driven PBV testing machine. This means that the fatigue life can be predicted with fair accuracy by RFCC in which modified Miner rule and CA S-N curve are adopted. It is also shown that RFCC leads to a little conservative estimate of failure lives under conditions chosen.

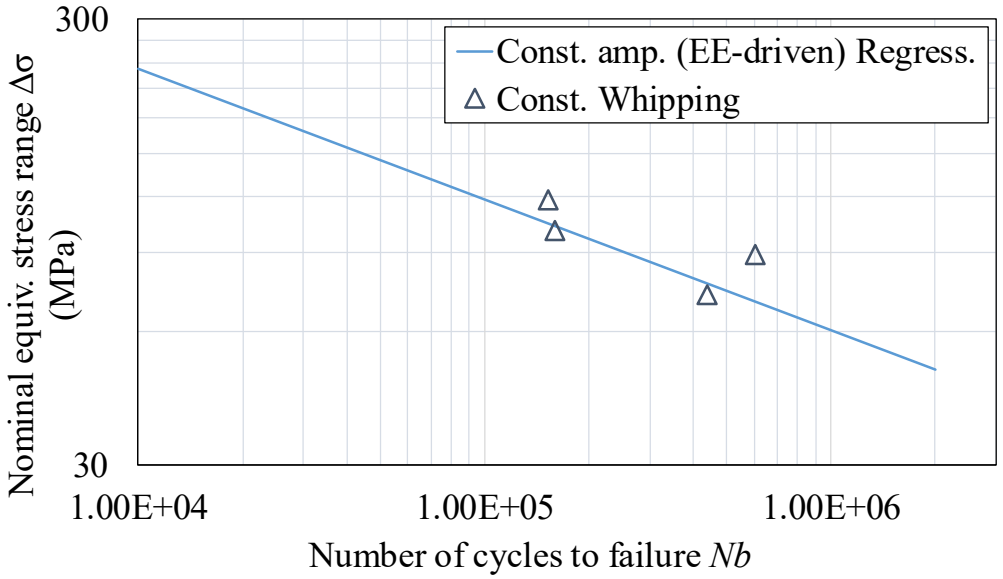

Fig. 5.7 The relation between $\Delta\sigma_{eq,rf}$ and N_b for constantly whipping superimposed fatigue tests.

5.4.3 Intermittently whipping superimposed loading tests

The stochastic characteristics of whipping HVSSW from the NLHEA simulation shows that slamming impact occurs once in every 3 to 5 PW cycles. This means that the whipping vibration is not constant on ships. Therefore, to emulate the variability of the whipping vibration, intermittently whipping superimposed loading fatigue tests are carried out by using the EE-driven PBV testing machine.

To define the testing waveform, a combination of n_{SUP} superimposed (SUP) cycles and subsequent n_{CA} constant amplitude (CA) cycles called 'load set' needs to be defined (see Fig. 5.8). $n_{total} = n_{SUP} + n_{CA}$ is the total number of cycles in one load set. Let $\Delta\sigma_{eq,rf}$ in SUP cycles be $\Delta\sigma_{SUP}$ and that in CA cycles $\Delta\sigma_{CA}$. Here, $\Delta\sigma_{CA}$ is chosen so that $\Delta\sigma_{CA}$ nearly equals $\Delta\sigma_{SUP}$. This case is called “IF (Intermittently superimposed with Fixed $\Delta\sigma_{eq}$)” series.

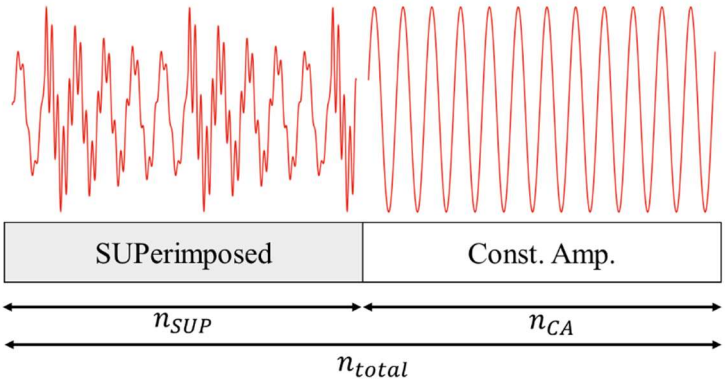

Fig. 5.8 Load set applied in intermittently superimposed loading tests.

Let N_0 be N_b estimated by CA *S-N* curve (Fig. 5.5) for the case with $\Delta\sigma=\Delta\sigma_{SUP}$. Load sets are applied repeatedly until the Ch1 strain amplitude shows a 65% drop. (n_{SUP}, n_{CA}) are chosen so that n_{SUP}/n_{total} is 0.5, and n_{total}/N_0 is 1/4. The loading conditions are listed in Table 5.3. In the same manner as the constantly superimposed cases, the number of PW cycles is treated as N in both SUP and CA cycles. The measured failure lives (N_b), DUF (D_{rf} up to N_b) and $\Delta\sigma_{eq,rf}$ for SUP cycles and that for whole life are shown in Table 5.3.

Table 5.3. Loading conditions, fatigue lives and accumulated damage of intermittently whipping superimposed loading tests.

test ID	Primary wave - PW		Hull vibration - HV			Slaming intvl (cycle)	Damping time (cycle)	$\Delta\sigma_{eq,rf}$ for SUP cycles	*Nb* (cycle)	*Nc* (cycle)	D_{rf}	$\Delta\sigma_{eq,rf}$ for whole life (MPa)
	$\Delta\sigma_{PW}$ (MPa)	Freq (Hz)	$\Delta\sigma_{HV}$ (MPa)	Freq (Hz)	Phase diff (x π rad)							
IF-1	85.90	4	85.90	16	0.27	5	12	116.80	136,420	30,940	2.172	135.25
IF-4	85.90		85.90					116.80	166,520	25,600	1.885	122.37
IF-5	51.54		51.54					70.08	512,960	92,400	1.067	74.50
IF-6	44.67		44.67					60.74	977,980	190,300	1.003	60.56
IF-7	38.66		38.66					52.56	2,693,800	749,600	1.833	53.70

It is observed in Table 5.3 that D_{rf} for intermittently whipping superimposed loadings ranges from about 1.003 to 2.172, and the average is 1.592. Intermittently whipping superimposed EE-driven PBV fatigue test results are presented as an *S-N* plot of $\Delta\sigma_{eq,rf}$ and N_b in Fig. 5.9 using open square marks.

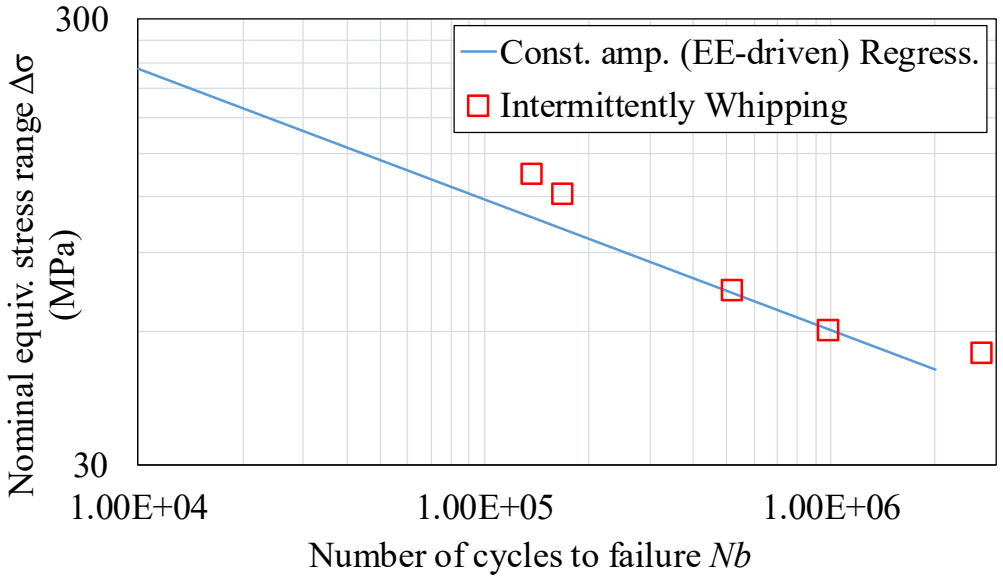

Fig. 5.9 The relation between $\Delta\sigma_{eq,rf,}$ and N_b for intermittently whipping superimposed fatigue tests.

This result is similar to those of the constantly whipping superimposed loading tests in section 5.3, that is, the fatigue life could be predicted with fair accuracy by RFCC in which modified Miner rule and CA *S-N* curve was adopted. It is shown that RFCC leads to conservative estimates of failure lives, and it is likely that the mean D_{rf} of intermittently superimposed cases is larger than that of constantly superimposed cases under conditions chosen. Although in the mechanism of fatigue crack growth during each load cycle there still exist several unknown phenomena, it is considered that under variable loading condition, in general, a load interaction (e.g. retardation/acceleration of the crack growth) occurs every cycle, resulting in quite a different situation in the overall loading cycles. The traditional fatigue life evaluation method based on the *S-N* curve approach with RFCC has been proved to give reasonable fatigue life estimation when considering constant amplitude loading. However, under variable amplitude loading conditions, the primary factor causing variability of fatigue life is the sequence of load cycles.

The preliminary results suggest that the RFCC conservative estimates of fatigue life under superimposed loading tests are partially explained since

retardation/deceleration in fatigue crack growth and variable amplitude loading when small stress cycles followed a high level of applied stress cycles, which is typical in the case of whipping after the slamming impact. The retardation of the fatigue crack growth is apparently lead by an increase of the thickness of the plastic wake on the crack surface after a large level of applied stress. Therefore, it is no expected the retardation effect under constant amplitude loading. On the other hand, there still debate on this topic since Fricke et al. (2014) reported that for a limited number of fatigue tests with measured stress history, which included primary wave and whipping vibration stress components, show that fatigue life based on the *S-N* curve approach with RFCC tends to be overestimated.

As mentioned previously, there are still some mechanisms of fatigue crack growth during each load cycle that are unknown. Therefore, in order to have a better understanding of the effect of the whipping vibration on the fatigue life when considering RFCC, it is needed to perform a more large number of fatigue test that includes a wide range of conditions which include different stress ratios between superimposed stress waveform and the primary wave stress, different stress levels, etc. Furthermore, studies based on numerical simulation of fatigue crack propagation with the consideration of hull vibration superimposed stress waveforms would be of great interest in order to enhance the comprehension of the effect of the high-frequency stress effect on the fatigue assessment of ship structures.

5.5 Summary

First, this chapter introduces the new EE-driven PBV fatigue testing machine that is adapted for intermittently whipping superimposed loading tests. Then, CA fatigue test results of the EE-driven PBV test are shown compared to those reported by Osawa et al. (2015) using an EM-driven PBV testing machine. Furthermore, it is

confirmed that the intermittently whipping superimposed waveforms of driving load and strain generated by the EE-driven PBV testing machine showed good linearity. This means that the actuator load follows the input waveform precisely. After that, the application of the modified Miner rule to RFCC in which whipping occurs intermittently is presented.

Chapter 6 Conclusions

6.1 Contribution and Major Findings

In this thesis, a basic methodology for a reliable and quantitative assessment of the fatigue induced by whipping vibration is proposed. The method to examine the stochastic characteristics of hull vibration superimposed stress waveform (HVSSW) experienced in ship examined by non-linear hydro-elasticity analysis (NLHEA) for various sea conditions/ship speed/heading angle have been proposed. Based on these NLHEA results, the HVSSW which are applied in high-frequency effect fatigue tests is chosen. Then, the validity of the rainflow cycle stress counting (RFCC) for real ship structure subject to whipping superimposed loading is examined by carrying out fatigue tests with stress histories which emulate intermittent occurrence of whipping vibration. The following main findings may be derived from the work of the thesis:

On the probabilistic model for whipping occurrence

- The variations of the frequency of whipping vibration are more sensitive to the changes in the ship speed than that for the wave height.

- In general, the frequency of whipping vibration linearly increases when the ship speed is increased from 10 kt to 22 kt, under the condition chosen. It is considered that the increase is associated with larger pitch motion at a higher speed. Then, increasing the slamming impact occurrence and finally resulting in an increase in the hull vibrations.

- The characteristics of the frequency of whipping vibration can be simplified so that the slamming impact occurs once in every 3 to 5 primary waves cycles.

- The changes on the slamming impact stress range are almost linearly in proportion with the wave height.

- The maximum stress range due to slamming impact can be comparable to the primary wave stress range.

- The proposed method to examine the relationship between the occurrence probability of a slamming induced hull vibration and the sea state is applicable for both numerical simulation and full-scale measurements.

On the fatigue testing considering whipping vibration

- The waveform characteristics are very important for fatigue testing. An approach to defining a 'reference whipping superimposed waveform', with comparable waveform's characteristics as the simplified HVSSW derived from NLHEA is presented.

- The developed electric exciter (EE)-driven plate bending vibration (PBV) fatigue testing machine can apply a given whipping superimposed waveform' to out-of-gusset welded joint specimens with good linearity between load and strain at high speed.

- The fatigue life of out-of-gusset welded joints subject to constantly and intermittently whipping superimposed loadings could be predicted with fair accuracy by RFCC in which modified Miner rule and constant amplitude *S*-*N* curve were adopted.

- It was shown that the RFCC led to conservative estimates of failure lives, and it was likely that the fatigue damage up to the failure of intermittently superimposed cases was larger than that of constantly superimposed cases under conditions chosen.

6.2 Recommendations for Future Works

The following recommendations related to this thesis are:

- It is known that the container ships are more prone to the wave-induced vibrations. However, the wave-induced vibration phenomenon is experienced by another type of vessels. Therefore, more studies are recommended to examine the statistical characteristics of wave-induced vibrations and wave-induced stresses of another type of vessels in order to complement the knowledge and improve the assessment of the structural influence of whipping on the fatigue strength.

- The structural rigidity of ultra-large container ships, having a carrying capacity of over 10,000 TEU, may become relatively smaller than that of the majority of ships currently in operation due to the increased size, and increased length in particular. Then, it is recommended apply the proposed model to bigger ships, especially large-container ships which are more susceptible to wave-induced vibrations.

- Most research studies focused on the effect of whipping on both the extreme load and fatigue damage accumulation. Recently, however, only a few investigate the effects of the whipping vibration on the mechanism of fatigue crack propagation. Studies to investigate the effect of the whipping vibration

on the mechanism of fatigue crack propagation would greatly enhance the understanding of the effect of whipping on the fatigue strength of marine structures.

- This thesis tested a limited number of specimens. It is unclear whether similar results can be found in generality of cases. Thus, it is recommended to continue and carry out numerous fatigue tests under various wave loading cases considering the high-frequency vibration.

Appendix 1: Stress Response Amplitude Operator of a Container Carrier's Structural Member

The stress amplitude operator, also known as RAO, of a container ship's butt weld on the upper deck, is considered in this study. The RAO presented in Fig. A1.1 is determined by the Japanese Ship Research Panel 219 (SR219 1996).

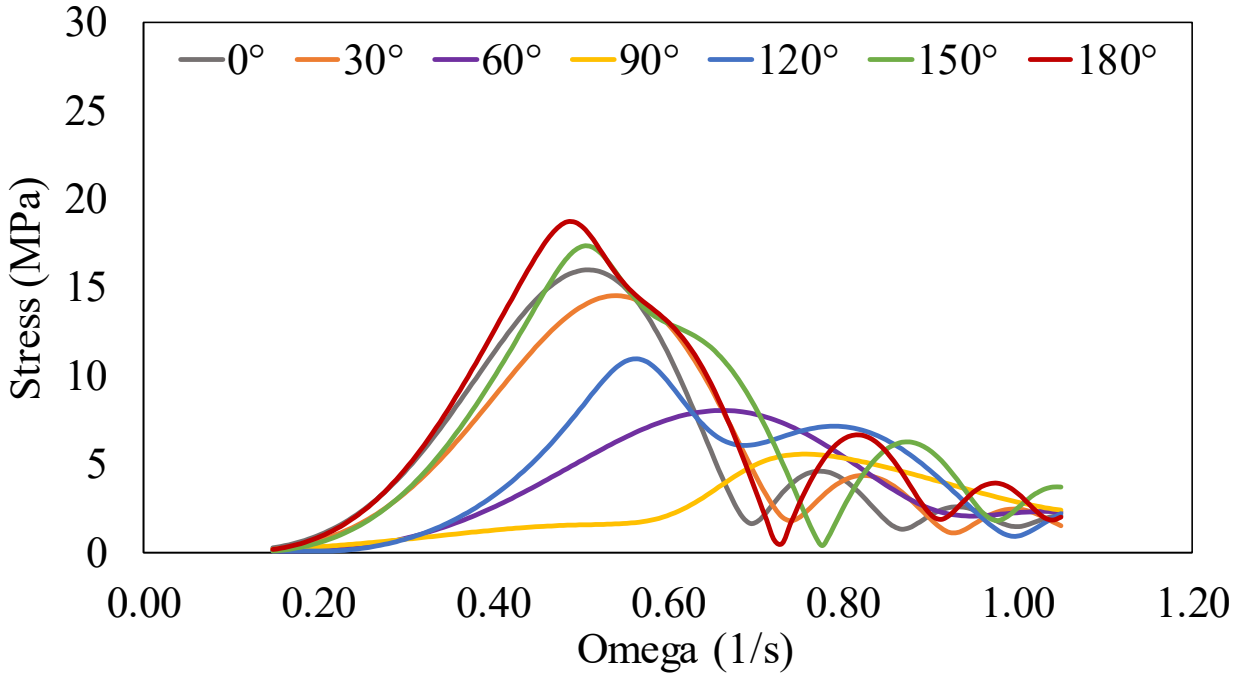

Fig. A1.1 Stress response amplitude operator of a container ship's butt weld on the upper deck for different heading angles.

Appendix 2: Parameters used for Fatigue Damage Calculation

In this research, the fatigue damage calculations are based on the recommendation given by DNVGL-CG-0129 (DNVGL 2015) curve D.

$$D = \sum_{i=1}^{n_{total}} \frac{n_i}{N_i} \tag{A2.1}$$

$$FatLife = \frac{L_D}{D} \tag{A2.2}$$

where:

L_D = ship's design life

n_{total} = total number of stress range blocks

n_i = number of stress cycles in *i*-th stress range block

N_i= number of stress cycles to failure at constant stress range block

i = stress range block index

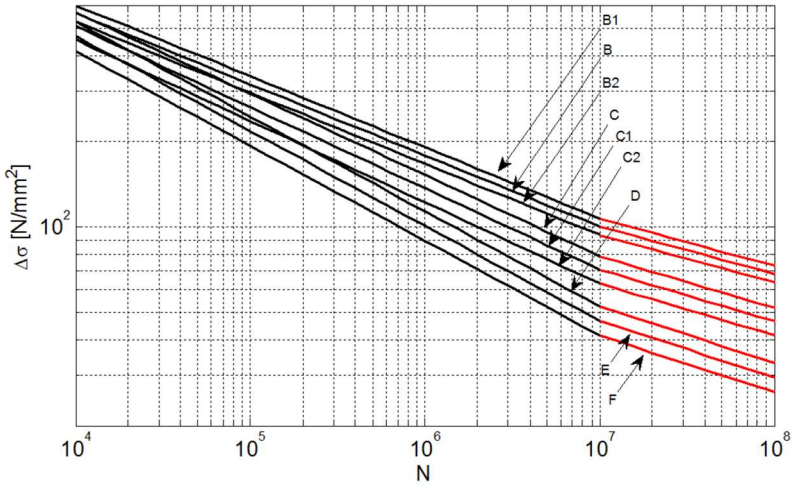

Fig. A2.1 Design *S-N* curve (DNVGL 2015).

Appendix 2 Parameters used for Fatigue Damage Calculation

Table A2.1 S-N parameters for air (DNVGL 2015).

S-N Curve	Reference stress at $2 \cdot 10^6$ cycles (FAT)	Reference stress at 10^7 cycles (knuckle), $\Delta\sigma$	Structural stress concentration embedded in the detail and taken at $2 \cdot 10^6$ (10^7) cycles	N ≤ 107		N > 107	
	N/mm2	N/mm2	-	log K2	m	log K2	m+Δm
B1	160	107	0.56 (0.49)	15.118	4	19.176	6
B	150	100.31	0.60 (0.52)	15.005	4	19.008	6
B2	140	93.62	0.64 (0.56)	14.886	4	18.828	6
C	125	78.92	0.72 (0.57)	13.64	3.5	17.435	5.5
C1	112	70.72	0.80 (0.74)	13.473	3.5	17.172	5.5
C2	100	63.14	0.90 (0.83)	13.301	3.5	16.902	5.5
D	90	52.63	1.00 (1.00)	12.164	3	15.606	5
E	80	46.78	1.13 (1.13)	12.01	3	15.35	5
F	71	41.52	1.27 (1.27)	11.855	3	15.091	5
FAT	X	0.585·X	90/X (90/X)	6.301+3·log(X)	3	7+5·log(0.585·X)	5

Appendix 3 Sensitivity Analysis

A3.1 Uncertainties

Structural performance prediction of ships under sea loading is subjected to uncertainties inherent in the load conditions, material properties, damage propagation, and cross-sectional dimensions. In this section, part of the sensitivity study results as for the wave spectrum, threshold T_{HRES} to extract the $\Delta\sigma_{PK}$ as a whipping vibration due to the slamming impact are given.

To examine the influence of the wave spectrum and T_{HRES} on the various parameters (coefficient of whipping interval C_{wh}, slamming impact stress range $\Delta\sigma_{PK}$, and primary wave stress range $\Delta\sigma_{PW}$), rough short-sea states that have a large contribution to the fatigue damage are considered. It is assumed that the significant wave heights change from 7.5 m to 11.5 m every 2 m, while the mean wave period change from 8.5 s to 11.5 s, every 1 s. Further, the sensitivity analysis is examined for the numerical simulation results in head wave condition, and three ship speeds are used.

A3.2 Wave Spectrum

It assumes that we can describe the sea as a stationary random process. Herein the influence of the JONSWAP (Joint North Sea Wave Project) spectral formulation on the C_{wh}, $\Delta\sigma_{PW}$, and $\Delta\sigma_{PK}$ is examined compared to those results obtained using the ISSC wave spectrum. The peak enhancement factor γ^r was set to 10. Figure A3.1 shows the relationship between significant wave height H_S and the average coefficient of whipping interval C_{wh} for the JONSWAP and ISSC wave spectrum results. It is observed that in general there are small variations between the JONSWAP and ISSC results for C_{wh} coefficient. In most cases, the C_{wh} generated by

using the JONSWAP wave spectrum tends to decrease compared to that obtained by using the ISSC spectral definition.

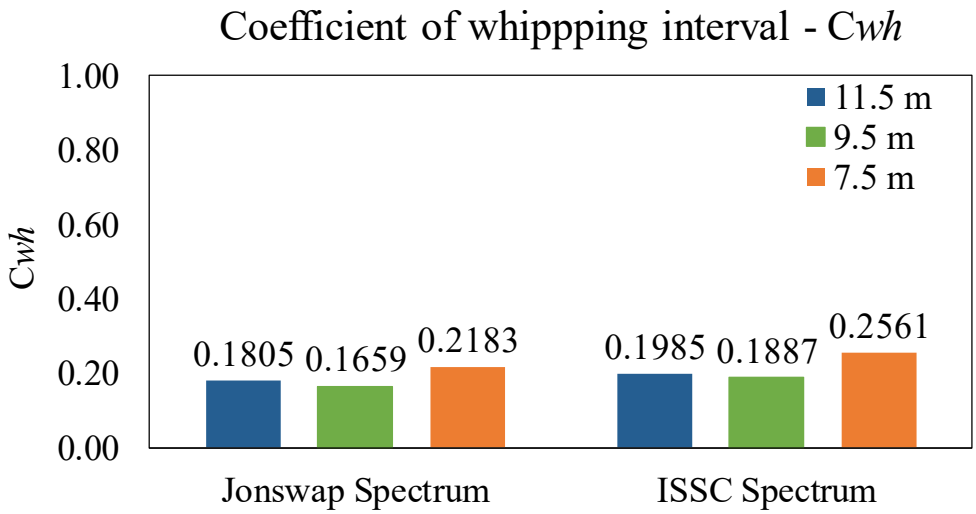

Fig. A3.1 The relation between significant wave height H_S and coefficient of whipping interval C_{wh}.

In Fig. A3.2 it is presented the variation of the average slamming peak stress range $\Delta\sigma_{PK}$ for short sea with various significant wave heights and ship speeds in head sea condition. It is shown that the difference in $\Delta\sigma_{PK}$ increment with *Hs* when comparing the two wave spectrum results. An increment in the slamming peak stress range up to 30% increment can be expected when using the JONSWAP spectrum compared to that of the ISSC spectrum for the same short-sea state, especially in rough seas (for example at 11.5 m waves), under the condition chosen. Furthermore, Fig. A3.3 presents the variation of the average primary wave stress range $\Delta\sigma_{PW}$ for short sea with various significant wave heights and ship speeds in head seas generated by the JONSWAP and ISSC spectrums. As expected, there are slight differences in the primary wave stress range $\Delta\sigma_{PW}$ since the wave spectra are different. These results show that the change in the wave spectra has a limited dependency on the primary wave component. Under the condition chosen, the differences in $\Delta\sigma_{PW}$ are at most 10% (e.g. 7.5 m case). These results indicate the

importance of the wave spectra on the hull vibration components which depend more on the spectrum assumed than C_{wh} or $\Delta\sigma_{PW}$.

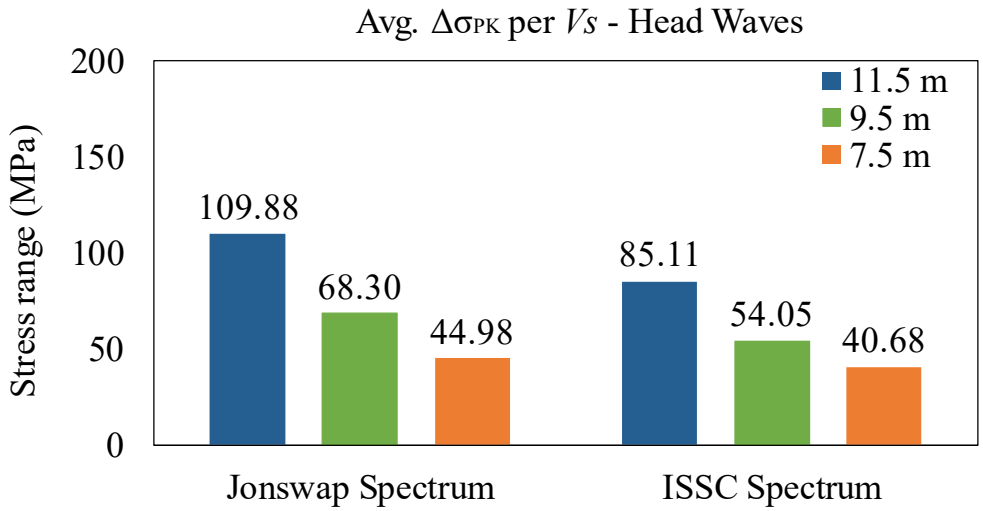

Fig. A3.2 The variation of the average slamming peak stress range $\Delta\sigma_{PK}$ for short sea with various significant wave heights and ship speeds –head seas-.

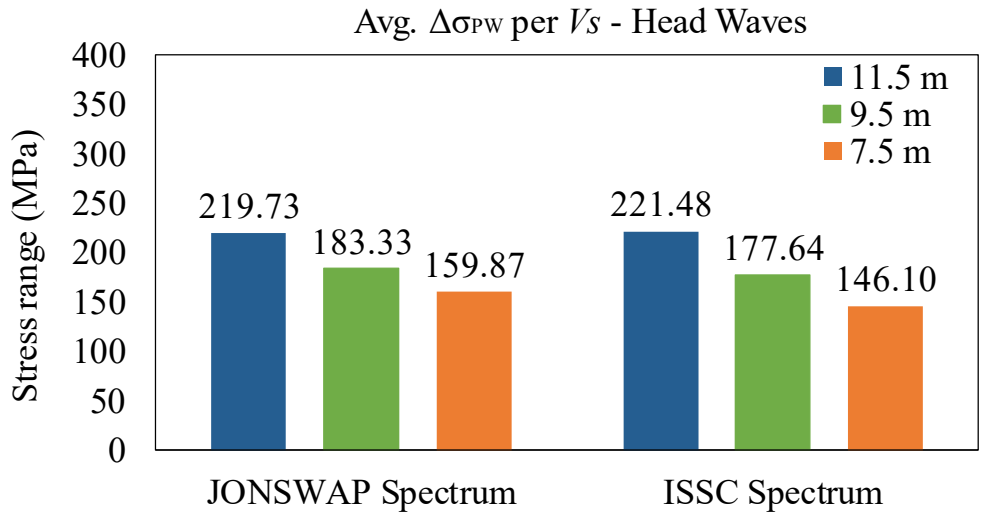

Fig. A3.3 The variation of the average primary wave stress range $\Delta\sigma_{PW}$ for short sea with various significant wave heights and ship speeds –head seas-.

A3.3 Structural Damping

In this thesis, it is assumed less than 2% critical damping for the respective flexible modes, and only the symmetric modes are considered. In order to examine the effect of different damping coefficient on the coefficient of whipping interval, slamming impact stress range and primary wave stress range, the percentage of damping coefficient is changed as follow: 2.4%, 3%, 4%, and 5% for the respective flexible modes. The sea state considered for this examination is the following *Hs*=5.5m, *Ts*=9.5s, in head waves. Figure A3.4 shows the relation of the coefficient of whipping interval with various percentage of structural. It is noted that the probability of whipping slightly decrease, and if are considered changes to the structural damping for the order of 4% and 5% are expected small increment. In Fig. A3.5 it is shown the relation of the stress ratio $\Delta\sigma_{PK}/\ \Delta\sigma_{PW}$ with various percentage of structural damping. It is observed a continuous decrease in the effect of the slamming impact stress range on the primary wave stress range as expected. The results showed in this section are under the condition chosen (only symmetric modes) and it may derive a different tendency if damping of antisymmetric hull distortion are considered since these motions entail horizontal bending and simultaneous twisting of the ship hull.

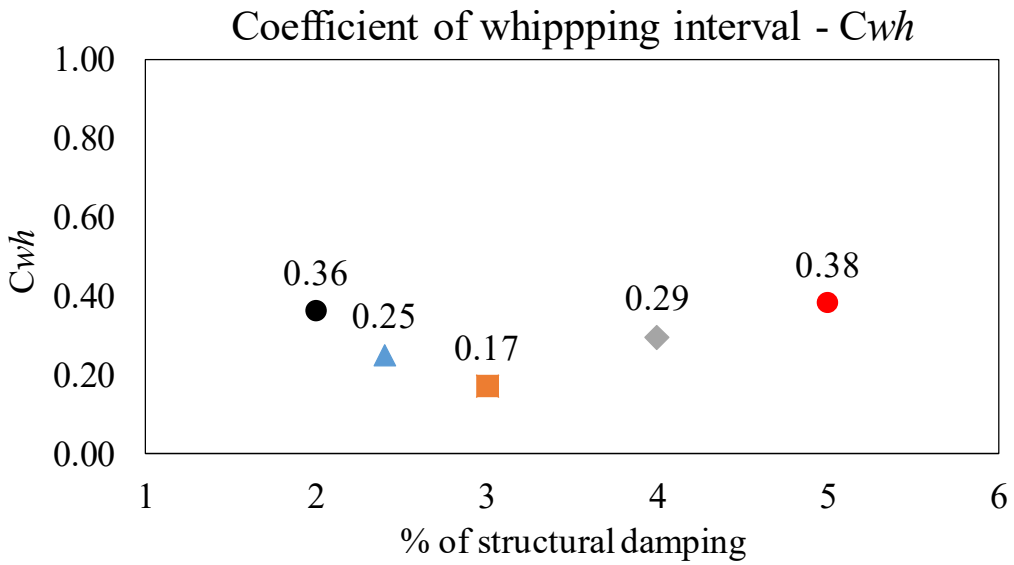

Fig. A3.4 The relation of the coefficient of whipping interval with various percentage of structural damping (*Hs*=5.5m, *Ts*=9.5s, head waves).

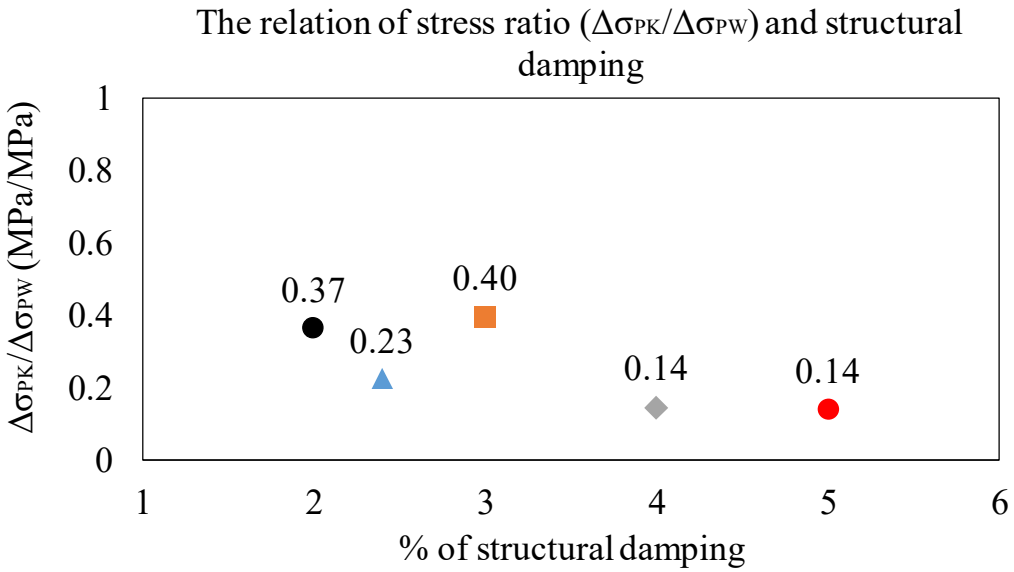

Fig. A3.5 The relation of the stress ratio $\Delta\sigma_{PK}/\Delta\sigma_{PW}$ with various percentage of structural damping (*Hs*=5.5m, *Ts*=9.5s, head waves).

A3.4 Threshold to Slamming Impact Detection

The non-dimensional factor *a* varied from 1.0 to 2.0 to examine the sensitivity on the coefficient of whipping interval C_{wh}. The reference *a* is 1.5 which correspond

to the factor used in this thesis as presented in Section 4.1 and highlighted in Table A3.1. Two wave conditions are examined for significant wave height of 6.5 m and 7.5 m and mean wave period 10.5s. In Table A3.1 it is presented the variation of the coefficient of whipping interval C_{wh} with a for short sea with various Hs, and Vs in head seas. The larger a means that less slamming impact peaks are detected, according to the definition in Eq. 4.2. Further, in general, it is observed that with the increase of the ship speed the C_{wh} variation increases. For 6.5 m waves, C_{wh} is more sensitive to the variation of a than that found for 7.5 m waves. C_{wh} varies from 0.13 to 0.41 for 6.5 m wave cases, which suggest that whipping may happen once every 2 to 7 primary waves. While for 7.5 m the variation on C_{wh} suggest that whipping may happen 3 to 6 primary waves. Moreover, it is observed the importance of threshold to the slamming impact detection on the coefficient of whipping interval. As natural concluded, it is possible that a different threshold would produce different results.

Table A3.1 The variation of the coefficient of whipping interval C_{wh} with the non-dimensional factor a for short sea with various significant wave heights and ship speeds –head seas-.

***Hs* (m)**	***Ts* (s)**	***Vs(kt)***	***a***	***Cwh***	**Slamming per primary wave**
6.5	10.5	19	1.00	0.4153	2
			1.20	0.3022	3
			1.50	0.2053	5
			1.70	0.1692	6
			2.00	0.1353	7
7.5	10.5	13	1.00	0.3500	3
			1.20	0.2963	3
			1.50	0.2275	4
			1.70	0.2053	5
			2.00	0.1692	6

References

1. Almar-Naess A (1985) Fatigue handbook: Offshore Steel Structures. Tapir, Trondheim.
2. ASTM (1985) Standard Practices for Cycle Counting in Fatigue Analysis. American Society for Testing and Materials E 1049-85.
3. Baxevani A, Caires S, Rychlik I (2009) Spatio-temporal statistical modeling of significant wave height. Environmetrics, 20:14–31.
4. Boesten E (2006) The M/S Estonia disaster and the treatment of human remains. In: Bierens JJLM (Eds.) Handbook on Drowning, 650–652.
5. BV (2016) Guidelines for Fatigue Assessment of Steel Ship and Offshore Units, NI 611. France.
6. Cardone VJ, Pierson WJ, Ward EG (1976) Hindcasting the directional spectra of hurricane generated waves. J. Petrol. Technol. 28:385-394.
7. Dessi D, Ciappi E (2013) Slamming clustering on fast ships: From impact dynamics to global response analysis. Ocean Engineering, 62:110-122. https://doi.org/10.1016/j.oceaneng.2012.12.051.
8. DNV GL (2014) Recommended Practice DNV-RP-C205 Environmental conditions and environmental loads. April 2014.
9. DNV GL (2015) Fatigue Assessment of Ship Structures, DNVGL-CG-0129. Høvik, Norway.
10. DNV GL (2018) Maritime Impact: Raisin the baseline for Ultra Large Container Vessel – ULCV. December 2018.
11. Dowling NE (2004) Mean stress effects in stress-life and strain-life fatigue. Fatigue 2004: Second SAE Brazil International Conference on Fatigue.
12. Drummen I, Storhaug G, Moan T (2008) Experimental and numerical investigation of fatigue damage due to wave-induced vibrations in a container ship in head seas. Journal of Marine Science Technology 13:428–445.
13. Europe Centre for Medium-Range Weather Forecasts (ECMWF) www.ecmwf.int.
14. Faltinsen OM (1993) Sea loads on ships and offshore structures solutions. Cambridge University Press, Cambridge.
15. French BJ, Thomas GA, Davis MR (2015) Slam occurrences and loads of a high-speed wave piercer catamaran in irregular seas. J Engineering for the Maritime Environment, 229(1)45-57.
16. Fricke W, Cui W, Kierkegaard H, Kihl D, Koval M, Mikkola T, Parmentier G, Toyosada M, Yoon J, (2002) Comparative fatigue strength assessment of a structural detail in a containership using various approaches of classification societies. Mar Struct 15(1)1-13. https://doi.org/10.1016/S0951-8339(01)00016-8.

References

17. Fricke W, Paetzold H (2012) Experimental Investigation of the Effect of Whipping Stresses on the Fatigue Life of Ships. In: Proceedings of the International Marine Design Conference - IMDC'2012, Vol. 3, pp. 3–10.

18. Fricke W, Paetzold H. (2014) Effect of whipping stresses on the fatigue damage of ship structures. Weld World, 58:261. https://doi.org/10.1007/s40194-014-0111-5.

19. Fukasawa T, Mukai K (2014) On the effects of hull-girder vibration upon fatigue strength of a Post-Panamax container ship disaggregated by short-term sea state. J. Jpn. Soc. Nav. Archit. Ocean Eng. 6(2)431-441. https://doi.org/10.2478/IJNAOE-2013-0190.

20. Fukasawa T, Ogawa Y, Iijima K, and Mikami, T (2011) Comparative Study on Computational Method to Estimate Dynamic Response of a Ship in Waves Including Hull-Girder Vibration. In: The 25th Asian-Pacific Technical Exchange and Advisory Meeting on Marine Structures (TEAM), Incheon, South Korea, pp. 301–308.

21. Gerber H (1874) Bestimmung der zulassigen Spännungen in Eisen-konstrctionen. Zeitschrift des Bayerischen Architeckten und Ingenieur-Vereins, 6:101-110.

22. Goodman J (1899) Mechanics Applied to Engineering. London: Longmans Green. pp. 631–636.

23. Gotoh K, Matsuda K, Kitamura O (2012) Numerical Simulation of Fatigue Crack Propagation under Superposed Loading Histories with Two Different Frequencies. In: Proceedings of Hydroelasticity in Marine Technology 2012, pp. 287-297.

24. Hagiwara H (1989) Weather routing of (sail-assisted) motor vessels. Ph.D. thesis, TU Delft.

25. Haltiner GJ, Hamilton HD, Arnason G (1962) Minimal-time ship routing. Journal of Applied Meteorology 1:1–7.

26. Heggelund SE, Storhaug G, Oma N (2010) Consequences of whipping and springing on fatigue and extreme loading for a LNG vessel based in onboard measurements. In: Proceedings of 11th International Symposium On Practical Design of Ships and other Floating Structures.

27. Hirdaris SE, Bai W, Dessi D, Ergin A, Gu X, Hermundstad OA, Huijsmans R, Iijima K, Nielsen UD, Parunov J, Fonseca N, Papanikolaou A, Argyriadis K, Incecik A (2014) Loads for use in the design of ships and offshore structures. Ocean Engineering, 78:131-174, https://doi.org/10.1016/j.oceaneng.2013.09.012.

28. Hirdaris SE, Price W G, Temarel P (2003) Two- and three- dimensional hydroelastic modeling of a bulker in regular waves. Mar. Struct. 16:627–658.

29. Hirdaris SE, Temarel P (2009) Hydroelasticity of ships: recent advances and future trends. In: Proceedings of the Institution of Mechanical Engineers, Part M: Journal of Engineering for the Maritime Environment, 223(3)305–330.

30. Hogben N, Dacunha NM, Olliver F (1985) Global wave statistics, British Maritime Technology Ltd.

References

31. Hopkins SW, Mitchell MR, Menigault J (2005) Role of Variable Amplitude Fatigue Standards in Improving Structural Integrity. Fatigue Testing and Analysis Under Variable Amplitude Loading Conditions, ASTM STP 1439, ASTM International, pp. 24-35.

32. Hwang JH, Park JS, Won SI, Jung BH (2015) Ultimate strength assessment of ultra large container ships considering hydroelastic responses. In: Proceedings of the 7th international conference on hydroelasticity in marine technology, Split.

33. Iijima K (2011) Evaluation of Effects of Wave-Induced Vibrations on Fatigue Damage of Large Ships. J. Jpn. Soc. Nav. Archit. Ocean Eng. 14:27–37.

34. Iijima K, Hermundstad O A, Zhu S, Mian T (2009) Symmetric and Antisymmetric Vibrations of a Hydroelastically Scaled Model. In: Hydroelasticity in Marine Technology. Southampton, UK, pp. 173-182.

35. Iijima K, Itamura N, Fujikubo M (2011) Comparison of Long-Term Fatigue Damage in Bulk Carrier, VLCC and Container Carrier Subjected to Wave-Induced Vibrations. In: 8th International Workshop on Formal Aspects of Security and Trust (FAST2011), Honolulu, pp. 547–554.

36. Iijima K, Ueda R, Fujikubo M (2017) Numerical Investigation into Uncertainty of Wave-Induced Vibration of Large Container Ships due to Ship Operation. ASME. International Conference on Offshore Mechanics and Arctic Engineering, Volume 9: Offshore Geotechnics; Torgeir Moan Honoring Symposium ()V009T12A046. doi:10.1115/OMAE2017-62336.

37. Iijima K, Ueda R, Tamaru H, Fujikubo M. (2019) Effects of Weather Routing on Maximum Vertical Bending Moment in a Ship Taking Account of Wave-Induced Vibrations. ASME. J. Offshore Mech. Arct. Eng. 141(3)031101-031101-11. doi:10.1115/1.4041997.

38. Iijima K, Yao T, Moan T (2008) Structural response of a ship in severe seas considering global hydro elastic vibrations. Marine Structures 21:420-445. https://doi.org/10.1016/j.marstruc.2008.03.003.

39. Im HI, Vladimir N, Malenica S, Ryu HR, Cho DS (2015) Fatigue analysis of HHI Sky Bench TM 19000 TEU ultra large container ship with springing effect included. In: Proceedings of the 7th international conference on hydroelasticity in marine technology, Split.

40. International Association of Classification Societies (1978) Unified Requirement (UR) S7 – Minimum Longitudinal Strength Standards, Rev. 2, London.

41. International Ship and Offshore Structures Congress - ISSC 2015 Committee I.1 Environment Report. Proc. ISSC 2015, 1, Lisbon, Portugal.

42. International Ship and Offshore Structures Congress – ISSC. ISSC 2012 Committee I.1 Environment Report. Proc. ISSC 2012, 1, 1-78, Rostock, Germany.

43. James RW (1957) Application of wave forecasts to marine navigation. Ph.D. thesis, New York University.

References

44. Jensen JJ, Dogliani M (1996) Wave-induced ship hull vibrations in stochastic seaways. Mar. Struct. 9:353–387.

45. Jiao J, Jiang Y, Zhang H, Li C, Chen C (2019) Predictions of Ship Extreme Hydroelastic Load Responses in Harsh Irregular Waves and Hull Girder Ultimate Strength Assessment. Appl. Sci., 9, 240.

46. Kahl A, Fricke W, Paetzold H., Selle HV (2015) Whipping Investigations based on Large-Scale Measurements and Experimental Fatigue Testing. International Journal of Offshore and Polar Engineering (IJOPE), 25(4)247-254. http://dx.doi.org/10.17736/ijope.2015.sh14.

47. Kawabe H (2002) Contribution of supposed wave condition on the long-term distribution of a wave-induced load. J Mar Sci Technol 6:135-147.

48. Ki HG, Park SG, Jang IH (2015) Full scale measurement of 14k TEU container ship. In: Proceedings of the 7th international conference on hydroelasticity in marine technology, Split.

49. Kim JH, Kim Y (2014) Numerical analysis on springing and whipping using fully-coupled FSI models. Ocean Engineering 91:28-50. https://doi.org/10.1016/j.oceaneng.2014.08.001.

50. Kim JH, Kim Y (2018) Prediction of extreme loads on ultra-large containerships with structural hydroelasticity. J Mar Sci Technol, 23:253. https://doi.org/10.1007/s00773-017-0471-9.

51. Kim JH, Kim Y, Yuck RH, Lee DY (2015) Comparison of slamming and whipping loads by fully coupled hydroelastic analysis and experimental measurement. Journal of Fluids and Structures 52:145-165. https://doi.org/10.1016/j.jfluidstructs.2014.10.011.

52. Kim Y, Kim JH (2016) Benchmark study on motions and loads of a 6750-TEU container-ship. Ocean Engineering 119:262-273. https://doi.org/10.1016/j.oceaneng.2016.04.015

53. Kim Y, Kim KH, Kim Y (2009) Analysis of hydroelasticity of floating ship-like structures in time domain using a fully coupled hybrid BEM-FEM. J. Ship Res 53(1)31-47.

54. Kitamura O, Sugimura T, Nakayama S, Hirota K (2012) A study of the results of fatigue crack propagation tests under combination loads of high & low cycles -Consideration to the effect of whipping on the fatigue strength-, 2012S-OS1-4. In: Conference Proceedings of the Japan Society of Naval Architects and Ocean Engineers, Vol.14, pp. 13-16. (in Japanese).

55. Korobkin A, Scolan Y (2006) Three-dimensional theory of water impact. Part 2. Linearized Wagner problem. Journal of Fluid Mechanics, 549:343-373. doi:10.1017/S0022112005008049.

56. Liao, P. K., Lee, Y. J., Lin, H. J., Tsai, S. C., Chien, H. L., Chang, B. C. & Luo, G. M. 2015. Springing effect on the fatigue life of an 8000 TEU container ship. In: Shenoi, G. S. (ed.) Analysis and Design of Marine Structures. UK.

57. Lundgren J, Rönnqvist M, Värbrand P (2010) Optimization. Student litteratur AB, Lund.

References

58. Magoga TF, Aksu S, Cannon S, Ojeda R, Thomas G (2014) Identification of slam events experienced by a high-speed craft. Safety & Reliability of Ships, Offshore & Subsea Structures International Conference, Scotland, UK, 1-13.

59. Malenica S, Tuitman JT (2008) 3D FEM-3D BEM model for springing and whipping analysis of ships. In: Proceedings of the International Conference on Design and operation of Containerships, London.

60. Mao W, Prasetyo F, Ringsberg JW, Osawa N (2013) A Comparison of Two Wave Models and Their Influence on Fatigue Damage in Ship Structures. In: ASME. International Conference on Offshore Mechanics and Arctic Engineering, Volume 2A: Structures, Safety and Reliability ()V02AT02A010. doi:10.1115/OMAE2013-10114.

61. Mao W, Ringsberg J, Rychlik I, Storhaug G (2009) Comparison Between a Fatigue Model for Voyage Planning and Measurements of a Container Vessel. ASME. International Conference on Offshore Mechanics and Arctic Engineering, Volume 2: Structures, Safety and Reliability ()173-180. doi:10.1115/OMAE2009-79235.

62. Mao W, Ringsberg JW, Rychlik I (2010a) Development of a Fatigue Model Useful in Ship Routing Design. Journal of Ship Research 54(4)281-293.

63. Marine Accident Investigation Branch – MAIB (2008) Report on the investigation of the structural failure of MSC Napoli, English Channel on 18 January 2007. MAIB report No. 9/2008. Southampton, UK.

64. Matsuishi M, Endo T (1968) Fatigue of Metals Subjected to Varying Stress. In: Proceedings of the Kyushu Branch of Japan Society of Mechanics Engineering, pp. 37-40.

65. Miner MA (1945) Cumulative Damage in Fatigue. Journal of Applied Mechanics, 12:A159-A164.

66. Minoura M, Naito S (2004) A Stochastic Model For Evaluation of Seakeeping Performance. In: International Society of Offshore and Polar Engineers Conference. ISOPE-I-04-444.

67. Minoura M, Naito S (2006) Stochastic Sea Climate Simulation Based On Hindcast Data. In: International Society of Offshore and Polar Engineers Conference. ISOPE-I-06-219.

68. Moe E, Holtsmark G, Storhaug G (2005) Full Scale Measurements of the Wave Induced Hull Girder Vibrations of an Ore Carrier Trading in the North Atlantic. In: Transactions of Royal Institution of Naval Architects, Conference on design and operation of bulk carriers, London, UK.

69. Morrow J (1968) Fatigue properties of metals, Section 3.2. Fatigue Design Handbook. Pub. No. AE-4, Soc. of Automotive Engineers, Warrendale, PA. Section 3.2 is a summary of a paper presented at Division 4 of the SAE Iron and Steel Technical Committee.

70. Oberhagemann J, Shigunov V, Radon M, Mumm H, Won SI (2015) Hydrodynamic load analysis and ultimate strength check of an 18000 TEU containership. In: Proceedings of the 7th international conference on hydroelasticity in marine technology, Split.

References

71. Ochi MK (1964) Prediction of occurrence and severity of ship slamming at sea. 5th Symp. Naval Hydrodynamics, Bergen.

72. Ogawa Y, Kitamura O, Toyoda M (2012) A study for the statistical characteristic of slamming induced vibration of large container ship. In: Proceedings of the Hydroelasticity in Marine Technology 2012, pp. 321-330.

73. Olsen AS, Schrøter C, Jensen JJ (2005) Wave Height Distribution Observed by Ships in the North Atlantic. Journal Ships and Offshore Structures, 1(1)1-12.

74. Osawa N, Nakamura T, Yamamoto N, Sawamura J (2013) Development of a New Fatigue Testing Machine for High Frequency Fatigue Damage Assessment. In: ASME. International Conference on Offshore Mechanics and Arctic Engineering, Volume 2B: Structures, Safety and Reliability ()V02BT02A051. doi:10.1115/OMAE2013-11582.

75. Osawa N, Nakamura T, Yamamoto N, Sawamura J (2015a) Experimental Study on Fatigue Strength of Ship's Welded Joint under Intermittently High Frequency Superimposed Load considering Actual Encountered Condition. In: International Society of Offshore and Polar Engineers. ISOPE-I-15-829.

76. Osawa N, Nakamura T, Yamamoto N, Sawamura J (2015b) Study on Fatigue Strength of Welded Joints Subject to High Frequency Superimposed Wave Loadings by Using Plate-Bending-Vibration Type Fatigue Testing Machines. Journal of the Japan Society of Naval Architects and Ocean Engineers, 22:175-185. https://doi.org/10.2534/jjasnaoe.22.175. (in Japanese).

77. Osawa N, Nakamura T, Yamamoto N, Sawamura J. (2014) Experimental Study on high-frequency Effect on Fatigue Strength of Welded Joint by using Plate-Bending-Vibration Type Fatigue Testing Machine. In: ASME. International Conference on Offshore Mechanics and Arctic Engineering, Volume 4B: Structures, Safety and Reliability ()V04BT02A003. doi:10.1115/OMAE2014-23856

78. Palmgren A (1924) The endurance of ball bearings (in German). Z. Ver. Deut. Ing. 68:339-341.

79. Papanikolaou AD, Schellin TE (1992) A three-dimensional panel method for motions and loads of ships with forward speed. Ship Technol Res 39:145–56.

80. Perakis, A. N., Papadakis, N. A., 1989. Minimal time vessel routing in a time dependent environment. Transportation Science 23, 266–276.

81. Prasetyo F (2013) Study on Advanced Storm Model for Fatigue Assessment of Ship Structural Member. Doctoral Thesis, Osaka University, Japan.

82. Prasetyo F, Osawa N., Kobayashi T (2012) Study on Preciseness of Load History Generation based on Storm model for Fatigue Assessment of Ship Structures Members. In: Proceeding of 22nd International Offshore and Polar Engineering Conference (ISOPE). Rhodes, Greece, pp 709-712.

83. Prpić-Oršić J, Parunov J, Šikić I (2014) Operation of ULCS - real life. International Journal of Naval Architecture and Ocean Engineering 6(4)1014-1023. https://doi.org/10.2478/IJNAOE-2013-0228.

References

84. Savitzky A., Golay M.J.E. (1964) Smoothing and Differentiation of Data by Simplified Least Squares Procedures. Analytical Chemistry 36 (8)1627-1639. https://doi.org/10.1021/ac60214a047.

85. Sen D, Padhy CP (2015) An Approach for Development of a Ship Routing Algorithm for Application in the North Indian Ocean Region. Appl. Ocean Res. 50:173–191.

86. Shao W, Zhou P, Thong SK (2012) Development of a novel forward dynamic programming method for weather routing. Journal of Marine Science and Technology 17:239–251.

87. Ship Research Panel 245 – SR245 (2000) Study on Ship Structural Life of the Double Hull Tanker. The Shipbuilding Research Association of Japan (JSRA). (in Japanese).

88. Simonsen M, Larsson E, Mao W, Ringsberg JW (2015) State-of-the-Art Within Ship Weather Routing. In: ASME. International Conference on Offshore Mechanics and Arctic Engineering, Volume 3: Structures, Safety and Reliability()V003T02A053. doi:10.1115/OMAE2015-41939.

89. Smith JO (1942) The Effect of Range of Stress on the Fatigue Strength of Metals. Bulletin No. 334, University of Illinois, Engineering Experiment Station, Urbana, IL.

90. Soares C, Santos TA (2015) Maritime Technology and Engineering, Taylor & Francis Group, London, UK, pp. 857-864.

91. Soderberg CR (1939) Factor of safety and working stress. Transactions of the American Society of Mechanical Engineers, 52:13-28.

92. Storhaug G (2007) Experimental Investigation of Wave Induced Vibrations Increasing Fatigue Damage in Ships (Ph.D. dissertation). Norwegian University of Science and Technology, Tronheim, Norway.

93. Storhaug G, Kahl A (2015) Full scale measurements of torsional vibrations on Post-Panamax container ships. In: Proceedings of the 7th international conference on hydroelasticity in marine technology, Split.

94. Storhaug G, Moe E, Holtsmark G (2006) Measurements of Wave Induced Hull Girder Vibrations of an Ore Carrier in Different Trades. ASME. J. Offshore Mech. Arct. Eng. 2007, 129(4)279-289. doi:10.1115/1.2746398.

95. Storhaug G, Moe E, Piedras TA (2007) Whipping Measurements Onboard a Midsize Container Vessel Operating in the North Atlantic. In: Marintec China Proceedings (RINA, CMP, and SNAME), International Symposium on Ship Design and Construction, pp. 55-70.

96. Storhaug G, Vidic-Perunovic J, F. Rüdinger F, Holtsmark G, Helmers JB, Gu X (2003) Springing/whipping response of a large ocean going vessel—a comparison between numerical simulations and full scale measurements. In: Proceedings of hydroelasticity in marine technology. Oxford, UK, pp 117–129.

References

97. Sumi Y (2012) The effect of slam-induced whipping stress for fatigue crack growth under random seaway loading. In: Conference Proceedings of the Japan Society of Naval Architects and Ocean Engineers 2012S-OS1-3, 14:9-12. (in Japanese).

98. Sumi Y (2014) Fatigue crack propagation in marine structures under seaway loading. International Journal of Fatigue, 58:218-224. https://doi.org/10.1016/j.ijfatigue.2013.03.002.

99. Szlapczynska J, Smierzchalski R (2007) Adopted isochrones method improving ship safety in weather routing with evolutionary approach. International Journal of Reliability, Quality & Safety Engineering 14:635–645.

100. Takami T, Oka M, Iijima K (2017) Study on Application of CFD and FEM Coupling Method to Evaluate Dynamic Response of Ship Under Severe Wave Condition. ASME. International Conference on Offshore Mechanics and Arctic Engineering, Volume 7A: Ocean Engineering ()V07AT06A053. doi:10.1115/OMAE2017-61553.

101. Tamaru H (2016) About the Optimum Route by the Weather Routing. In: Conference Proceeding of the Japanese Society of Naval and Ocean Engineers. Okayama, pp. 109-114.

102. Tamaru H, Hagiwara H, Sugai K, Kusaka Y (1999) A Study on Weather Routing of High Speed Ship. In: Proceedings of the Fifth International Conference on Fast Sea Transportation (FAST'99), pp. 219-229.

103. Thomas G, Winkler S, Davis M (2011) Slam events of high-speed catamarans in irregular waves. Journal of Marine Science and Technology, 16:8-21.

104. Tick LJ (1958) Certain probabilities associated with bow submergence and ship slamming in irregular seas. Journal of Ship Research, 2:30-36.

105. Tomita Y, Matoba M, Kawabe H (1995) Fatigue crack growth behavior under random loading model simulating real encountered wave condition. Mar Struct 8:407-422.

106. Toyoda K, Matsumoto T, Tamamoto N, Terai K (2012) Simplified Fatigue Assessment considering the Occurrence Probability of Hydro-Elastic Response in Actual Sea State Conditions. In: Proceedings of the Hydroelasticity in Marine Technology 2012, pp. 367-375.

107. Tuitman JT (2010) Hydro-Elastic Response of Ship Structures to Slamming Induced Whipping (Ph.D. dissertation). Delft University of Technology, Delft, The Netherlands.

108. Vettor R, Soares C (2016) Development of a ship weather routing system. Ocean Engineering 123:1-14. https://doi.org/10.1016/j.oceaneng.2016.06.035.

109. Von Karman T (1929) The Impact on Seaplane Floats During Landing," National Advisory Committee for Aeronautics, Washington, DC, Report No. NACA-TN-321.

110. Wan S, Shinkai A (1995) The statistical characteristics of global wave data and appraisal for long-term prediction of ship response. J Soc Nav Archit Jpn 178: 289-296. (in Japanese).

References

111. Wang S, Guedes Soares C (2016a) Experimental and numerical study of the slamming load on the bow of a chemical tanker in irregular waves. Ocean Engineering, 111:369-383.

112. Wang S, Guedes Soares C (2016b) Stern slamming of a chemical tanker in irregular seas. Ocean Engineering, 122:322-332.

113. Wang S, Guedes Soares C (2017) Review of Ship Slamming Loads and Responses. Journal of Marine Science and Application, (4)427-445. doi:10.1007/s11804-017-1437-3.

114. Ward EG, Borgman LE, Cardone VJ (1979) Statistics of hurricane Waves in the Gulf of Mexico. OTC 3229. 10th Annual Offshore Technology Conference, Houston, TX.

115. Yamada K (2006) Some new approaches to fatigue evaluation of steel bridges. Steel Structures, 6:319-326.

Publications related to this Thesis

Peer-review Publications

1. Osawa N, De Gracia L, Iijima K, Yamamoto N, Matsumoto K (2019): Study on Fatigue Strength of Welded Joints Subject to Intermittently Whipping Superimposed Wave Load. In: International conference proceeding on Practical Design of Ships and Other Floating Structures (PRADS). (in printing).
2. De Gracia L, Wang H, Mao W, Osawa N, Rychlik I, Storhaug G (2019): Comparison of Two Statistical Wave Models for Fatigue and Fracture Analysis of Ship Structures. Ocean Engineering, Volume 187, 106161. doi.org/10.1016/j.oceaneng.2019.106161.
3. De Gracia L, Osawa N, Iijima K, Fukasawa T, Tamaru H (2018): A Study on the Stochastic Aspects of the Whipping Vibrations in a Container Ship. In: ASME, International Conference on Offshore Mechanics and Arctic Engineering, Volume 3: Structures, Safety, and Reliability ():V003T02A027. doi:10.1115/OMAE2018-77888.
4. De Gracia L, Tamaru H, Osawa N, Fukasawa T (2017): A Study on the Influence of Weather Routing on the Preciseness of Ship Structure's Fatigue Assessment. In: Proceeding of 27th International Offshore and Polar Engineering Conference (ISOPE), pp. 957-963.

Conference Proceedings

1. De Gracia L, Wang H, Mao W, Osawa N, Rychlik I, Storhaug G, Ruiz H (2019): Comparative Study on Two Statistical Wave Load Models and Their Application to Fatigue Assessment. In: Conference Proceeding of The Japan

Society of Naval Architects and Ocean Engineers, Volumen 28, 2019S-GS18-3, pp. 459-461.

2. De Gracia L, Osawa N, Iijima K, Yamamoto N, Ruiz H (2018): A Study on the Fatigue Damage Estimation with the consideration of Wave-induced Vibrations. In: Conference Proceeding of The Japan Society of Naval Architects and Ocean Engineers, Volumen 27, 2018A-GS16-4, pp. 445-449.
3. De Gracia L, Osawa N, Iijima K, Fukasawa T (2017): A Study on the effect of the Stochastic Characteristics of Whipping Vibrations in a Container Carrier. In: Conference Proceeding of The Japan Society of Naval Architects and Ocean Engineers, Volumen 25, 2017-GS2-16, pp. 353-357.
4. De Gracia L, Osawa N, Iijima K, Fukasawa T (2017): A Study on the Stochastic Characteristics of Wave Load Sequences including Whipping Vibrations in a Container Ship. In: International conference proceeding of the 31st Asian-Pacific Technical Exchange and Advisory Meeting on Marine Structures (TEAM 2017), pp. 780-785.